

COTUTELLE THESIS PRESENTED
TO OBTAIN THE QUALIFICATION OF

**DOCTOR OF
THE UNIVERSITY OF BORDEAUX
AND THE UNIVERSITY OF THE BASQUE COUNTRY (UPV/EHU)**

DOCTORAL SCHOOL of Life and Health Sciences (UB)
DOCTORAL SCHOOL of Pharmacology (UPV/EHU)

By **Lise GUILHEMSANG**

**NETWORK DYNAMIC OF BASAL GANGLIA CIRCUITS
IN NORMAL AND PARKINSONIAN CONDITIONS**

Under the supervision of

Mrs. Teresa MORERA-HERRERAS	University of the Basque Country (UPV/EHU)
Mr. Thomas BORAUD	University of Bordeaux

Viva on December 16, 2022

Members of the examination panel:

Mr. Philippe DE DEURWAERDERE	Professeur des universités (University of Bordeaux)	President
Mrs. Maria TORRECILLA	Associate Professor (University of the Basque Country)	Examiner
Mrs. Marianne AMALRIC	Senior researcher (Aix-Marseille University)	Examiner
Mr. Pierre-Olivier FERNAGUT	Senior researcher (University of Poitiers)	Reporter
Mrs. Ledia F. HERNANDEZ	Associate Professor (Complutense University)	Reporter

Research units

- Departamento de Farmacología. Facultad de Medicina y Enfermería. Universidad del País Vasco (UPV/EHU). Barrio Sarriena s/n 48940-Leioa (Spain).
- Dynamique des Réseaux de l'Apprentissage Procédural. Institut des Maladies Neurodégénératives (IMN). CNRS UMR 5293. Université de Bordeaux. Centre Broca Nouvelle-Aquitaine. 3ème étage, 146 rue Léo Saignat. 33076-Bordeaux (France).

This Doctoral thesis has been supported by funds from the University of the Basque Country (GIU19/092), and the MINECO fund SAF2016-77758-R (AEI/FEDER, UE). Lise Guilhemsang has held a predoctoral UPV/EHU fellowship in Cotutelle with the University of Bordeaux for the period 2019-2023.

Conflict of interest

The authors declare no conflicts of interest.

ACKNOWLEDGEMENTS / REMERCIEMENTS

Throughout my thesis, I have had the opportunity to work with some great people that I would like to thank because each and one of them, in one way or another, played a role in my thesis.

First of all, I would like to thank the jury members for evaluating my work and for giving me the opportunity to defend this thesis. Thank you to **Ledia F.Hernandez** and **Pierre-Olivier Fernagut** for having accepted to be reporters and thanks to **Philippe De Deurwaerdère**, for being the president of the jury panel.

I would like to thank my supervisors **Teresa** and **Thomas**, for allowing this adventure to happen in the first place (and yes Thomas, on paper you are my supervisor). Thank you for having accepted me in your respective laboratories.

Teresa, thank you for having given me the chance to discover the joint PhD possibility with what the cotutelle has to offer. I will never forget your welcome when I first arrived in Bilbao, your smile and your kindness, and of course, all of our morning coffee breaks at 9:30am! Thank you for making my stay in Spain so unforgettable. I will remember the birthday choir and the candle for a very long time! It is really a shame that lockdown prevented me from staying longer in Leioa.

There is the official and the unofficial! A huge thanks to **Nico**, my third supervisor. Thank you for first getting me interested in electrophysiology in vivo during my master's internship, and for having stayed one entire night to write my master report together... and depositing it 4 minutes before the deadline (we have made some progress)! Thank your help in the writing of this thesis, which this time, did not end with an all-nighter! I truly admire your passion for science. I am very grateful to have witnessed your scientific approach of always finding the positive in 'failed' experiences.

Gracias a todo el equipo de Leioa: **Luisa, Cristina, Elena, Mario, Asier y Sergio** por la acogida y todos vuestros consejos durante mi estancia. Gracias también por hacerme descubrir la maravillosa ciudad que es Bilbao y a **Sergio**, sin el cual no habría podido recuperar mi coche del depósito a buen precio. Os recordaré siempre con vuestras sonrisas españolas y esa amabilidad que siempre calienta el corazón. Eskerrik asko !

Je tiens également à remercier tous les membres de l'équipe 4, pour ces moments de science mais aussi de détente. Un merci plus particulier à **Victor** pour le travail fourni sur ce projet, je sais à quel point regarder des souris vues de dessous ce n'est pas facile. **Clara**, merci pour ces fraises du mercredi matin ! Et **Sophie** que je ne connaissais finalement pas tant que ça avant de partager une chambre, que dis-je un lit lors de la FENS. Merci pour les chocolatinas restantes de l'open space qui ont ravi quelques unes de mes soirées d'écriture.

Enfin je remercie toutes ces personnes croisées dans les couloirs de l'IMN et qui ont soulagé mes week-ends en partageant le suivi post-opératoire des souris, **Zoé, Léa, Alexia**, les **membres du PIV, Lorena**. Lorena que j'aurais pu remercier en espagnol finalement. Merci pour les échanges sur les dyskinésies, les arky, ton aquarelle toujours exposée chez moi et puis ta recette de mascarpone sucré/salé ! Un immense Merci à Raphaëlle, pour ta patience

quant à mon anglais, ton courage pour relire encore et encore mon manuscrit. J'espère que tu continueras de profiter pleinement de ton passage à Leioa !

Un grand Merci à mes amis, qui ont fait de ces 3 dernières années autre chose qu'une thèse. **Teresa S**, pour tes cours de vocabulaire espagnol, les citrons et la tequila, que nous ne sommes pas prêtes d'oublier. **Oihana**, pour nos virées d'après boulot, nos convoits à travers la frontière. Mon passage à Bilbao n'aurait certainement pas été le même sans ton soutien et ta bonne humeur. **Lauriane**, pour les ventes de plantes, les balades à vélos, les vendredis détentés et les kebabs infects dont on oubliera l'adresse. **Marine**, mon double, parce qu'avec toi tout est toujours improbable mais si vivifiant. **Kit**, Pernelle, parce que "*les connaissances sans le caractère ne sont que la croûte sans le pâté*". **Manon**, ces repas du midi au RU, ces séances d'escalades (et de torture ensuite), m'ont toujours aidé à faire une pause, changer d'air et merci pour ça ! **Barth**, merci pour tes commentaires. Et puis **Élodie**, merci pour cet exposé sur l'altruisme en première année de master, là où tout a commencé, puis a continué en stage et après. Ta bienveillance et ta positivité font que nos retrouvailles sont toujours aussi ressourçantes ! Cette thèse elle est un peu pour toi, parce que même si la route est longue, l'important c'est ce qu'on en fait et de toujours rebondir, ta force à ce sujet, m'a toujours impressionnée. Et Merci à tous ceux que je n'ai pas cités mais qui ont contribué de près ou de loin à ce que cette aventure soit plus folle !

Mais que serait cette thèse sans le soutien inconditionnel de ma famille ? Un merci ne serait pas assez fort. **Claire**, tes petits messages d'encouragements qui font toujours tant de bien, tu as toujours le chic pour les envoyer au bon moment. **Julien** pour tes conseils avisés dans cette aventure, **Chub**, parce qu'avoir un beau frère qui travaille dans la bio c'est toujours sympa pour trouver des stages de licence ! Et enfin **Papa** et **Maman**, de croire en moi depuis le début, de m'avoir poussée à poursuivre mes rêves et aider à les financer. Je n'oublierai pas toute l'aide que vous m'avez apportée, notre frigo non plus. Mais pas de panique je vais pouvoir (enfin) vous laisser tranquille (que sur ce point). Je vous remercie du fond du cœur.

Et puis, **Thomas**. Ah que dire de synthétique pour te remercier. Tu es présent à chaque instant. Tu es un vrai soutien pour moi, tant au niveau technique que moral. Merci pour ces visio Python depuis la Norvège, pour avoir si bien traduit le langage d'un biologiste à un informaticien et toujours trouver une façon de m'aider. Cette thèse elle est un peu la tienne. Tu sais me faire rire, me rassurer, en bref, merci de m'avoir si bien soutenu et accompagné même ces dernières semaines, un peu moins faciles. Ce sera ton tour plus vite que tu ne le penses et je serai là.

A mes étoiles, et à ce qui ne se voit pas,

A difficulty is no longer one from the moment you smile and confront it.

Baden Powell

ABSTRACT

Basal ganglia (BG) circuits are involved in different functions from movement control to cognitive/motivational processes. The loss of dopamine (DA) in these circuits triggers Parkinson's disease (PD) characterised by devastating motor impairments known as akinesia and bradykinesia. In addition to DA depletion, PD patients present an early serotonergic (5-HT) alteration at the level of the BG nuclei.

5-HT modulates the activity of BG circuitry by acting on a large variety of 5-HT receptor subtypes. Among them, the 5-HT_{2A} receptor is expressed in both motor and associative/limbic territories of the BG nuclei being implicated in regulation of motor, executive and cognitive functions, as well as automatisms. In addition, 5-HT_{2A} receptors may also play a role in diseases linked to BG dysfunction, such as PD. However, the role of the 5-HT_{2A} receptor in cortical-BG information processing is still not well understood.

Therefore, in the first part of my PhD, we investigated the specific contribution of 5-HT_{2A} receptors on the dynamic response of BG output nucleus to motor and medial prefrontal (mPF) cortical information. For that purpose, *in vivo* single-unit extracellular recordings of lateral and medial *substantia nigra pars reticulata* (SNr) neurons along with simultaneous electrical stimulation of the motor and mPF cortex were used to assess the effect of 5-HT_{2A} receptor activation/blockade. The results showed a topographical-dependent dissociation in the effects triggered by the 5-HT_{2A} agonist TCB-2, which specifically increased the medial SNr neuron activity and had preferential action on mPF cortical information processing through the striato-nigral direct pathway. These findings provide novel evidence about the specific signature of 5-HT_{2A} receptors on the dynamic regulation of BG circuits.

The second part of my PhD was focused on the study of BG dynamics in pathological conditions. In PD, dopaminergic therapy such as the administration of the precursor levodopa reduces the symptomatology and improves movement execution in the early stage of the disease, but quickly triggers abnormal and involuntary movements known as levodopa-induced dyskinesia (LID). LID is very debilitating and refractory to any further drug treatment. Hence, understanding the neuronal mechanism underlying LID is fundamental to develop new therapeutic strategies. Recent studies have shown that LID is caused by excessive neuronal activity in the striatum, however, how such striatal activity impacts BG downstream circuits such as the external globus pallidus (GPe) to generate LID is still unknown. In addition, a subpopulation of GPe neurons called the arkypallidal (Arky-GPe) neurons, directly form a negative feedback loop with the striatum to powerfully control action inhibition in normal

conditions. Importantly, the activity and contribution of this GPe action-suppressing pathway during LID is totally unknown.

For these reasons, the objective of this project was to characterise the dynamic changes of activity present in Arky-GPe neurons across different disease states, going from healthy condition to the pathophysiological states of PD and LID. In this work, we used optical methods (i.e. fiber photometry and miniscope) to monitor *in vivo* the calcium activity of Arky-GPe neurons across different motor and disease states. Having characterised the abnormal changes of activity, we then used optogenetic manipulation to test their causal contribution to LID generation. We found that optogenetic reactivation of Arky-GPe neurons during LID reduces hyperkinetic behaviour and promotes normal-like motor behaviour. These results pave the way to understand the complex mechanisms involved in the generation and maintenance of LID.

Keywords: Basal ganglia circuits, Parkinson's disease, levodopa-induced dyskinesia, serotonin, 5-HT_{2A} receptor, external *globus pallidus*, arkypallidal neurons, optogenetic manipulation

RÉSUMÉ

Les circuits des ganglions de la base (GB) sont impliqués dans différentes fonctions allant du contrôle des mouvements aux processus cognitifs/motivationnels. La perte de dopamine (DA) dans ces circuits déclenche la maladie de Parkinson (MP) caractérisée par des déficiences motrices dévastatrices connues sous le nom d'akinésie et de bradykinésie. En plus de la déplétion en DA, les patients atteints de la MP présentent une altération sérotoninergique (5-HT) précoce au niveau des noyaux des GB.

La 5-HT module l'activité des circuits des GB en agissant sur une grande variété de sous-types de récepteurs 5-HT. Parmi eux, le récepteur 5-HT_{2A} est exprimé dans les territoires moteurs et associatifs/limbiques des noyaux GB ainsi que dans la régulation des fonctions motrices, automatiques, exécutives et cognitives. De plus, il a été montré que les récepteurs 5-HT_{2A} pourraient jouer un rôle dans des maladies liées à un dysfonctionnement des GB comme la MP. Cependant, des informations précises sur le rôle des récepteurs 5-HT_{2A} dans ces circuits sont encore manquantes.

Par conséquent, dans la première partie de mon projet de thèse, nous nous sommes intéressés à la contribution de ces récepteurs sur la réponse dynamique des noyaux de sortie des GB aux aires corticales motrice et préfrontale (mPF). Dans le but d'évaluer l'effet de l'activation ou du blocage des récepteurs 5-HT_{2A}, nous avons réalisé des enregistrements extracellulaires *in vivo* sur les neurones latéraux et médians de la substance noire pars reticulata (SNr) combinés à une stimulation électrique du cortex moteur ou préfrontal médian. Les résultats ont montré une dissociation topographique-dépendante dans les effets induits par le TCB-2, un agoniste 5-HT_{2A}. Ce dernier ayant spécifiquement augmenté l'activité des neurones de la SNr médiane et agit sur le traitement de l'information corticale venant du mPF par la voie directe striato-nigrée. Ces résultats fournissent des preuves de la signature spécifique des récepteurs 5-HT_{2A} dans la régulation dynamique des circuits des GB.

Dans la deuxième partie de mon doctorat nous nous sommes intéressés à la dynamique des GB en conditions pathologiques. Au stade précoce de la MP, l'administration du précurseur de la DA, L-DOPA, réduit les symptômes en améliorant l'exécution des mouvements mais déclenche rapidement des mouvements anormaux et involontaires connus sous le nom de dyskinésies induites par la L-DOPA (LID). Les LID sont très invalidantes et réfractaires à tout autre traitement médicamenteux. Il est donc fondamental de comprendre les mécanismes neuronaux qui sous-tendent les LID afin de développer de nouvelles stratégies thérapeutiques. De récentes études ont montré que les LID sont causées par une activité neuronale aberrante dans le striatum, cependant, on ne sait toujours pas comment cette dernière affecte les circuits

des GB. En outre, il est connu que les neurones arkypallidaux du GPe (Arky-GPe) forment directement une boucle négative vers le striatum contrôlant l'inhibition de l'action en conditions normales. Cette activité en conditions pathologiques étant encore inconnue, ce projet a eu pour objectif de caractériser les changements d'activité des Arky-GPe à travers différents stades, état sain, MP et LID. Dans ce travail, nous avons utilisé des méthodes de photométrie par fiber et miniscopie afin de mesurer et suivre in vivo l'activité calcique des neurones cibles. Après avoir caractérisé leurs changements d'activité, nous avons testé leur contribution causale dans la génération des LID. Pour cela nous avons directement manipulé ces neurones grâce à des méthodes d'activation optogénétiques et constaté une diminution de la sévérité des dyskinésies et une restauration d'un comportement moteur pseudo-normal. Ces résultats ouvrent la voie à la compréhension des mécanismes complexes impliqués dans la genèse et le maintien des LID, étape indispensable pour concevoir le développement de nouvelles cibles thérapeutiques.

Mots-clés: Ganglions de la base, Maladie de Parkinson, L-DOPA induisant des dyskinésies, récepteur 5-HT_{2A}, Globus pallidus externe, neurones arkypallidaux, manipulation optogénétiques

RESUMEN

Los circuitos de los ganglios basales (GB) están implicados en diferentes funciones, desde el control del movimiento hasta los procesos cognitivos/motivacionales. La pérdida de dopamina (DA) en estos circuitos desencadena la enfermedad de Parkinson (EP), caracterizada por devastadoras alteraciones motoras conocidas como acinesia y bradicinesia. Además de la depleción de DA, los pacientes con EP presentan alteraciones serotoninérgicas (5-HT) tempranas a nivel de los núcleos de los GB. La 5-HT modula la actividad de los circuitos de los GB actuando sobre varios subtipos de receptores 5-HT. Entre ellos, el receptor 5-HT_{2A} se expresa tanto en territorios motores como en asociativos/límbicos de los núcleos de los GB, estando implicado en la regulación de las funciones motoras, ejecutivas y cognitivas, así como en automatismos. Además, los receptores 5-HT_{2A} también podrían estar implicados en enfermedades relacionadas con la disfunción de los GB como la EP. Sin embargo, se desconoce el papel del receptor 5-HT_{2A} en la regulación dinámica de los circuitos de los GB.

En la primera parte de la tesis, investigamos la contribución específica de los receptores 5-HT_{2A} en la respuesta dinámica del núcleo de salida de los GB a la información cortical motora y prefrontal medial (mPF). Para ello, se realizaron registros uni-extracelulares *in vivo* de las neuronas de la *substantia nigra pars reticulata* (SNr) lateral y medial junto con estimulación eléctrica simultánea de la corteza motora y mPF para evaluar el efecto de la activación/bloqueo de los receptores 5-HT_{2A}. Los resultados mostraron una disociación dependiente de la topografía en los efectos desencadenados por el agonista 5-HT_{2A} TCB-2, que aumentó específicamente la actividad de las neuronas SNr mediales y tuvo una acción preferente sobre el procesamiento de la información mPF a través de la vía directa estriato-nigral. Estos hallazgos muestran la modulación específica de los receptores 5-HT_{2A} en la regulación dinámica de los circuitos de los GB.

La segunda parte de la tesis se centró en el estudio de la dinámica de los GB en condiciones patológicas. En la EP, la administración del precursor levodopa, reduce la sintomatología y mejora la ejecución del movimiento en etapas iniciales, pero rápidamente desencadena movimientos anormales e involuntarios conocidos como discinesias inducidas por levodopa (LID). Las LID son muy debilitantes y refractarias a cualquier tratamiento farmacológico. Por ello, comprender el mecanismo neuronal subyacente a las LID es fundamental para desarrollar nuevas estrategias terapéuticas. Estudios recientes han demostrado que las LID son causadas por una actividad neuronal excesiva en el estriado, pero aún se desconoce cómo dicha actividad estriatal afecta a los circuitos descendentes de los GB, como el globo pálido externo (GPe), para generar las LID. Además, una subpoblación de neuronas del GPe, denominadas neuronas arquipalidales (Arky-GPe), forman directamente un bucle de

retroalimentación negativa con el estriado que controla la inhibición de la acción en condiciones normales. Es importante destacar que la actividad y la contribución de esta vía de supresión de la acción del GPe durante las LID son totalmente desconocidas.

Así, el segundo objetivo de este proyecto fue caracterizar los cambios dinámicos de la actividad de las Arky-GPe en condiciones fisiológicas, EP y LID. En este trabajo, utilizamos métodos ópticos (fotometría de fibra y miniscopio) para monitorizar *in vivo* la actividad del calcio de las neuronas Arky-GPe en diferentes estados motores y de enfermedad. Una vez caracterizado el cambio anormal de actividad, utilizamos la manipulación optogenética para probar su contribución causal a la generación de las LID. La reactivación optogenética de las Arky-GPe durante las LID redujo el comportamiento hiperkinético y promovió el comportamiento motor normal. Estos resultados ayudan a comprender los complejos mecanismos implicados en la generación y el mantenimiento de las LID.

Palabras clave: Circuitos de los Ganglios Basales, enfermedad de Parkinson, discinesias inducidas por levodopa, serotonina, receptor 5-HT_{2A}, *globus pallidus* externo, neuronas arquipalidales, manipulación optogenética

INDEX

INTRODUCTORY NOTES	21
FIGURES INDEX	23
ABBREVIATION LIST	26
1. INTRODUCTION	29
1.1. Basal ganglia	29
1.1.1. Basal Ganglia nuclei	30
1.1.2. Basal Ganglia circuit dynamic	39
1.2. Parkinson's disease	44
1.2.1. History	44
1.2.2. Pathophysiology	44
1.2.3. Clinical features	45
1.2.4. Parkinson's disease treatments	46
1.2.5. Levodopa-induced dyskinesia	48
1.2.6. Animal models	51
1.3. Basal ganglia nuclei in Parkinson's disease and levodopa-induced dyskinesia	55
1.3.1. Basal ganglia nuclei in Parkinson's disease	55
1.3.2. Basal ganglia nuclei in L-DOPA-induced dyskinesia	56
1.4. The serotonergic system in Basal Ganglia	59
1.4.1. The serotonergic system in Parkinson's disease	61
1.4.2. The serotonergic system in levodopa-induced dyskinesia	62
2. HYPOTHESIS AND OBJECTIVES	64
3. STUDY I	66
3.1. Material and methods	67
3.1.1. Animals	67
3.1.2. Pharmacology	67
3.1.3. Electrophysiological procedures	69
3.1.4. Electrophysiological data analysis	72
3.1.5. Statistical analysis	73
3.1.6. Verification of the recording and stimulation sites	74
3.2. Results	76
3.2.1 Modulatory action of 5HT _{2A} receptor on spontaneous and cortically evoked activity of SNr neurons	76
3.2.2 Role of the endogenous 5-HT in the effects triggered by TCB-2	82
3.3. Discussion	87
4. STUDY II	91

4.1. Material and methods	92
4.1.1. Animals	92
4.1.2 Drugs.....	92
4.1.3 Viral vectors.....	93
4.1.4 Stereotaxic surgery.....	94
4.1.5 Behavioural studies	97
4.1.6 Protocols of optogenetic stimulations.....	101
4.1.7 Histological procedures	102
4.1.8 Electrophysiological procedures	103
4.1.9 Calcium imaging procedures	104
4.1.10 Analysis of data	106
4.2 Results.....	108
4.2.1 Characterisation of Arkypallidal activity across healthy and pathological PD conditions.....	108
4.2.2 Causal contribution of Arky-GPe neurons in the genesis of L-DOPA-induced dyskinesia	118
4.3 Discussion	126
4.4 Annex	131
5. CONCLUSIONS	132
6. BIBLIOGRAPHY.....	134

INTRODUCTORY NOTES

The basal ganglia (BG) form a highly organised network that integrates information from several cortical areas, conforming segregated anatomical circuits that process different functional domains, from movement control to cognitive/motivational processes. In a classical view of the BG, the flow of cortical information is transmitted to the different BG nuclei via distinct integration pathways that will be described in the first section of the introduction. Under physiological conditions, the integration of cortical inputs is the result of a complex dynamic that transfers the information in a temporally organised manner within the BG pathways.

Conversely, under pathological conditions, such as in Parkinson's disease (PD), the loss of *substantia nigra pars compacta* (SNc) neurons induces drastic alterations in information transfer, which results in the spatio-temporal disorganisation of cortical information processing across BG circuits leading to disabling motor deficits.

Understanding the dynamical properties of these circuits in functional and dysfunctional BG was the starting point of this PhD project. The thesis was carried out under the joint supervision of Dr. Morera (University of Basque Country, Spain) and Dr. Boraud/ Dr. Mallet (University of Bordeaux, France). Thus, according to the respective host laboratories, two studies were designed, aimed to answer different aspects related to the functionality of BG networks. The Study I, performed in Dr. Morera's lab, focused on the modulatory action of serotonergic 5-HT_{2A} receptor subtype on the dynamic regulation of BG circuits in control conditions. On the other hand, in the Study II, performed in Dr. Boraud/Dr. Mallet's lab, I studied the population dynamics of external *globus pallidus* (GPe) neurons, namely arkyppallidal neurons, under normal and parkinsonian conditions. Therefore, my PhD research aimed to dissect the impact of 5-HT and GPe GABAergic transmissions on the dynamical properties of BG circuits in both normal and pathological conditions. In addition, because long-term administration of levodopa (L-DOPA) as gold standard treatment of PD symptomatology can induce disabling motor complications including abnormal involuntary movements (L-DOPA induced dyskinesia, LID), in the Study II, we also investigated the BG network dynamic during LID.

My PhD project started with the Study I at the University of the Basque Country in June 2019. Initially, the main goal of this study was to investigate the modulatory role exerted by serotonergic 5-HT_{2A} receptors on the dynamic regulation of BG circuits in control, parkinsonian and dyskinetic animals. However, due to the exceptional situation generated by the COVID-19 pandemic, the academic and research activity was suspended (in March 2020) and once

resumed, we decided to continue my training in the Bordeaux laboratory. Although we continued to work on the Study I in Bordeaux, it was only possible to complete the study on control animals. Nevertheless, interesting data were obtained and are currently part of a publication under review in "*The Journal of Neuroscience*". In this study, we provide evidence about the specific and preferential signature of 5-HT_{2A} receptors on the dynamic regulation of BG circuits in physiological conditions.

At the same time, in the Bordeaux laboratory I also started to conduct experiments in the context of the Study II, which I have been working on until the thesis was deposited. In this study, we characterised the role of the GABAergic GPe-striatum transmission in healthy vs. Parkinsonian vs. dyskinetic conditions. Furthermore, we investigated whether the manipulation of this transmission during LID could have a therapeutic potential with a recovery of motor function.

FIGURES INDEX

INTRODUCTION

Figure 1.1. Basal ganglia nuclei and their main connections

Figure 1.2. GPe neuron composition

Figure 1.3. Molecular markers and projection targets of prototypic and arkypallidal neurons

Figure 1.4. Anatomical, molecular and electrophysiological signatures of prototypical neurons

Figure 1.5. Anatomical, molecular and electrophysiological signatures of arkypallidal neurons.

Figure 1.6. Prototypic and arkypallidal functional inputs organization and disynaptic circuit in GPe

Figure 1.7. Activation of arkypallidal neurons is sufficient to reduce locomotion inhibition induced by iMSN stimulation

Figure 1.8. Schematic representation of sensorimotor and medial prefrontal basal ganglia circuits

Figure 1.9. Schematic representation of the cortico-nigral transmission circuits.

Figure 1.10. Schematic illustration of the L-DOPA action mechanism for the treatment of motor symptoms of PD

Figure 1.11. Relationship between LID and L-DOPA plasma concentration

Figure 1.12. Handling of L-DOPA in LID physiopathology

Figure 1.13. Schematic representation of the BG motor circuit in healthy, parkinsonian and dyskinetic states.

Figure 1.14. Rostral raphe nuclei and serotonergic innervation of the Basal Ganglia circuits.

STUDY I

Figure 3.1. Schematic representation of the experimental design

Figure 3.2. Peristimulus time histogram showing the characteristic triphasic response evoked in an SNr neuron after MC or mPFC stimulation

Figure 3.3. Representative coronal brain slices showing the placement of the stimulation and recording electrodes

Figure 3.4. Effect of systemic administration of cumulative doses of the selective 5-HT_{2A} receptor agonist TCB-2 on spontaneous activity of lateral and medial *substantia nigra pars reticulata* neurons

Figure 3.5. Effect of systemic administration of TCB-2 on cortically evoked responses in lateral and medial *substantia nigra pars reticulata* neurons

Figure 3.6. Blockade of the effects of TCB-2 by the previous administration of the selective 5-HT_{2A} receptor antagonist MDL11939 on the spontaneous activity of lateral and medial *substantia nigra pars reticulata* neurons

Figure 3.7. Blockade of the effects of TCB-2 by the previous administration of the selective 5-HT_{2A} receptor antagonist MDL11939 on cortically evoked responses in lateral and medial *substantia nigra pars reticulata* neurons

Figure 3.8. Effects of the systemic administration of a cumulative dose of the non-selective 5-HT antagonist methiothepin on the spontaneous and cortically evoked activity of lateral and medial *substantia nigra pars reticulata* neurons

Figure 3.9. Effect of the administration of the 5-HT synthesis inhibitor pCPA (300 mg/kg/day, i.p 3 days) or the selective 5-HT reuptake inhibitor fluoxetine (10 mg/kg, i.p) on the spontaneous activity of lateral and medial *substantia nigra pars reticulata* neurons

Figure 3.10. Patterns of response evoked in lateral and medial *substantia nigra pars reticulata* neurons by motor or mPF cortex stimulation

Figure 3.11. Effect of the treatment with vehicle, pCPA and fluoxetine on the cortically evoked responses in lateral and medial *substantia nigra pars reticulata* neurons

Figure 3.12. Effect of the systemic administration of cumulative doses of the 5-HT_{2A} receptor agonist TCB-2 on the spontaneous activity and cortically evoked responses of lateral and medial *substantia nigra pars reticulata* neurons from pCPA-treated rats

STUDY II

Figure 4.1. Experimental designs of the three studies developed

Figure 4.2. Behavioural test setup

Figure 4.3. L-DOPA-induced dyskinesia in mice with unilateral 6-OHDA lesion

Figure 4.4. Protocols of optogenetic manipulations

Figure 4.5. Calcium imaging pipeline using Inscopix Data Processing Software

Figure 4.6. Experimental design of locomotor analysis

Figure 4.7. Motor assessment across different physio/pathological states using SNc-lesioned mice.

Figure 4.8. Comparison of calcium transient properties across healthy vs. PD vs. LID conditions.

Figure 4.9. Comparison of calcium photometric signals between the contralateral and the ipsilateral side of the lesion across healthy, PD, and LID conditions.

Figure 4.10. Longitudinal recordings of the calcium transients in Arky-GPe and STR neurons across different health states.

Figure 4.11. In vivo electrophysiological recordings and optotagging strategy in the GPe.

Figure 4.12. Stimulation of Arky-GPe neurons drastically reduces dyskinetic behaviour, in the MFB-lesioned model.

Figure 4.13. Stimulation of Arky-GPe neurons drastically reduces dyskinetic behaviour in the SNc-lesioned model.

Figure 4.14. Validation of the excitatory opsin vs. CTL virus in the behavioural effect.

Figure 4.15. Effect of optogenetic inhibition of Proto-GPe neurons during LID in MFB-lesioned mice.

Figure 4.16. Effect of chemogenetic inhibition of Proto-GPe neurons during LID in MFB-lesioned mice.

Annex 1. Analysis of the impact of Arky-GPe neurons opto-excitation on the motor-state transition in LID mice using an unsupervised classification method.

ABBREVIATION LIST

MPTP	1-methyl-4-phenyl-1,2,3,6-tetrahydropyridine
5-HT	Serotonin or 5-hydroxytryptamine, serotonergic
5-HT_{2A}	5-hydroxytryptamine-2A receptor or serotonin-2A receptor
6-OHDA	6-hydroxydopamine
AIMs	Abnormal Involuntary Movements
ALO	Axial, limb and orolingual
ANOVA	Analysis of the variance
Arky-GPe	Arkypallidal GPe neurons
AUC	Area Under the Curve
BBB	Blood Brain Barrier
BG	Basal Ganglia
ChR2	Channelrhodopsin-2
CONTRA	Contralateral
CV	Coefficient of variation
DA	Dopamine
DBS	Deep Brain Stimulation
DRN	Dorsal Raphe Nucleus
EE	Early Excitation
ECoG	Electrocorticogram
EP	<i>Entopeduncular nucleus</i>

GABA	Gamma-aminobutyric acid
Glu	Glutamate
GPe	External (segment of the) <i>Globus Pallidus</i>
GPI	Internal (segment of the) <i>Globus Pallidus</i>
I	Inhibition
IPSI	Ipsilateral
i.p.	Intraperitoneal
i.v.	Intravenous
L-DOPA	Levodopa or 3,4-Dihydroxy-L-phenylalanine methyl ester
LE	Late Excitation
LGE	Lateral ganglionic eminence
LHb	Lateral habenula
LID	L-DOPA-induced dyskinesia
LFP	Local field potential
MC	Motor cortex
mPF	Medial prefrontal
mPFC	Medial prefrontal cortex
MSNs	Medium Spiny Neurons
NA	Noradrenergic
PBS	Phosphate saline buffer
PD	Parkinson's disease
PV+	Parvalbumin-positive
Proto-GPe	Prototypical GPe neurons

SERT	Serotonin transporter
SM	Sensorimotor
SN	<i>Substantia nigra</i>
SNc	<i>Substantia nigra pars compacta</i>
SNr	<i>Substantia nigra pars reticulata</i>
SSRI	Serotonin selective reuptake inhibitor
STN	<i>Subthalamic nucleus</i>
STR	Striatum
TH	Tyrosine hydroxylase
VGAT	Vesicular transporter for GABA

1. INTRODUCTION

1.1. Basal ganglia

The basal ganglia (BG) are a highly organised functional network composed of different subcortical structures and circuits that connect the cortex with the thalamus, forming different cortico-BG-thalamo-cortical loops (Figure 1.1). The BG are primarily engaged in motor functions, together with a wider variety of roles such as motor learning, executive functions, behaviour and emotions (Haber, 2003; Middleton & Strick, 2000). Therefore, disturbances in this complex network could lead to a wide range of behavioural disorders, for instance Parkinson's disease (PD) (Tremblay et al., 2015).

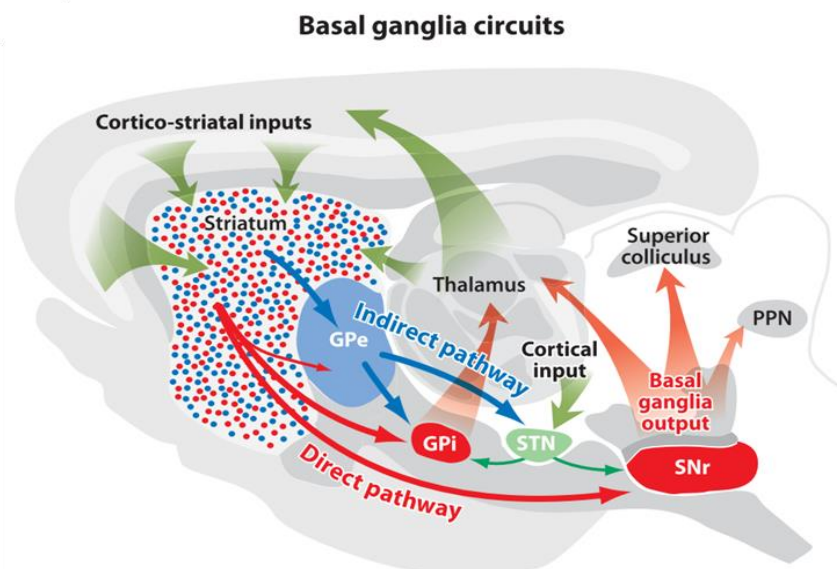


Figure 1.1. Basal ganglia nuclei and their main connections. Scheme representing the main connections of the BG network in a sagittal section of the rodent brain. In the striatum, medium spiny neurons from the direct pathway (dMSNs) are represented in red and medium spiny neurons from the indirect pathway (iMSNs) in blue. BG output pathways arise from the GABAergic neurons in the internal *globus pallidus* and the *substantia nigra pars reticulata*. GPe: external *Globus Pallidus*; GPi: internal *Globus pallidus*; STN: *Subthalamic nucleus*; SNr: *Substantia nigra pars compacta*; PPN: *Pedunculopontine nucleus*.

1.1.1. Basal Ganglia nuclei

The BG are a set of nuclei including the striatum (STR), the external and internal *globus pallidus* (GPe, GPi or entopeduncular nucleus (EP) in rodents), the *substantia nigra* (*pars compacta*, SNc and *pars reticulata*, SNr) and the subthalamic nucleus (STN). These structures are explained in detail in the following sections.

1.1.1.1. Striatum

The STR is considered the main input nucleus of the BG responsible for integrating information from the entire cerebral cortex. It is composed of 95% of GABAergic neurons called medial spiny neurons (MSNs) or spiny projection neurons (SPN). Despite their morphological similarities, MSNs can be divided into two subpopulations based on their molecular profile and axonal projection patterns. Approximately half of MSNs project to the SNr or EP forming the so-called 'direct' or striato-nigral pathway (**dMSNs**), while the other half projects to the GP establishing the so-called 'indirect' or striato-pallidal pathway (**iMSNs**) (Albin et al., 1989). The dMSNs express dynorphin (or substantia P) and dopaminergic D₁ receptors, while iMSNs express enkephalin and dopaminergic D₂ receptors (Gerfen et al., 1990). Striatal dMSNs are activated by dopamine (DA), while iMSNs are inhibited (Gerfen & Surmeier, 2011). *In vivo*, MSNs are quite silent and need an excitatory glutamatergic synaptic input from the cortex to fire action potentials.

The STR also has a diverse array of interneurons representing 5% of all striatal neurons. According to the distinct electrophysiological, molecular and synaptic profiles, these interneurons can be classified as cholinergic or GABAergic, although they might release other signalling molecules as well, like glutamate (Higley et al., 2011). Cholinergic interneurons (**ChaT+** to Choline acetyltransferase) represent 1-3% of the total STR neuronal population. Also known as tonically active interneurons, they extend their axonal arborisations throughout the whole STR playing a key role in the control of striatal function (Bonsi et al., 2011; Tepper et al., 2018; Zhou et al., 2002). GABAergic interneurons can be further classified as fast-spiking, low-threshold, calretinin-expressing, tyrosine hydroxylase (TH)-expressing, neurogliaform, fast adapting or spontaneous active bursty interneurons (Faust et al., 2015; Ibáñez-Sandoval et al., 2010, 2011; Kawaguchi et al., 1995; Tepper et al., 2018).

In addition to cortical inputs, the STR receives serotonergic (5-HT) projections from the *dorsal raphe nucleus* (DRN) (Huang et al., 2019; Steinbusch, 1981) and discrete noradrenergic innervation from the *locus coeruleus* (Fitoussi et al., 2013).

1.1.1.2. External Globus Pallidus

The GPe is a GABAergic nucleus, and a key component of the indirect pathway in cortico-BG circuits. The GPe has long been considered as a simple relay between the STR and the STN (Hitoshi Kita et al., 1999; Parent & Hazrati, 1995). However, recent findings highlight the molecular and functional complexity of the GPe and identify different neuronal subpopulations with distinct anatomical, embryonic origin, structural, behavioural and molecular properties. We will discuss these differences throughout this section.

In this line, three GPe neuron subtypes can be distinguished: cholinergic neurons (ChaT+) and GABAergic prototypic and arkypallidal neurons (Figure 1.2) (Dodson, Larvin, Duffell, et al., 2015; Fujiyama et al., 2015; Mallet et al., 2012; Mastro et al., 2014; Oh et al., 2017; Saunders et al., 2015).

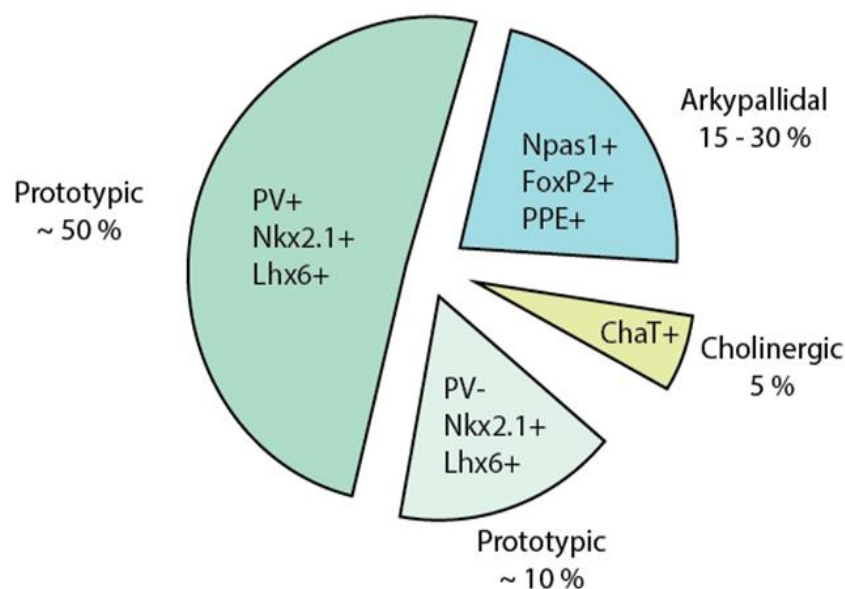


Figure 1.2. GPe neuron composition. Three subtypes of neurons were identified based on their molecular signature, electrophysiological characteristics and projection patterns. Inside the slice, molecular markers were specified. The area of each marker represents the approximate percentage of each subpopulation. FoxP2+, Forkhead box protein P2-positive; Lhx6+, LIM homeobox 6-positive; Nkx2.1+, Nk2 homeobox 1-positive; Npas1+, Neuronal PAS domain protein 1-positive; ChaT+, Choline acetyltransferase-positive .

ChaT+ neurons correspond to approximately 5% of GPe neurons and express cholinergic and GABAergic markers suggesting a co-release of GABA by these neurons (Saunders et al., 2015). Although close to the nucleus basalis of Meynert, ChaT+ neurons are present in the ventro-caudal region of the GPe (Herna et al., 2015) and receive input from both iMSN and dMSN forming a distinct group of GPe neurons.

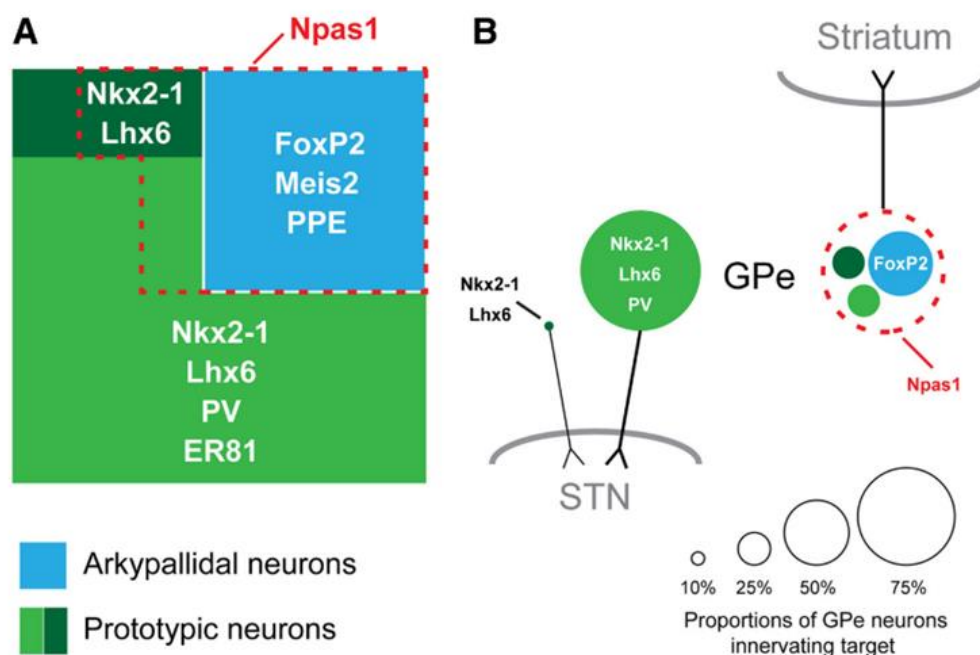


Figure 1.3. Molecular markers and projection targets of prototypic and arkypallidal neurons. A, Summary of the two major GABAergic cell types in the rat GPe. Arkypallidal neurons (blue) and prototypic neurons (light and dark greens) are represented in respect to all GABAergic GPe neurons. The molecular markers seen in both subtypes are also indicated. **B,** Diagram of the major GPe cell types innervating the STN (left) or dorsal striatum (right). Whereas the majority of prototypic neurons innervate the STN, arkypallidal neurons seem to innervate the STR. Image taken from Abdi et al., 2015.

Prototypic (Proto-GPe) neurons derive from the medial ganglionic eminence (MGE) and represent 70% of the GPe neurons that express the transcription factor Nkx2.1 (Figure 1.3). Proto-GPe neurons show a tonic and regular fast-spiking discharge, independent of cortical activity (Figure 1.4) (Abdi et al., 2015; Mallet et al., 2016). In addition to Nkx2.1, a large population of Proto-GPe neurons ($\frac{3}{4}$ approximately) are also parvalbumin-positive (PV+) and massively constitute the pallido-subthalamic pathway innervating the STN (Abdi et al., 2015). However, the percentage of PV+ Proto-GPe neurons varies across studies (Herna et al., 2015) and it seems that a PV-/Lhx6+ constitute a second subpopulation of Proto-GPe neurons (Mastro et al., 2014). Besides, Proto-PV+, which represent ~50% of the GP neurons, provide

the major arborisation to the SNr/SNc and EP (Fujiyama et al., 2015; Saunders et al., 2016). Synapses between Proto-GPe neurons and other BG neurons are formed from proximal dendrites or cellular bodies that place this population as a hub to control activity in the BG (Bolam et al. 2009; Smith, Shink, and Sidibe 1998). In this line, Mastro and colleagues showed that in DA depleted mice, movement can be persistently rescued by manipulations of PV+ GPe neurons, therefore highlighting the functional importance of this cell-type, and potentially of the GPe-SNr pathway (Mastro et al., 2017).

Moreover, it has been shown that a small population of Proto-GPe neurons also projects back to the STR and selectively contacts interneurons (Bevan, 1998). The physiological impact of these pallido-striatal projections is still unknown, however it has been proposed to play a role in the selection/execution of appropriate striatal programs (Gage et al., 2010).

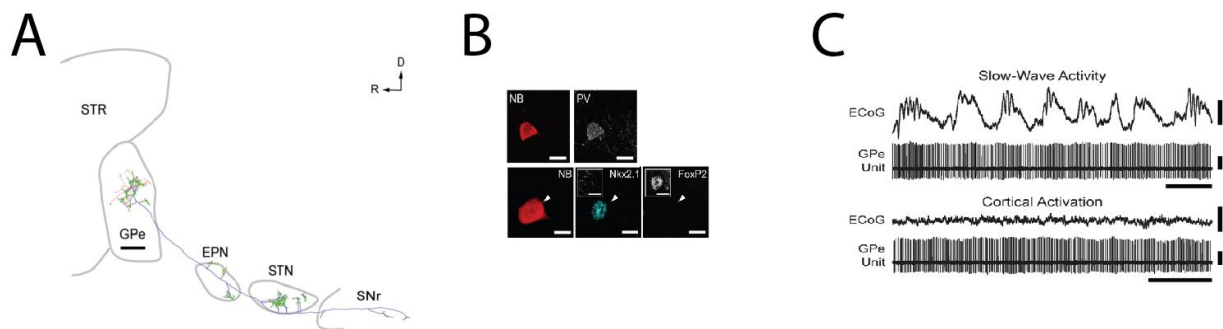


Figure 1.4. Anatomical, molecular and electrophysiological signatures of prototypical neurons. **A**, Full reconstruction of a Proto-GPe neuron (soma and dendrites are in red, the axon in blue and each varicosity is in green). This Proto-GPe sends an axon to downstream BG: entopeduncular nucleus (EPN) and subthalamic nucleus (STN). It also sends a sparse axon up to the striatum (STR). **B**, Images showing the molecular signature of Proto-GPe. Red: the neurobiotin (NB); Grey: Parvalbumin (PV); Blue: Nkx2.1 and the absence of the FoxP2 marker. **C**, Example of raw recordings in the natural slow-wave sleep (top) and awake state (bottom). ECoG: electrocorticogram. (A and B taken from Mallet et al., 2012, C taken from Abdi et al., 2015)

Arkypallidal (Arky-GPe) neurons derive from the lateral ganglionic eminence (LGE) and represent between 15 - 30 % of GPe neurons. Arky-GPe neurons can be distinguished by the specific expression of preproenkephalin (PPE) and the transcription factor FoxP2 (Azzedine Abdi et al., 2015; Dodson, Larvin, Butt, et al., 2015) (Figure 1.3). Although all Arky-GPe neurons co-express Npas1, it is not a specific marker of this subpopulation due to its expression by some Proto-GPe neurons (Azzedine Abdi et al., 2015; Herna et al., 2015). Arky-GPe neurons display a low and irregular firing discharge highly dependent on cortical activity (Azzedine Abdi et al., 2015), with tonic firing during cortical activation state and becoming silent

at slow wave activity transition (Figure 1.5). Differences in electrical signatures between Proto-GPe and Arky-GPe neurons, are a way to distinguish them with a high confidence, in particular in freely-moving animals (Mallet et al., 2016). Moreover, contrary to Proto-GPe neurons, all the Arky-GPe neurons massively innervate all types of striatal neurons (interneurons and MSNs) (10 fold more) with an axonal length considerably longer than those of Proto-GPe neurons (Figure 1.5) (Bevan, 1998; Mallet et al., 2012). Indeed, one Arky-GPe neuron could form more than 10.000 boutons in the STR which is, at a single cell level, the largest extrinsic source of GABAergic inputs to STR ever discovered (Mallet et al., 2012). This suggests their direct control of striatal microcircuits.

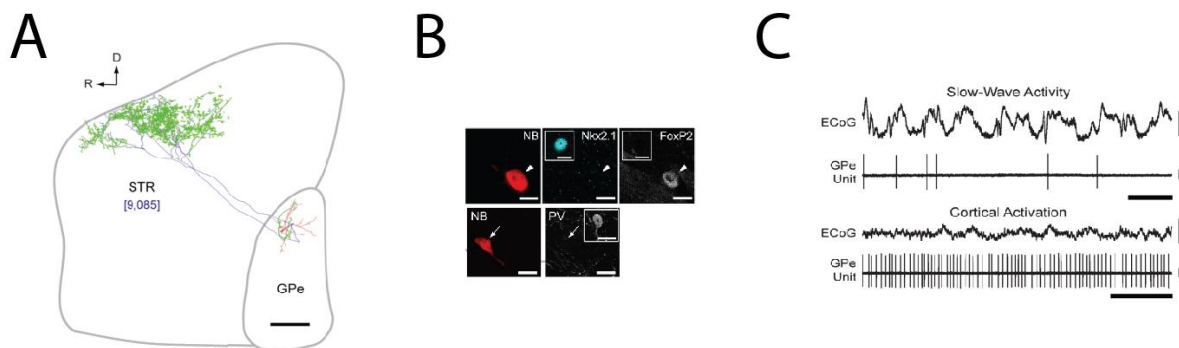


Figure 1.5. Anatomical, molecular and electrophysiological signatures of arypallidal neurons.

A, Full reconstruction of an Arky-GPe neuron (soma and dendrites are in red, axon in blue and each varicosity is in green). The dense striatal axon covers a large area in the striatum (STR). **B**, Images showing the molecular signature of Arky-GPe neurons. Red: the neurobiotin (NB); Grey: Parvalbumin (PV); Blue: Nkx2.1. FoxP2 is the only marker expressed in this neuron. **C**, Example of raw recordings in the natural slow-wave sleep (top) and awake state (bottom). ECoG: electrocorticogram. (A and B taken from Mallet et al., 2012, C taken from Abdi et al., 2015)

In return, Arky-GPe neurons receive inputs from the STN, the dMSN and iMSN and from Proto-GPe neurons in a non-reciprocal manner (Ketzel & Silberberg, 2021). Recently, it has been found that the inputs from the STN differ in terms of impact issues for both Arky and Proto-GPe neurons. Indeed, the opto-activation of STN induces an excitation of Proto-GPe neurons, while Arky-GPe neurons are being inhibited (Crompe et al., 2020). Regarding inputs from the iMSNs, a study using similar optogenetic methods shows that the opto-activation of iMSNs induces a strong inhibition of Proto-GPe neurons and an excitation of both Arky-GPe and STN neurons (Aristieta et al., 2021). In the same study, they elucidate the source of excitatory

responses observed in Arky-GPe neurons and showed that it came from a disinhibition from the collateral axon of Proto-GPe neurons (Figure 1.6). All the results obtained in this study demonstrate a new disynaptic circuit within the GPe, in which Proto-GPe neurons act as a relay between STR or STN inputs and Arky-GPe neurons.

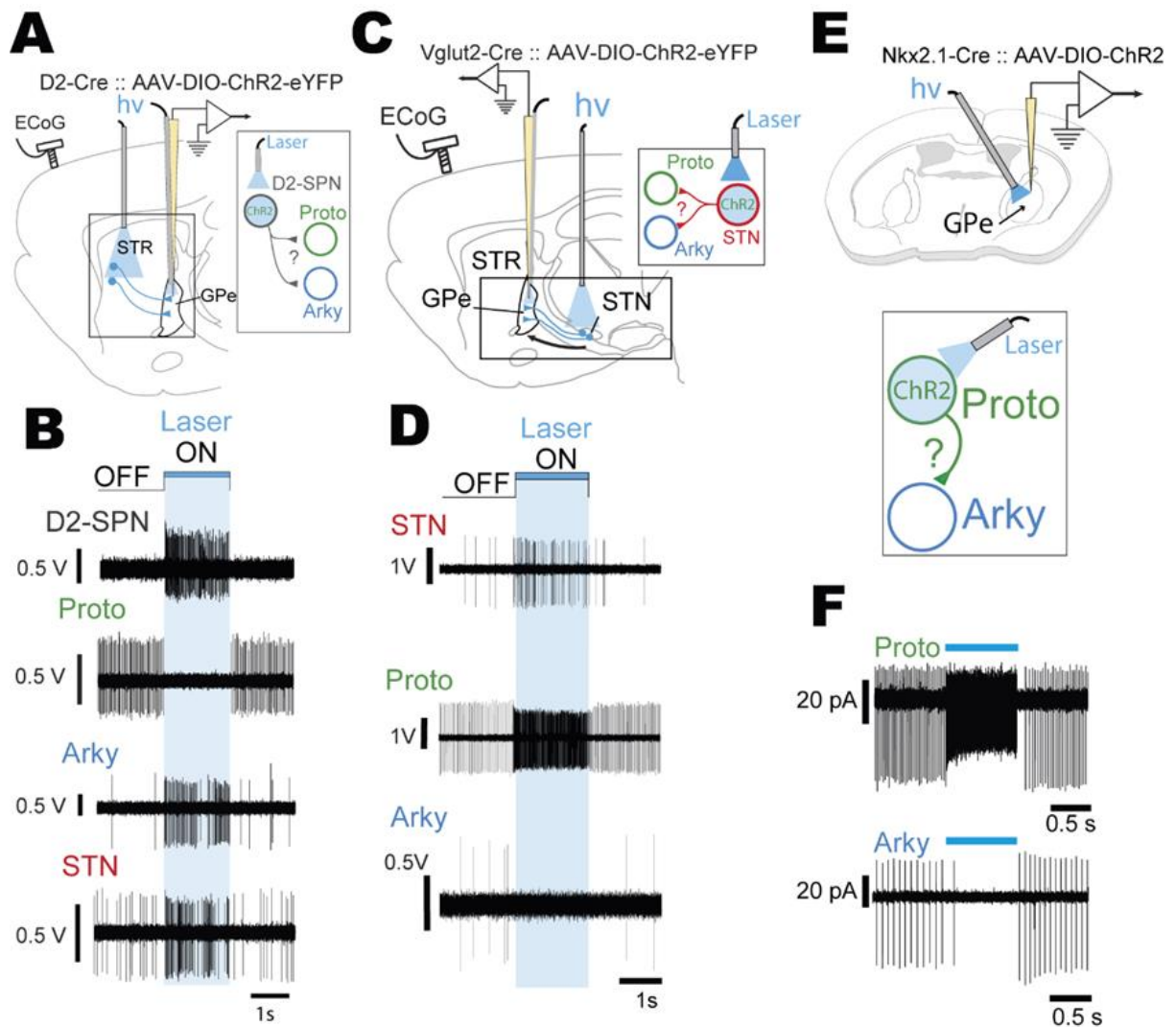


Figure 1.6. Prototypic and arkypallidal functional input organisation and disynaptic circuit in GPe. **A**, Schematic of the experimental design in D2-Cre mice injected with AAV-DIO-ChR2-eYFP in the striatum (STR). **B**, Representative examples of iMSN (D2-SPN) opto-excitation on the *in vivo* firing activity of identified iMSN (D2-SPN), Proto-GPe, Arky-GPe, and STN neurons. **C**, Schematic of the experimental design in Vglut2-Cre mice injected with AAV-DIO-ChR2-eYFP in the STN and recorded in the GPe. **D**, Representative examples of *in vivo* juxtacellular labeled STN, Proto-GPe, and Arky-GPe neurons showing the effect of STN opto-activation on their firing activities. **E**, Schematic of the *ex vivo* experiments using Nkx2.1-Cre mice injected with an AAV-DIO-ChR2-mCherry to study the effect of prototypic axon collaterals onto Arky-GPe neurons. **F**, Typical cell-attached activity of identified Proto-GPe (top) and Arky-GPe neurons (bottom) during OFF and ON epochs of laser stimulation (taken from Aristieta et al., 2021).

Importantly, since previous work has highlighted the role of Arky-GPe neurons in action cancelation (Mallet et al., 2016), Aristieta et al., also investigated if the increased activity of Arky-GPe neurons in response to iMSN opto-excitation played a role in the inhibition of movements classically observed after such stimulation. To test this, they trained mice to run on a treadmill and then used optogenetic tools to specifically activate iMSNs or Arky-GPe neurons during locomotion (Figure 1.7A). They showed that the activation of Arky-GPe neurons induced a strong suppression of locomotion (Figure 1.7D). Moreover, they showed that this effect by itself could account for the inhibitory response observed after the inhibition of iMSN (Figure 1.7B,C) (Aristieta et al., 2021).

These novel findings are changing the “classic” view of BG circuits, highlighting the putative importance of Arky-GPe neurons to form a novel “cancel” pathway that provides the animal with a mechanism to interrupt imminent actions independently from the traditional indirect “No Go” pathway.

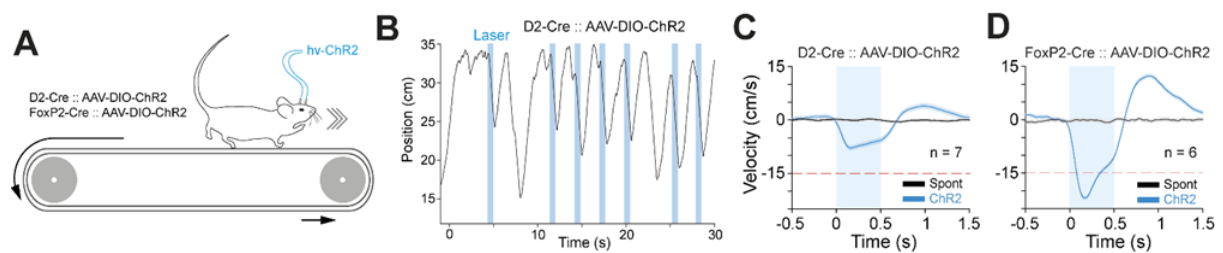


Figure 1.7: Activation of arypallidal neurons is sufficient to reduce locomotion inhibition induced by iMSNs stimulation. **A**, Schematic of the mice locomotion experiments using a motorised treadmill and online optogenetic control. **B**, Raw example of 30-s locomotion bouts in D2-Cre::AAV-ChR2 mice receiving blue light stimulation (500 ms long) at random times. **C-D**, Average velocity induced by the light stimulation (blue) or during spontaneous locomotion (black) in D2-Cre::AAV-ChR2 (**C**), or FoxP2-Cre::AAV-ChR2 (**D**) (taken from Aristieta et al. 2021).

1.1.1.3. Subthalamic nucleus

The STN is the only glutamatergic nucleus of the BG and is considered to be one of the main regulators of motor function. It plays a fundamental role within BG circuitry, being the second major gateway (Parent & Hazrati, 1997). The primate STN is subdivided into several areas, one directly related to motor tasks and others to emotional and cognitive functions (Haynes & Haber, 2013). The STN receives inputs from the GPe but also from other regions such as the

cortex, the thalamus or the SNc (Hammond et al., 2007) and sends projection to all proximal parts of BG nuclei (Bolam et al., 2009). For instance, electrical stimulation of STN induces excitatory responses in GP, SNr and EP neurons (Ammari et al., 2010). Indeed, the STN receives information from the sensorimotor cortex and the STR (Parent & Hazrati, 1995), but also receives 5-HT input, mainly from the DRN, that clearly modulates its neuronal activity (Di Matteo et al., 2008a). In particular, STN neuron excitation can drive SNr GABA neurons into burst firing, which may contribute to PD motor symptoms emergence and 5-HT modulation at the cell body in the STN or axon terminal in the SNr is one potential mechanism to explain this (Ding et al., 2013). In contrast, STN lesion and functional inhibition are able to partially revert the aberrant oscillatory firing and normalise the SNr firing pattern in animal models and PD patients (Murer et al., 1997; Tseng et al., 2001). However, STN-DBS can induce dyskinesia in both rodent models of PD and PD patients (Benabid et al., 2009; Oueslati et al., 2007).

1.1.1.4. Substantia nigra

Anatomically and functionally, the *substantia nigra* is composed of two main regions. The dorsal part contains DA neurons, called “*pars compacta*” (SNc), while the ventral part contains mainly GABAergic neurons, called “*pars reticulata*” (SNr).

The **SNc** is one of the most important DA nuclei in the central nervous system. DA neurons contain the DA precursor neuromelanin, a pigment that produces black colour seen in freshly extracted human brains. DA neurons exhibit slow firing rate *in vivo*, with a long duration action potential (around 2.5 ms) and a low frequency (1-4 Hz). In addition, they become bursty with movement onset, which proves their implication as a motor control ingredient (Dodson et al., 2016). The SNc receives GABAergic inputs from the STR, the GPe and the SNr, but also glutamatergic inputs from the STN, the cortex and the pedunculo pontine nucleus (PPN) (Watabe-Uchida et al., 2012). Axons from DA neurons provide rich innervation of the distant striatal complex with a ratio of one SNc neuron innervating 1mm³ of striatal tissue with a length of ~50 cm (Matsuda et al., 2009). Finally, it is important to mention that collaterals of the GABAergic SNr neurons have also been reported to affect the activity of DA SNc neurons (Tepper et al., 1995), which constitutes an ultra-short inhibitory pathway.

The **SNr** is the principal BG output nucleus in rodents. Although mainly composed of GABAergic neurons, discrete clusters of DA neurons can be found in its caudal-medial region (González-Hernández & Rodríguez, 2000) for a respective number of 30.000 to 7.000. Most GABAergic neurons express glutamic acid decarboxylase (GAD) and express PV. However, recent publications have shown that PV and GAD₂ are preferentially expressed in a distinct

SNr GABAergic population (Liu et al., 2020). Also, Rizzi and colleagues divided the SNr into two subpopulations of neurons, containing either vesicular transporter for GABA (VGAT) or PV (Rizzi & Tan, 2019). Interestingly, by using optogenetic manipulations of these two neuronal subtypes and employing a series of motor tests, these authors revealed that VGAT and PV SNr neurons govern different aspects of motor behaviour.

In awake rodents, SNr GABAergic neurons spontaneously discharge at very high frequencies (25-30 Hz), with a spike of short duration (~ 1 ms) (DeLong et al., 1983). The SNr receives inputs from different neurotransmitter sources: GABAergic from the STR via dMSNs (Gerfen et al., 1990) and the GPe, glutamatergic from the STN (Kita & Kitai, 1987), cholinergic from the PPN, DA from the SNc (Di Giovanni et al., 2009) and 5-HT from the DRN (Corvaja et al., 1993). Regarding all these inputs, receptor identification has been done and several DA (D₁, D₄ and D₅), glutamatergic (AMPA, NMDA, kainate), GABAergic, cholinergic or 5-HT (5-HT_{1A/1B/1D}, 5-HT_{2C}, 5-HT_{2A}, 5-HT₄, 5-HT₇) receptors were found (Chatha et al., 2000; Di Matteo et al., 2008).

For a long time, the motor part of the thalamus was considered the main target of SNr GABAergic neurons, where axons form synapses on the proximal dendrites and soma of relay neurons in the thalamus and the superior colliculus (Deniau et al., 2007; Kha et al., 2001; Zhou & Lee, 2011). However, McElvain and colleagues recently reported that the SNr is in reality projecting to an unexpectedly large number of targets. Using genetically restricted tracing virus, they highlighted 42 brain regions receiving input from the SNr. Among them, were 3 nuclei of BG (GPi, STN, SNc), 10 nuclei from the large target of the brainstem, 17 from small nuclei of the premotor brainstem and, 12 nuclei from the diencephalon (McElvain et al., 2021). Interestingly, these findings provide new thinking about BG output related to the motor system, and refine the closed-loop architecture of BG-thalamo-cortical circuit overlap.

1.1.1.5. Entopeduncular Nucleus

The EP, which is homologous to the internal segment of the GPi in primates, is one of the two BG output nuclei. Studies on the EP are limited compared with those on the SNr, however it is known that the EP is not only a GABA-releasing structure but also contains both glutamatergic and GABAergic neurons. More precisely, molecular studies show three different types of neurons: the somatostatin-positive neurons (SOM+) which project to the Lateral Habenula (LHb) and represent two fourths of the global population; the PV+ neurons which innervate the motor thalamus for one fourth of the global population, and the last quarter being SOM and PV negative neurons (Wallace et al., 2017). SOM+ and PV+ act as motor components playing a

role in motor outcome and motor program selection, respectively. Like the SNr, the EP expresses different types of receptors, such as DA (D_{1-5}) (Lavian et al., 2017), glutamatergic (AMPA and NMDA), cholinergic and 5-HT (5-HT_{1A/1B/1D}, 5-HT_{2A/2C}) (Di Matteo et al., 2008), and it receives projections from the STN, the prefrontal cortex, the GPe and the STR.

1.1.2. Basal Ganglia circuit dynamic

BG nuclei provide the substrate for a complex network that links cortex and thalamus, creating the known cortico-BG-thalamo-cortical loops or circuits. Almost the entire cortex projects to the STR following an anatomo-functional organisation, thus establishing functional subdivisions of this nucleus, depending on the cortical areas innervating that region. Recently, Foster and colleagues identified a novel cortico-BG projection and 6 parallel cortico-BG-thalamic subnetworks (Foster et al., 2021). Moreover, this apparent anatomo-functional compartmentalisation is not exclusive to the STR, as it is conserved throughout the BG nuclei. This suggests the existence of parallel and closed cortico-BG circuits through which specific functional information flows back to the cortex, after being processed within the BG nuclei. In 1990, Alexander and colleagues proposed the classical view of BG circuits in non-human primates, including five functionally distinct parallel loops (Alexander & Crutcher, 1990). Later, evidence suggested the involvement of associative BG territories in motor behaviour (Everitt et al., 2008; Sawada et al., 2014), thus opening a gateway in these ‘closed’ cortico-BG circuits for the information exchange between functionally distinct circuits.

Nowadays, it is generally accepted to group these circuits into three functional domains (Tremblay et al., 2015): (1) ‘motor’ and ‘oculomotor’ circuits fall into the sensorimotor (SM) domain, including premotor, motor and somatosensory cortices; (2) the ‘dorsolateral prefrontal’ and ‘lateral orbitofrontal’ circuits belong to the associative domain and (3) the ‘anterior cingulate’ circuit pertains to the limbic domain. In rodents, a distinction can be made between the **SM circuits**, that would belong to the SM domain, and the **medial prefrontal (mPF) circuits**, which would represent a mixed ‘associative/limbic’ domain (Aliane et al., 2009; Beyeler et al., 2010).

In a simplified way, cortical information through the SM and mPF BG circuits is transmitted to the output structures (i.e., SNr and EP) of the BG through three pathways: the hyperdirect trans-subthalamic pathway (cortex-STN-SNr), the direct (cortex-striatal dMSNs-SNr) and indirect trans-striatal pathways (cortex-striatal iMSNs-GPe-STN-SNr) (Albin et al., 1989; Maurice et al., 1999; Nambu et al., 2002). However, SM and mPF circuits are anatomically segregated and contact different territories: SM circuits through all the lateral parts of the

nuclei, while mPF circuits target the medial part of the nuclei (Figure 1.8). The way these pathways are constituted set the neural substrates for the functioning of BG circuits.

In addition to these classical three pathways, additional connections between BG nuclei have been described over the years, such as GPe-SNr, the reciprocally connected GPe-STN loop (Bevan et al., 2002), the GPe-STR pathway (Asier Aristieta et al., 2021; Mallet et al., 2012, 2016) and bridging collaterals from dMSNs to the GPe (Cazorla et al., 2014; Kawaguchi et al., 1995; Ketzef & Silberberg, 2021), from the STN to the STR (Dautan et al., 2020; Koshimizu et al., 2013), and from the cortex to the GPe (Abecassis et al., 2019; Karube et al., 2019).

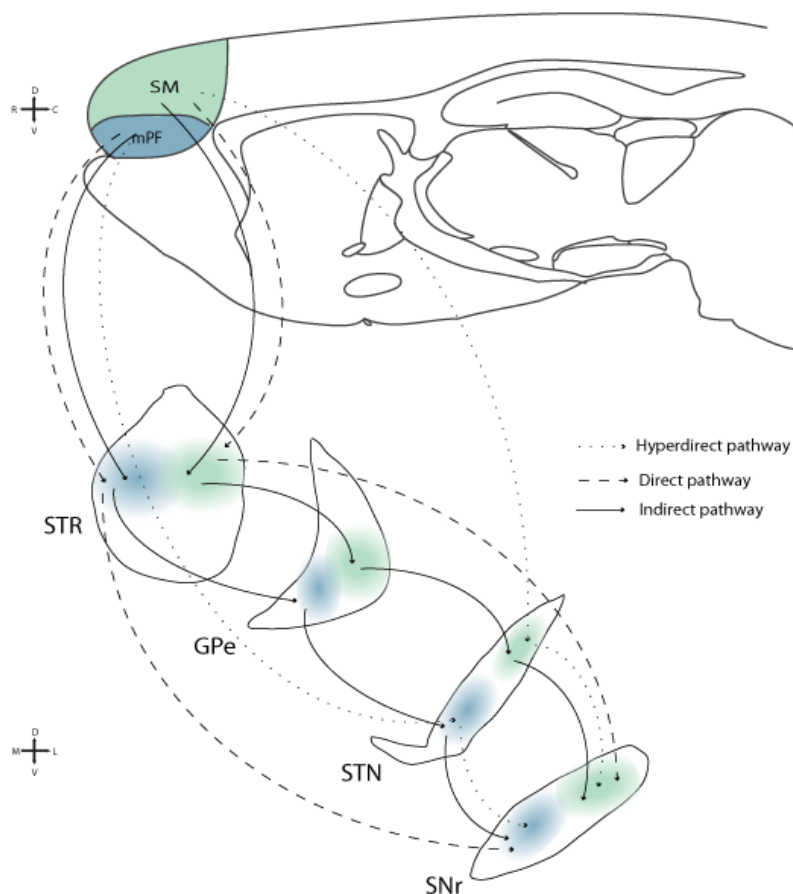


Figure 1.8. Schematic representation of sensorimotor (SM, green) and medial prefrontal (mPF, blue) basal ganglia (BG) circuits. These circuits convey cortical information to the BG output nuclei through three principal pathways: the hyperdirect (cortex-STN-SNr, dotted line); the direct (cortex-striatum-SNr, dashed line) and the indirect pathways (cortex-striatum-GP-STN-SNr, solid line). However, SM and mPF BG circuits are anatomically segregated. While SM circuits course through the lateral parts of the BG nuclei, the mPF circuits occupy the medial parts of these nuclei. DL/DM striatum, dorsolateral and dorsomedial striatum; GP, *globus pallidus*; mPFC, medial prefrontal cortex; MC, motor cortex; SNr, *substantia nigra pars reticulata*; STN, subthalamic nucleus.

In both SM and mPF circuits, a specific spatio-temporal organisation of the trans-striatal and trans-subthalamic pathways allows the indirect and hyperdirect pathways to control the

disinhibitory process through the direct pathway. This spatio-temporal organisation can be analysed by recording cortically evoked responses of single SNr neurons. Typically, cortical stimulation evoked characteristic triphasic responses in SNr neurons, consisting in different combinations of an early excitation (EE), an inhibition (I) and/or a late excitation (LE). As illustrated in Figure 1.9, EE is attributable to the activation of the “hyperdirect” cortico-subthalamo-nigral pathway, I to the activation of the “direct” cortico-striato-nigral pathway, and LE to the activation of the “indirect” cortico-striato-pallido-subthalamo-nigral pathway (Maurice et al., 1999).

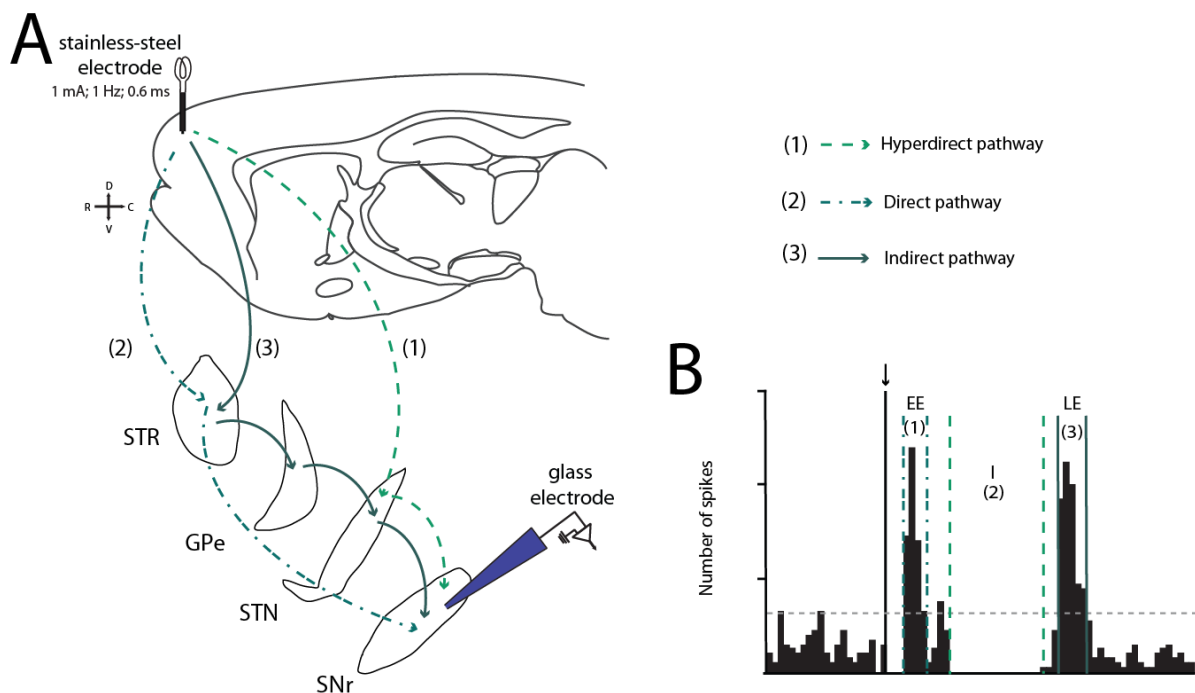


Figure 1.9. Schematic representation of the cortico-nigral transmission circuits. **A**, Schematic sagittal sections of the rat brain and coronal section of different BG nuclei showing their involvement in the different pathways that constitute BG circuits. Cortical information is transferred through the hyperdirect (1) (cortex-STN-SNr, dashed line), direct (2) (cortex-STR-SNr, dashed/dotted line) and indirect (cortex-STR-GPe-STN-SNr, solid line) pathways. **B**, Peristimulus histograms reflecting the response produced by cortical stimulation through each pathway. Arrow indicates cortical stimulus application. EE: Early Excitation, I: Inhibition, LE: Late Excitation.

As the name suggests, SM circuits process SM information provided by the motor and somatosensory cortices. These circuits are involved in modulating motor and sensory cortices in order to control motor output, allowing precise movement execution, learning motor sequences, and their correct expression (Gremel & Costa, 2013; Jin et al., 2014; Phillips et al., 1993). According to the classical functioning model of the BG, the direct and indirect pathways play opposite roles in movement control (Albin et al., 1989). This model predicts that activation

of dMSNs by cortical projection neurons, leads to the inhibition of BG output nuclei, decreasing the GABAergic inhibitory drive of these nuclei onto the thalamus, which in turn, increases the excitatory thalamo-cortical pathway, leading to excitation of the motor cortex and ultimately, movement facilitation. On the other hand, activation of iMSNs by cortical excitatory inputs reduces GPe activity, leading to STN disinhibition, and increases STN glutamatergic input onto the BG output nuclei. This would end up inhibiting thalamic neurons, thus reducing excitatory input onto the motor cortex, and promoting movement suppression. In studies using optogenetic approaches which enable selective activation of either dMSNs or iMSNs, evidence shows that activation of dMSNs inhibits the spontaneous firing rate of GABA projection SNr neurons and increases the locomotion, whereas activation of iMSNs has the opposite effect (Freeze et al., 2013; Kravitz et al., 2010). These results revealing a pathway-specific regulation of motor function confirmed the classical model of BG.

Theoretically, activation of STN neurons in the hyperdirect pathway by cortical inputs would increase excitatory drive onto the BG output nuclei, resulting in reduced thalamo-cortical input, inducing movement suppression. In agreement with this, ablation of this pathway induces hyperactivity in rodents, probably by increasing thalamo-cortical input (Koketsu et al., 2021). The specific role of this pathway in movement execution has been hypothesised to be the inhibition of competing motor programs, thus contributing to correct expression of motor patterns (Nambu et al., 2002). A similar role has been proposed for the indirect pathway in the inhibition of competing motor programs, while the direct pathway would be involved in selecting the desired motor programs (Mink, 2003). In line with this, dMSNs and iMSNs are active during the initiation and termination of action sequences, with mainly dMSNs being activated during sustained motor activity. Thus, revealing that balanced activity between both pathways is needed for correct motor program selection (Cui et al., 2013; Jin et al., 2014).

On the other hand, mPF circuits process information coming from mPF cortical areas (i.e., anterior cingulate, prelimbic and infralimbic cortices), and are involved in 'associative/limbic' aspects of behaviour like goal-directed and drug-seeking behaviours, and in the evaluation and revaluation of outcome values (Balleine & O'Doherty, 2010; Gremel & Costa, 2013; Nonomura et al., 2018). Although their behavioural correlates are not well understood, the activation of the pathways constituting these circuits would provoke physiological responses in the BG nuclei similar to those described for the SM circuits. Similar pathway-specificity is seen in the dorsomedial STR where dMSNs code positive outcomes, and iMSNs code for negative outcomes, and switch in action selection (Nonomura et al., 2018). Similarly, accumbal iMSNs are required for flexible learning (Yawata et al., 2012).

Abnormal functionality of the BG circuits is linked to several disorders. Indeed, dysfunction within the SM circuits is associated with movement disorders, such as PD.

1.2. Parkinson's disease

Parkinson's disease (PD) is the most common neurodegenerative disorder after Alzheimer's Disease, affecting 1-2% of the population over 65 years old (Brakedal et al., 2022; Tysnes & Storstein, 2017) and its prevalence is rapidly increasing as the population ages.

PD is likely a result of multiple factors: aging, genetic predispositions, and environmental risk factors. Advanced age is considered the main risk factor for PD. However, environmental risk factors, such as exposure to various toxins like 1-methyl-4-phenyl-1,2,3,6- tetrahydropyridine (MPTP) or pesticides like rotenone or paraquat (Betarbet et al., 2000; Calne & William Langston, 1983; Thiruchelvam et al., 2000) are key elements underlying the pathogenesis of idiopathic PD.

1.2.1. History

The first description of PD dates back to 1817, when Sir James Parkinson described it as a neurological condition in his publication "An essay on the shaking palsy". Six decades later, Jean Martin Charcot, a French neurologist studying tremors and palsy, renamed the disorder "Parkinson's disease" and established the clinical definition of the disease describing bradykinesia and rigidity. Between the 1950s and 1960s, the role of DA as a cerebral neurotransmitter and its relevance in the STR were discovered by Montagu and Carlsson (Carlsson, 1958; Montagu, 1957). Later, chemical differences (DA loss) in the brains of PD patients were identified (Ehringer and O. 1960), and DA signalling was shown to play a crucial role in motor control.

Following this discovery, Cotizás and his colleagues tried to reproduce the experiments done by Marcus Guggenheim in 1913, who isolated the DA precursor 3,4-dihydroxyphenylalanine or levodopa (L-DOPA). If the experiment of Guggenheim did not work, the small oral dose tried by Cotizás 60 years later in his patients improved motor symptoms and became the gold-standard treatment for PD.

1.2.2. Pathophysiology

PD is a progressive disorder characterized by the gradual degeneration of DA neurons in the SNc (Braak et al., 2003; Ehringer & O., 1954) causing a massive loss of DA in the STR. The degeneration of SNc neurons can be correlated with alpha-synuclein aggregations in the

cytoplasm called Lewy bodies. According to Braak's theory, Lewy bodies start to build up in cholinergic and monoaminergic midbrain neuron populations, as well as in the olfactory system. As the neurodegeneration progresses, Lewy bodies are also found in many other brain regions such as the amygdala, the PPN, the SNc, the cortical areas or the hippocampus (Braak et al., 2003; Braak et al., 2004).

At present, the exact pathophysiology of PD is still unknown, but several cellular and molecular mechanisms are being explored to understand the aetiology of this disorder, including mitochondrial dysfunction, protein homeostasis, neuroinflammation and excitotoxicity.

1.2.3. Clinical features

1.2.3.1. Motor symptoms

The clinical diagnosis of PD is based on the presence of characteristic motor symptoms induced by the DA depletion akinesia/bradykinesia, muscle rigidity, resting tremor and postural instability.

Akinesia is a term for the loss of voluntary movement abilities. The most common sign of akinesia is a "freezing" behaviour when aiming to move. **Bradykinesia** is the impairment of voluntary motor control expressed by slow movement or freezing. It can be expressed, for example, by shuffling or dragging one or both feet when a patient is walking or by the lack or absence of facial expressions. The combination of both of these motor symptoms results in a default to initiate voluntary movements and the presence of a new way of walking, typical for the disease.

Rigidity is described by the tension and the tightening of the muscles in an unwanted manner. Flexor muscles are principally affected which explains the flexed posture of PD patients.

Resting tremor occurs, as its name suggests, at rest when the patient is sitting or even while walking, but when he/she reaches out to shake hands with someone, tremors are less noticeable. Also described as "pill-rolling", this symptom generally occurs in the hand in a unilateral manner, especially during early stages of the disease. With disease progression, both sides may become affected like other parts of the body. Some people report an internal tremor like a shaking sensation inside the chest that cannot be seen. The frequency of these tremors is slow and is comprised between 3-7 Hz.

Postural instability is also one of the main symptoms of PD, which appears in the later stages of the disease. PD patients have issues with their balance, which makes them unsteady when standing.

1.2.3.2. Non-motor symptoms

Some non-motor symptoms can appear years before motor symptoms and well before the diagnosis of the disease. Few years before the confirmation of PD, patients present numerous symptoms such as a weakening sense of smell and taste, constipation, dizziness, sexual problems, etc. Although these symptoms are often discrete, some have a more important impact on the quality of life, like sleep disorders, an increase in pain or mood disorders including depression, compulsive behaviours or high anxiety.

1.2.4. Parkinson's disease treatments

At this moment, only symptomatic treatment of motor and non-motor symptoms is available for PD patients, with no strategic therapy aimed at slowing the disease's progression. Currently, DA replacement therapies are the first choice in PD treatment, although some patients show small benefits from medication and develop strong side effects and require surgical approaches.

1.2.4.1. Pharmacological treatments

The main goal of the pharmacological treatments is to compensate for the loss of DA. Depending on the age, progression of the disease and response to the treatment, different strategies are used: (1) Increasing DA synthesis through the administration of the DA precursor: L-DOPA; (2) Stimulating the DAergic receptors using agonists (3) Inhibiting the DA metabolism using a monoamine oxidase type B inhibitor (MAO) or a catechol O-methyl transferase inhibitor (COMT); (4) Increasing DA release using a NMDA receptor antagonist: Amantadine (See review of Connolly and Lang 2014).

Despite all the progress to find a complete molecule to treat PD symptoms, L-DOPA is still the gold standard treatment. In contrast to DA, L-DOPA can cross the blood brain barrier (BBB) and its administration exogenously replaces the DA deficit. L-DOPA is currently administered

together with a DA decarboxylase inhibitor, such as benserazide, carbidopa, or/and a COMTI that does not cross the BBB, in order to avoid the peripheral transformation of L-DOPA into DA (Figure 1.10). L-DOPA improves striatal DAergic transmission, producing a rapid improvement of motor symptoms of PD. Although L-DOPA does not stop the progression of the disease and its efficacy decreases over time, it can be used in all patients at any stage of the disease.

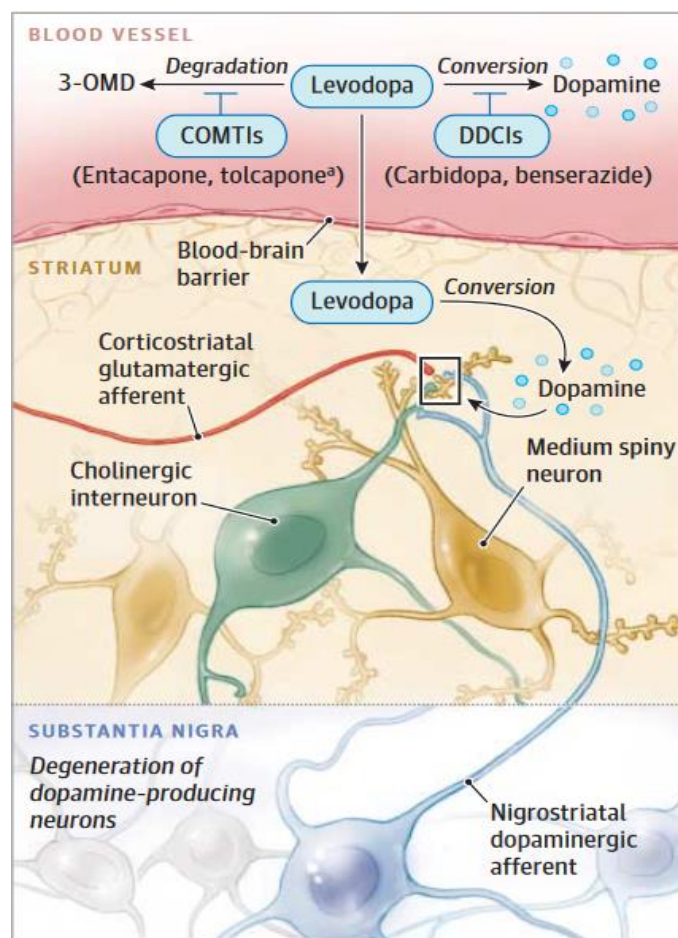


Figure 1.10. Schematic illustration of the L-DOPA action mechanism for the treatment of motor symptoms of PD. L-DOPA is co-injected with dopamine (DA) carboxylase inhibitor (DDCIs) (benserazide or carbidopa) or/and catechol O-methyltransferase inhibitor (COMTI) to block its transformation in DA before the crossing of the blood brain barrier (BBB). Once the L-DOPA crosses the BBB, it is transformed into DA and uptaken by striatal neurons. (Image taken from Connolly. B, 2014)

1.2.4.2. Surgical treatment

Deep brain stimulation (DBS) is an alternative treatment reserved for people whose symptoms are not adequately controlled with medication. DBS consists of the implantation of one or more electrodes in specific brain areas (STN, GPi, or PPN) and the application of electrical stimulations at frequencies between 100 and 200 Hz (Benabid, 2003). DBS is certainly the most important advancement since the development of L-DOPA: it remains flexible due to its reversibility, it offers the possibility to remove the electrodes in case of problems or parameters can be customised for each patient in case of side effects. Another advantage is that it offers the option to record the neuronal activity of the awake patient (Benazzouz et al., 2002; Dostrovsky et al., 2000). However, it has some limitations, such as the fragility of the electrode system and the elevated cost.

1.2.5. Levodopa-induced dyskinesia

The standard oral L-DOPA therapy is well established in the clinic and provides general satisfactory symptomatic relief. However, long-term L-DOPA treatment induces abnormal and involuntary movements called L-DOPA-induced dyskinesia (LID). Approximately 40% of PD patients develop LID after 4-6 years of L-DOPA treatment and 90% of patients after 10 years. Although the pathophysiological basis of LID is not fully understood, the onset of LID has been associated with several factors, such as earlier age at the onset of L-DOPA treatment, total L-DOPA exposure, female sex, and possible genetic factors (Zappia et al., 2005).

LID is characterized by choreic, dystonic or ballistic movements involving the limbs, the orofacial muscle and the trunk.

Choreic movements are defined by involuntary, irregular, abrupt, rapid and non-rhythmic movements that seem to flow from one part of the body to the other.

Dystonic movements can be described by sustained contractions of agonist and antagonist muscles.

Finally, **ballism** is another type of involuntary movement affecting the proximal limb musculature, manifested in jerking, flinging movements of the extremity. Usually, ballism is involved in one side of the body, resulting in hemiballism. These new symptoms can disable patients over time, impairing their quality of life, affecting their daily activities and routines (Ahlskog & Muenter, 2001).

LID has a variety of clinical forms, (1) “peak-dose dyskinesia”, the most common type of dyskinesia that often consists of stereotypic, choreic, or ballistic movements involving the head, trunk, and limbs and sometimes respiratory muscles and occurs at the peak of L-DOPA plasma concentrations; (2) “diphasic dyskinesia”, occurring at the beginning and the end of L-DOPA drug’s action; and (3) “off-period dystonia”, where the concentration of L-DOPA in the brain is low, manifesting in abnormal dystonic postures mainly affecting the lower limbs (Figure 1.11) (Bastide et al., 2015; Guridi et al., 2012).

Today, two effective strategies are used to treat LID. Initially approved by the FDA as an agent against influenza, the NMDA receptor antagonist, amantadine, is now the only effective and available antidyskinetic drug (Lyons, 2018). When antidyskinetic treatments are absent and LID strongly present, the DBS appears to be the last possibility. STN-DBS can reduce the required dose of L-DOPA and ameliorate LID, while GPi-DBS provides greater antidyskinetic effects without reduction of L-DOPA intake (Ramirez-Zamora & Ostrem, 2018).

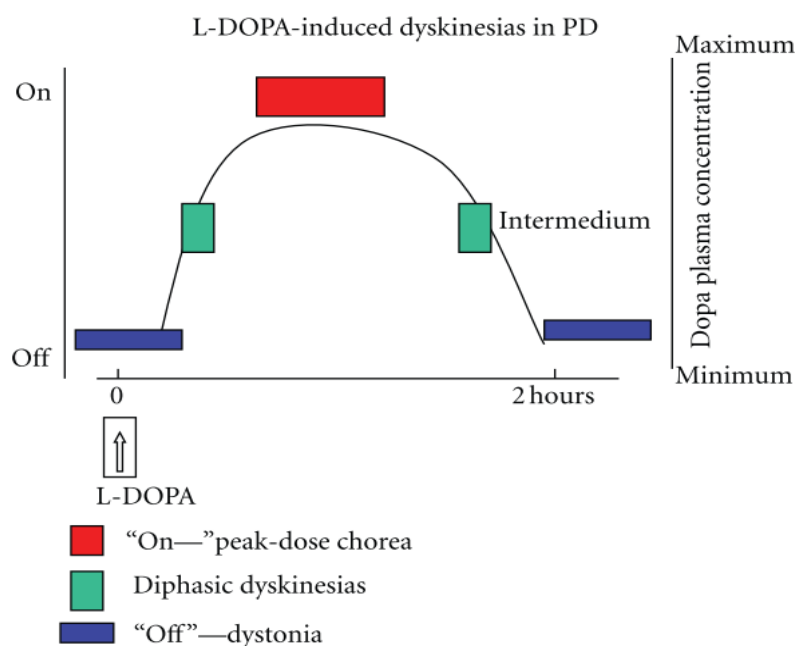


Figure 1.11. Relationship between LID and L-DOPA plasma concentration. “Peak of dose” or “on” period dyskinesia is correlated to high levels of L-DOPA and in parallel with the maximal clinical benefit. Diphasic dyskinesia appears at the onset and offset of the L-DOPA effect in relationship with increment or decrement of L-DOPA plasma level. “Off” period dystonia is characterised by painful postures in lower extremities and is correlated with the lowest L-DOPA level. Generally a full spectrum of the three types is present in PD patients with motor fluctuations Taken from (Guridi et al., 2012).

The classical model of BG functional organisation proposes that LID generation is a consequence of a striatal DAergic overstimulation that causes an inhibition of the output nuclei GPi/SNr. So, the magnitude of nigrostriatal degeneration is considered as the main factor for the development of LID (Bastide et al., 2015; Guridi et al., 2012). Therefore, numerous studies have been conducted to understand the implication of the DA system during LID. Molecular changes have been highlighted, such as an increase of FosB and prodynorphin expression at the striatal level, which are likely mediated by D₁ receptor overactivity and involved in the severity of LID in rodent models of PD (Cenci et al., 1998; Doucet et al., 1996). Besides, the increased sensitivity of the D₁ receptor enhances the activation of cAMP-dependent protein kinase A, which phosphorylates several proteins like DARP-32, and optogenetic blockade of this protein in MSNs has been shown to reduce LID symptoms in a rat model (Bateup et al., 2010).

However, in the last decades, many studies have shown the implication of different neurotransmitter systems in LID, including the glutamatergic, noradrenergic, 5-HT, cannabinoid, cholinergic, and opioid systems (Espay et al., 2018; Vijayakumar & Jankovic, 2016b, 2016a). Experimental and clinical findings have provided compelling evidence for the prominent role of the 5-HT system in the pathophysiology of PD and LID (Carta et al., 2007; Navailles et al., 2011). The mechanisms underlying LID are poorly understood, but there is a consensus that the 5-HT system plays a relevant role, since L-DOPA is transformed into DA and stored and released by the 5-HT terminals (Figure 1.12) (Carta et al., 2007; Miller et al., 1999).

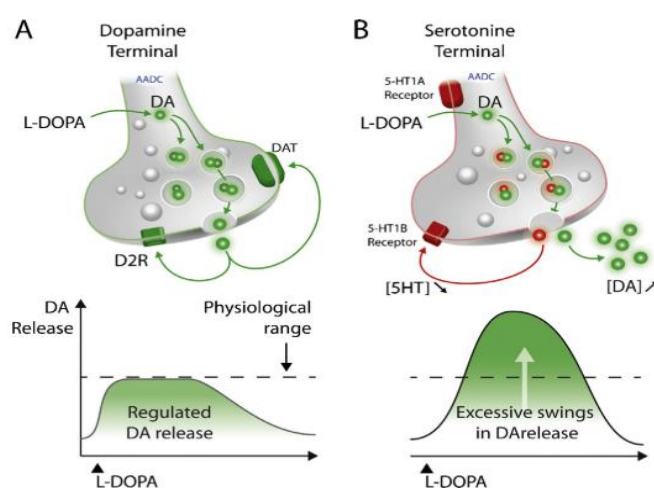


Figure 1.12. Handling of L-DOPA in LID pathophysiology. **A**, Normal L-DOPA handling. Dopaminergic terminals convert L-DOPA into dopamine (DA) which is released in the synaptic cleft in a controlled way due to the expression of a fine regulatory mechanism composed of the DAergic D2 receptor (D2R) and the DA active transporter (DAT) proteins. Indeed, D2R and DAT can regulate the firing rate of DA neurons and DA reuptake, respectively, leading to a regulated DA release. **B**, Aberrant L-DOPA handling. In a situation of advanced DA denervation, the serotonergic (5-HT) neurons become the main site of L-DOPA conversion to DA. However, the loss of the last spared DAergic terminals,

which could buffer 5-HT neuron-derived DA release, triggers the appearance of LID due to the absence of the D2R/DAT feedback control mechanism for DA release on 5-HT neurons. The absence of this mechanism makes 5-HT neuron-dependent DA release uncontrolled, contributing to swings in synaptic DA levels, and promoting pulsatile stimulation of striatal postsynaptic DA receptors (Figure adapted from Bastide et al., 2015).

1.2.6. Animal models

The use of animal models of PD is essential to study the pathophysiological mechanisms underlying parkinsonian motor symptoms and the generation of LID. One of the major constraints in modelling LID in animals relies on the generation of a PD model with enough DA depleted to reproduce dyskinetic movements with a high concentration of L-DOPA.

1.2.6.1. Animal models of PD

Neurotoxin-based animal models

MPTP model: Accidentally developed in the 70s, the MPTP has been used since it tends to induce parkinsonism in non-human primates (Mahlon R. DeLong, 1990). Nowadays, it is considered as the most representative model for mimicking PD symptomatology: akinesia, bradykinesia, rigidity and postural disorder. Only resting tremor is not developed by this model. In addition to clinical features, this model allowed the study of characteristic electrophysiological alterations (changes in the firing rate and firing pattern) in the BG nuclei. Finally, the contribution of this model is significant and allowed DeLong and his team to design the physiopathological model of BG in PD, which is described in section 1.3.

6-Hydroxydopamine (6-OHDA) model: 6-OHDA is the most commonly used toxin to modelise PD in rodents. Due to its inability to cross the BBB, 6-OHDA needs to be injected intracerebrally. Once reuptaken, 6-OHDA is rapidly oxidised and produces reactive oxygen responsible for neuronal death (Perese et al., 1989). Administration of 6-OHDA in different brain regions causes a distinctive pattern of neuronal degeneration. Depending on the degrees of depletion or the desired motor symptoms, the site of injection can differ between the SNc, the STR, or the Medial Forebrain Bundle (MFB). For instance, injection into the SNc leads to a rapid and massive destruction of DA neurons, while 6-OHDA injection directly into the STR causes a retrograde degeneration of nigrostriatal neurons, much longer and less effective (Dauer & Przedborski, 2003). In most cases, the administration of 6-OHDA is done in MFB where DAergic and noradrenergic (NA) axons are cross. A NA reuptake inhibitor (desipramine)

is then injected prior to the administration of 6-OHDA to protect NAergic fibers and specifically lesion DA neurons.

Rodents with bilateral lesions reproduce the characteristic motor impairment of PD, but they also show adipsia, seizure and high mortality. Therefore, unilateral 6-OHDA lesions are the most widely used, producing hemiparkinsonian syndrome, which includes asymmetries of body posture and contralateral SM deficits. Only tremor and postural instability are not reproduced by these models. As a result of the postural asymmetry, behavioural measures can be made. Mice or rats preferentially use their ipsilateral forelimb producing an asymmetric circling in the ipsilateral side of the lesion. This turning deficit depends on the degree of nigrostriatal lesion and is not due to the loss of ability to move the contralateral paw but by the loss of ability to exert force to displace the body (Schwartz & Huston, 1996).

Although widely used, the neurotoxic 6-OHDA model does not perfectly mimic the PD pathophysiology. First, the 6-OHDA toxin induces an acute neurodegeneration of DA neurons and, as such, it does not reproduce the progressive nature of PD. Second, this model does not reproduce the histological hallmark of PD that is the intraneuronal presence of alpha-synuclein aggregates called Lewy bodies (Schober, 2004).

Pesticide model: Correlation between agro-chemical exposure and increased risk for PD have been difficult to conclude, but pesticides and herbicides such as rotenone, paraquat and maneb were identified as possible environmental causes of PD. So far, these compounds have been used in rodents to model PD. Both rotenone and paraquat are identified to cause DA degeneration by inducing oxidative stress. In the rotenone model, first, due to its highly lipophilic properties, rotenone can easily cross the BBB and enter in DA neurons. Then, it blocks complex I activity, causing a massive formation of reactive oxygen species. Finally, rotenone inhibits proteasome activity generating proteolytic stress (Betarbet et al., 2000).

Chronic injections of paraquat induces a loss of DA cells in SNc but none in the STR, that is why it is not really used in a simple model of PD. Rotenone administration can induce motor and non-motor symptoms and show signs of alpha-synuclein aggregation but also lead to catecholamine depletion. These less-used models can allow the understanding of how environmental factors can influence the onset of PD.

Genetic models

Alpha-synuclein: Alpha-synuclein was the first gene linked to a dominant-type familial PD and is the main component of Lewy bodies. To date, many alpha-synuclein models have been developed. The first was created in 2000 by Masliah et al., but no significant DA loss was observed in mice which did not fully replicate the human pathology. After that, strategies of double mutant (A30P/A53T) were designed and reported neurites dystrophy and neuronal aggregates accompanied by motor activity impairments (Masliah et al., 2011). Although these models are useful to elucidate the alpha-synuclein function and its relation to PD, the clinical relevance is questionable and as with other transgenic models, the additional deficits are not yet known.

Parkin: Parkin is an E2 ubiquitin ligase that participates in the ubiquitin-proteasome system. In particular, parkin recognises proteins on the membrane of mitochondria and mediates the clearance of damaged mitochondria. In this way, parkin enhances cell survival by suppressing both mitochondrial-dependent and independent apoptosis. Mutations of this protein lead to neuronal death and aberrant metabolism seen in PD (Hang et al., 2015; Pickrell & Youle, 2015). Indeed, mutations in parkin are a cause of 50% of familial PD and 20% of idiopathic PD cases. Thus, knockout parkin mice have been generated but no success has been shown to this day. However, numerous studies about knockouts rendered DA neurons more sensitive to MPTP or 6-OHDA. The Parkin model is still far from being the new PD model, but it could be useful to study potential therapeutic targets (Greene et al., 2012).

Protein mutation: Numerous other protein mutations have been tested to generate a new PD model. For instance, mutations in PTEN-induced kinase 1 (PINK1) which is associated with a recessive form of the disease, induced neurite outgrowth in DA neurons but without any obvious PD pathology observed in the brain. As for the Parkin model, the mutation in DJ-1, also associated with a recessive form of PD, showed no DA deficit and a hypersensitivity towards the insults of MPTP or Rotenone, but in this case, DJ-1 knockout mice display locomotor deficit. Finally, transcription factors were also a target of mutation. The MitoPark model disrupts mitochondrial function in DA neurons by knocking out the mitochondrial transcription factor A (TFAM) in DAT-Cre mice. This model displayed progressive degeneration, motor impairments and more or less Lewy body like inclusions.

Despite all the advances to model PD, it is difficult to conclude whether these genetic models mirror the human condition, but at the moment, they are a valuable tool to study the molecular mechanisms implicated in PD.

1.2.6.2. Animal model of L-DOPA-induced dyskinesia

Since the 2000s, the 6-OHDA model has been used to produce stable and consistent motor symptoms of PD and constitutes the widely used model to study LID.

The chronic administration of a high dose of L-DOPA is sufficient to develop abnormal involuntary movements (AIMs) affecting orofacial, trunk and forelimb muscles on the contralateral side of the lesion (Lundblad et al., 2004). MFB or striatal 6-OHDA models can be used but the threshold dose of L-DOPA for the induction of LID differs, as well as the degrees of LID. A daily dose of 18 mg/kg is necessary in striatally-lesioned mice, whereas the dose needed is much lower for inducing AIMs in MFB-lesioned mice with doses ranging between 1-6 mg/kg (Francardo et al., 2011). As mentioned above, in order to cross the BBB without peripheral transformation into DA, L-DOPA is co-administered with a peripheral DOPA decarboxylase inhibitor, benserazide, which cannot cross the BBB, at a fixed of 12.5 mg/kg (Figure 1.10).

However, L-DOPA does not usually induce LID in partial DA-lesioned animals that remain resistant to the development of AIMs. Therefore, MFB-lesioned models characterised as more invasive and showing a stronger reduction in DAergic fibers, remain the most widely used in rodent studies.

1.3. Basal ganglia nuclei in Parkinson's disease and levodopa-induced dyskinesia

Chronic loss of DA results in significant changes in the firing activity of BG nuclei. The “classical” model predicts that parkinsonian motor features are related to increased firing rate of BG output neurons, whereas LID is associated with decreased firing rate of these neurons (DeLong, 1990).

1.3.1. Basal ganglia nuclei in Parkinson's disease

In PD, the model suggests that the lack of DA generates a hyperactivity of STN neurons and reduces the activity of dMSNs, resulting in the reduction of inhibition over the GPi/EP and SNr, with the consequent over-inhibition of the thalamus (Figure 1.13). This over-inhibition reduces the activation of cortical motor regions and leads to motor impairment, such as akinesia/bradykinesia. This is supported by clinical studies in PD patients showing increased neuronal firing rates in output nuclei and in the STN (Bergman et al., 1994; Obeso et al., 2002). At the striatal level, the loss of DA innervation decreases D₁ receptor activation and STR-SNr transmission but promotes D₂ receptor activation, increasing GP-SNr and STN-SNr transmissions (Aceves et al., 2011). However, the model fails to explain other features of neuronal firing that are observed in PD, such as the increased burst firing activity and the increased synchronisation and oscillatory activity, particularly in the beta frequency band in BG nuclei (Wichmann & Dostrovsky, 2011).

The oscillatory activity is a property of neurons, defined as rhythmic neuronal fluctuations that occur periodically. This may be reflected in single-unit spikes in the electrocorticogram (ECoG), or in local field potentials (LFP). While several theories exist to explain the role of these oscillations in neuronal processing, most propose that neuronal oscillations are crucial for efficient communication within brain circuits and have been involved in different processes such as cognition, locomotion, learning, and alertness (Fries, 2009; Haider & McCormick, 2009; Uhlhaas & Singer, 2006). Moreover, these oscillations can be subdivided into 5 types characterised by their frequency and location: theta (2-7 Hz), alpha (7-13 Hz in visual cortex), beta (11-30 Hz), gamma (30-80 Hz), and mu (7-12 Hz in the SM cortex) oscillations (Hutchison et al., 2004).

Abnormal oscillatory activity in the beta frequency band is the most prominent change detected in PD patients and has been related to tremor and akinesia syndromes (Dostrovsky & Bergman, 2004; Kühn et al., 2006). The functional coupling between the motor cortex and periphery is strongest in the beta frequency range during sustained contraction or rest and has

been proposed to promote maintenance of the existing motor output (Gilbertson et al., 2005). On the other hand, the gamma frequency band is thought to be pro-kinetic and to underlie the priming and maintenance of LID (Güttler et al., 2021; Wiest et al., 2021).

However, it is important to note that none of these studies demonstrate correlation between the level of beta oscillation expression and the degree of symptoms (Stein & Bar-Gad, 2013).

1.3.2. Basal ganglia nuclei in L-DOPA-induced dyskinesia

Chronic L-DOPA therapy tends to over-stimulate iMSNs and dMSNs that leads to an inhibition of the indirect pathway and an over-activation of the direct pathway. This time, the SNr/GPi outputs are inhibited, leading to an increase in glutamatergic thalamo-cortical transmission, resulting in an excess of motor movements seen in LID (Figure 1.13).

The study of LFP showed the presence of gamma oscillations during LID. If in healthy humans, gamma oscillations have been associated with a pro-kinetic action (Brücke et al., 2012), it raises the possibility that abnormal levels of gamma oscillation are responsible for involuntary movement seen in LID.

Classically, the effect of DA replacement results in a reduced activity of the STN-GPi pathway (Crossman et al., 1988) and a decreased firing activity in GPi output neurons (Olanow et al., 2009). The same results have been observed after recording LFP from the SNr in 6-OHDA rats with LID (A. Aristieta et al., 2016; Lacombe et al., 2009; Meissner et al., 2006). However, findings in parkinsonian monkeys and PD patients demonstrate that the destruction of the GPi by a surgical procedure called pallidotomy abolishes LID (Baron et al., 1996). The antidyskinetic effect observed with pallidotomy has led to the revision of the pathophysiology of LID which is not only the result of GPi hypoactivity, but is also due to abnormal firing patterns in BG output neurons (Güttler et al., 2021; Obeso et al., 2000).

After that, numerous studies have been done on the entire BG nuclei and the STR comes through as being a good target. Over the past few years, evidence supports the role of striatal D₁ receptors in the development of LID (Darmopil et al., 2009; Murer & Moratalla, 2011). It has been shown that, contrary to D₂ receptor knockout mice, D₁ receptor knockout mice do not show AIMs upon prolonged L-DOPA treatment. Most of the studies using optogenetic approaches confirmed this notion. For instance, the optogenetic inhibition of one subpopulation of D₁ neurons showed the importance of this population as necessary and sufficient to reverse AIMs (Girasole et al., 2018). Indeed, they first reduced the level of LID with the opto-inhibition of D₁ neurons, and then generated LID with the inverse experiment: the activation of the same

population of D₁ neurons. In line with this, optogenetic activation of STR-SNr terminals is able to generate a full dyskinetic state in DA-depleted wild-type mice (Keifman et al., 2019).

The necessity to have DA depletion to trigger LID is also demonstrated in the study of Hernandez and colleagues, where the optogenetic stimulation of striatal projections is able to evoke LID with and without L-DOPA but only on DA-depleted rats. Moreover, in this study they looked at c-fos level and confirmed the higher expression of FosB in dMSN (Hernández et al., 2017). Consequently, these results suggest that the dMSN-SNr transmission could be an attractive therapeutic target for future strategies aimed at reducing LID.

In contrast, other studies challenge this point of view that dMSN over-activity alone can explain LID, showing the participation of iMSN in LID maintenance. Alcacer and colleagues showed that chemogenetic co-stimulation of dMSNs and iMSNs induced dyskinesia in PD rats (Alcacer et al., 2017). Moreover, iMSN and dMSN seem to interact in different motor patterns as set out in the study of Andreoli et al., where D₁ and D₂ receptors modulation mediate distinct patterns of dyskinetic and dystonic movements (Andreoli et al., 2021). In this study, they separately studied AIMs subtypes. Whereas D₁ receptor mediates forelimb and orofacial AIMs, the D₂ receptor controls the axial subtypes that can be related to a dystonic character (Andreoli et al., 2021). Beyond the new insight of dMSN/iMSN part of LID maintenance, they introduced a new scale and a new method of behaviour analysis. Similarly, Parker and colleagues refined this complexity of an intermingled role of dMSN/iMSN in PD and LID genesis. Interestingly, they used calcium imaging to follow the patterns of striatal neurons across conditions (healthy vs. PD vs. LID). Both dMSN and iMSN showed modification of activity. Not surprisingly, dMSN became hyperactive and iMSN hypoactive, however the novelty was in the spatial clustering response. dMSN lost their spatial coordination of movement evoked response, thus iMSN became more responsive to motion onset (Parker et al., 2018). Although they add complexity in the LID circuits mechanism, these results pave the way in the understanding of complex aspects of dyskinetic behaviour.

Finally, it has become evident that striatal interneurons are major determinants of network activity and behaviour in PD and LID (Zhai et al., 2019). In accordance with this, a recent optogenetic study has revealed the critical role played by striatal cholinergic interneurons in tuning the intensity of LID. The authors have shown that short pulse stimulation of cholinergic interneurons enhanced LID while longer pulse stimulation of cholinergic interneurons reduced them (Bordia et al., 2016). Raising the question of whether other brain regions or neuronal types can be implicated in the maintenance or generation of dyskinetic behaviour.

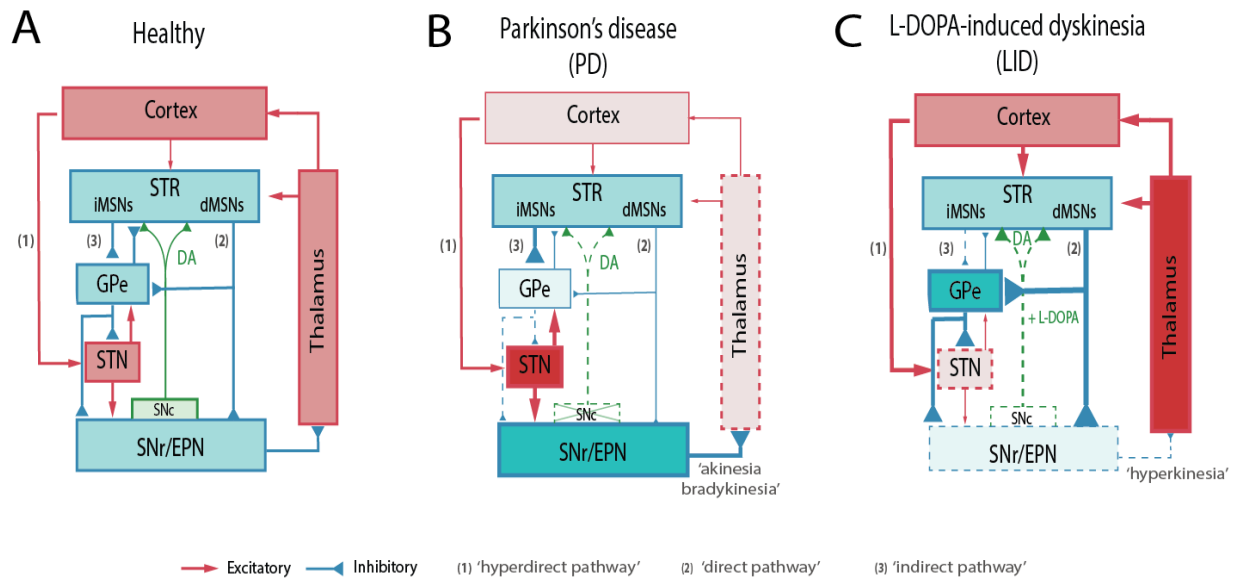


Figure 1.13. Schematic representation of the BG motor circuit in (A) healthy, (B) parkinsonian and (C) dyskinetic states. Dopaminergic, GABAergic (inhibitory), and glutamatergic (excitatory) projections are depicted in green, blue, and red, respectively. The thickness of the arrows corresponds to their presumed activity. DA: dopamine; EPN: entopeduncular nucleus; GPe: external *globus pallidus*, MSNs: medium spiny neurons from the direct (dMSNs) or indirect (iMSNs) pathway; SNc: *substantia nigra pars compacta*; SNr: *substantia nigra pars reticulata*; STN: subthalamic nucleus; STR: striatum.

1.4. The serotonergic system in Basal Ganglia

The 5-HT is synthesised from tryptophan, a neutral amino acid originating from alimentation and able to cross the BBB. After being synthesised by the enzyme tryptophan hydroxylase, 5-HT accumulates in secretory granules via a vesicular monoamine transporter before being released to the synaptic cleft. 5-HT acts via 5-HT receptors, which are classified into seven families and at least 14 different subtypes, including the G-protein-coupled receptor subtypes (5-HT₁, 5-HT₂, 5-HT₄₋₇) and ligand-gated ion channels (5-HT₃) (Hoyer et al., 2002). In the central nervous system, 5-HT reuptake is possible via the 5-HT reuptake transporter (SERT) located in 5-HT axon terminal.

The main population of serotonergic neurons are located in the DRN (Peyron et al., 1997), which provides extensive innervation to almost the entire brain and controls multiple functions such as mood, cognition, emotion, motor behaviour, sleep, appetite, and the regulation of the circadian rhythm (Benarroch, 2009). BG nuclei, such as ventral pallidum, EP, SNr and STR receive innervation from the DRN (Figure 1.14) (Huang et al., 2019) and contain SERT and all the 5-HT receptor subtypes. The numerous receptors located in and around the BG makes the study of the effect exerted by 5-HT on BG nuclei difficult, since they are the result of the direct activation of 5-HT receptors in the different nuclei plus the activation of those located on 5-HT neurons that project to the BG (Migueluez et al., 2014). Despite the complexity to study the effects of 5-HT drugs on BG nuclei, it is well documented that the 5-HT system modulates activity of the BG (Benarroch, 2009; Di Matteo et al., 2008).

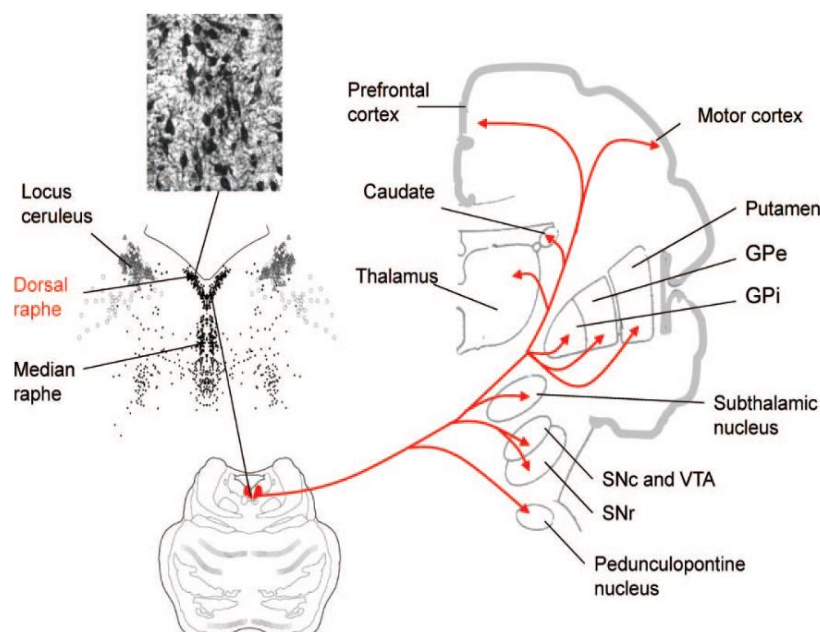


Figure 1.14. Rostral raphe nuclei and serotonergic innervation of the Basal Ganglia circuits. The dorsal raphe nucleus sends serotonergic projections to all components of the BG: the striatum

(caudate/putamen), external and internal globus pallidus (GPe, GPi), substantia nigra pars compacta and pars reticulata (SNc, SNr), and subthalamic nucleus. Other nuclei such as the prefrontal and motor cortex, the pedunculopontine nucleus and the ventral tegmental area (VTA) also receive afferences from the dorsal raphe nucleus (Taken from Benarroch, 2009).

The density and pattern of 5-HT innervation is not homogeneous for all the BG nuclei, but the SNr seems to be the nucleus receiving the heaviest 5-HT input from the DRN (Corvaja et al., 1993). Indeed, a high level of 5-HT receptors (5-HT_{1A-1B-1C}, 5-HT_{2A-2C}, 5-HT₃, 5-HT₄) is present and located on the somatodendritic and terminal region of SNr neurons (Di Matteo et al. 2008). For instance, low levels of binding were found for the 5-HT_{1A} and 5-HT_{1D} subtypes contrary to 5-HT_{1B} which presents the highest level of protein bindings (Castro et al., 1998; Compan et al., 1998). Moderate levels of the 5-HT_{2A} receptor are found in the SNr and SN (Pompeiano et al., 1994; Wright et al., 1995), while in the GPe, the presence of this subtype is more recently highlighted, but well described with 70% of neurons expressing the 5-HT_{2A} receptor projecting to the STR (Bubser et al., 2001). The STR receives inputs from multiple 5-HT neuron subtypes and high concentration of both receptor mRNA and protein of the different receptor subtypes have been found, such as the 5-HT_{1A-1B}, 5-HT_{2A-2C}, 5-HT₆ and the 5-HT₇ receptors. The 5HT_{2A} receptor subtype is present in the STR of various mammal species with an increase of its gradients in the rostrocaudal and mediolateral directions (Migueluez et al., 2014; Wright et al., 1995). In fact, the 5-HT_{2A} receptor distribution displays topographical differences, showing higher expression in associative/limbic structures than in the motor ones (Ito et al., 1998; López-Giménez et al., 1997; Morilak & Ciaranello, 1993; Pinborg et al., 2003; Riad et al., 1999; Riss et al., 2011). The 5-HT_{2A} and 5-HT_{2C} receptors have similar pharmacological profiles and cellular signalling pathways making it difficult to separate them. One way to differentiate anatomical and functional features of the 5-HT_{2A} and 5-HT_{2C} subtypes originates from their expression within the STN. Whereas the 5-HT_{2C} receptor subtype is highly expressed in the STN and directly regulates it (Aristieta et al., 2014; Stanford et al., 2005), the 5-HT_{2A} receptor expression is low and seems not to participate in the control of STN neuron activity (Pompeiano et al., 1994).

Interestingly, behavioural studies have pointed to the implication of the 5-HT_{2A} receptor subtype in the regulation of motor, automatism, executive, and cognitive BG functions (Aznar & Hervig, 2016; Zhang & Stackman, 2015). In addition, the 5-HT_{2A} receptor may also play a role in many diseases associated with BG dysfunction. Nowadays, the 5-HT_{2A} receptor is a pharmacological target in treatment development for neuropsychiatric disorders such as schizophrenia (Miyamoto et al., 2005), or PD psychosis (Chang & Fox, 2016).

Finally, although their presence in BG nuclei are well described, abundant and contradictory results from *in vitro* and *in vivo* studies indicate that there are complex interactions between 5-

HT and other systems like the DA system at the levels of BG. So, more studies are needed to understand the implication of 5-HT in BG modulation.

1.4.1. The serotonergic system in Parkinson's disease

According to Braak's theory (H. Braak et al., 2003), the pathological process in PD occurs in a gradual way, starting from the olfactory nucleus in presymptomatic stages and spreading to the pons and the midbrain. In stage 2, Lewy bodies and Lewy neurites start affecting the median raphe nuclei, which are totally involved in stage 3.

Post-mortem studies reported an important 5-HT depletion in the STR, hypothalamus or frontal cortex as well as its metabolite 5-hydroxyindoleacetic acid (5-HIAA) in brains of PD patients. Besides, PET analysis showed SERT changes and a decrease of 5-HT terminals in raphe, thalamus, ventral STR (Pagano et al., 2018). This 5-HT damage in the STR and anterior cingulate cortex of PD patients, is correlated with the severity of neuropsychiatric disorders such as depression, apathy and anxiety (Castrioto et al., 2016).

Numerous studies carried out in PD patients and animal models have shown that 5-HT dysfunction was also characterised by an alteration of the receptor subtypes (Huot et al., 2011; Leal et al., 2019). Modification of the receptor expression will also be associated with disorders developed by PD patients. For instance, an increase in 5-HT_{2A} receptors in the temporal cortex is related to visual hallucinations induced by L-DOPA (Ballanger et al., 2010; Huot et al., 2010). Other effects of this alteration can be observed with the reduction in 5-HT_{1A} receptors, greater in the temporal, orbitofrontal and amygdala cortices in depressed PD patients (Ballanger et al., 2012).

However, studies in animal models of PD gave heterogeneous results about the 5-HT system, showing either no changes or striatal hyperinnervation. Sprouting of 5-HT axon varicosities was revealed using MPTP monkeys, in the STR and GPe/GPi, while the density and morphology of 5-HT neurons in the DRN remained unchanged (Gagnon et al., 2018). Thus, the hyperinnervation may reflect the role of the over sprouting of 5-HT neurons which produce a compensatory mechanism due to the loss of striatal DA (Carta et al., 2007). Indeed, in animal PD models, alterations have been identified involving the 5-HT system that depend on the loss of DA (Migueléiz et al., 2014). Finally, it was described that the distribution of 5-HT receptors and transporters in DA regions plays an important role in the interaction of DA/5-HT (De Deurwaerdère & Di Giovanni, 2017).

Importantly, immunohistochemical studies diverge about the impact of 5-HT on DA neuronal activity within the STR and other cortical areas (see De Deurwaerdère and Di Giovanni 2017). Some studies, using electrophysiological recordings, highlight neuronal projections between DRN, SN, and VTA, and argue that these projections could be associated with the inhibitory activity of 5-HT on both DA and 5-HT neurons (Dray et al., 1976; Gervais & Rouillard, 2000). Moreover, the use of the 5-HT agonists or antagonists modulate other neurotransmitters such as GABA, an inhibitory one (De Deurwaerdère & Di Giovanni, 2017; Huot et al., 2011). However, some DRN projections co-express glutamate, so under certain conditions, this neuronal activity could be excitatory.

Finally, the degeneration of 5-HT terminals is a process that starts early in the course of PD. However, it does not follow the linearity of the degeneration observed in the DA system. The 5-HT system may contribute to PD symptomatology, and while mainly involved in non-motor symptoms such as mood disorder, it also has an important pivotal role in parkinsonian resting tremor.

1.4.2. The serotonergic system in levodopa-induced dyskinesia

It has been shown, using the microdialysis technique, that L-DOPA induces a regionally dependent release of DA and 5-HT (Migueluez et al., 2016; Navailles et al., 2011). This release of DA via the 5-HT neurons is largely implicated in the generation of LID (Carta & Bezard, 2011; Carta & Tronci, 2014; De Deurwaerdère & Navailles, 2012; Politis et al., 2014).

We have already addressed in section 1.2.5, the disturbance of the 5-HT system in LID. As a matter of fact, 5-HT terminals are able to convert L-DOPA into DA, store it in vesicles and release it, but the absence of the D₂ receptors/DAT feedback control for DA release makes the release uncontrolled, which can cause excessive DA level in several brain region (De Deurwaerdère & Di Giovanni, 2017). This DA released in the STR by 5-HT terminals is induced by the L-DOPA administration and acts as a “false neurotransmitter”, important in the genesis of LID (Carta et al., 2008; Navailles et al., 2011). Another consequence is the alteration of 5-HT neurons themselves. The synthesis of DA by the entrance of L-DOPA is supported by the enzyme MAO, which allows the degradation of DA and auto-oxidation mechanisms (Stanley & Yamamoto, 2014). However, the oxidative stress promoted by this mechanism generates free radicals and causes 5-HT cell death and the depletion of 5-HT content in a subregion of the DRN (Navailles et al., 2011).

Most studies have investigated the role of 5-HT_{1A} and 5-HT_{1B} receptors in LID. Preclinical studies in animal models of LID by using the 5-HT_{1A} receptor partial agonist buspirone have shown an antidyskinetic effect (Bibbiani et al., 2001; Politis et al., 2014). However, in a clinical trial with dyskinetic PD patients, the 5-HT_{1A} agonist did not counteract LID better than placebo. Regarding the 5-HT_{2A} receptor, evidence is not sufficient to elucidate its potential utility, even if promising results have been obtained using the selective 5-HT_{2A} receptor inverse agonist Pimavanserin. Moreover, other studies targeting SERT or 5-HTT have also shown beneficial effects without approval for patient use. More studies are therefore needed to elucidate the role that 5-HT-based drugs could play in the management of PD and LID symptoms.

2. HYPOTHESIS AND OBJECTIVES

Along with the increase in life expectancy, the prevalence of neurodegenerative diseases has increased dramatically. Indeed, it is estimated that the number of patients suffering from neurodegenerative diseases will double over the next 40 years with the consequent increase in social and health costs. Today, the pathophysiology of PD is not fully understood and the pharmacological treatment available does not prevent or stop the neurodegenerative progress. In addition, the use of L-DOPA is associated with long-term motor complications such as LID that are even more invalidating than the disease itself. Therefore, defining the neurobiological mechanisms that are directly causing LID and the search of new targets/useful pharmacological tools that alleviate LID are of primary interest in PD therapeutics. As a result, there could be a great social benefit and economic savings for the Health System.

In this context, our **hypothesis** is that the 5-HT system and the Arky-GPe have a modulatory role in the dynamic regulation of BG function and dysfunction. As such, characterising the regulatory action of the 5-HT_{2A} receptor on BG circuits and the Arky-GPe activity during PD and LID could be useful to identify and develop new treatment-candidates useful for the clinical management of these movement disorders.

As a result of the cotutelle we subdivided this PhD research project into two studies with the following aim objectives:

Objective of study I: To characterise *in vivo* the modulatory action of 5-HT_{2A} receptors on the dynamic regulation of mPF and SM BG circuits.

For this purpose, we performed simultaneous *in vivo* cortical electrical stimulation and single-cell extracellular recordings of SNr neurons in anaesthetised rats. The specific objectives of this study were:

- 1- To study whether the 5-HT_{2A} receptor stimulation has a preferential action on the dynamic regulation of the BG circuits, in favour of one circuit over another.*
- 2- To characterise the modulatory role of the 5-HT_{2A} receptor on spontaneous and cortically evoked activity of lateral and medial SNr neurons.*
- 3- To elucidate the participation of the endogenous 5-HT in the effects triggered by the 5-HT_{2A} receptor activation.*

Objective of study II: To define the contribution of arkypallidal neurons in the genesis and maintenance of LID.

In order to best achieve this objective, we separated it into two parts:

1 - To characterise the Arky-GPe activity in different conditions: from healthy to pathological states of PD and LID.

For this purpose, we performed calcium imaging recordings of Arky-GPe neurons in each condition using the fiber photometry and miniature endoscope techniques.

2 - To test if the causal manipulation of Arky-GPe neurons during LID is able to restore normal motor behaviour.

For this purpose, we employed optogenetic approaches to compare the effect of our manipulation during dyskinetic behaviour.

3. STUDY I

Preferential modulatory action of 5-HT_{2A} receptors on the dynamic regulation of Basal Ganglia circuits

In the present chapter, you will find the work done in the first period of my PhD, under the supervision of Dr. Morera-Herreras. As mentioned in the introductory notes, this study gave rise to the writing of a paper currently under review. So, as a preview you can find a similar version in the following sections.

Summary

Motor and medial prefrontal (mPF) basal ganglia (BG) circuits play an important role in integrative brain functions like movement control or cognitive/motivational behaviour, respectively. Although these neuronal networks express 5-HT_{2A} receptors, the expression is higher in the associative/limbic structures than in the motor ones. In this study, we show a topographical-dependent dissociation in the effects triggered by the 5HT_{2A} agonist TCB-2, which specifically increases the medial SNr neuron activity and has a preferential action on mPF information processing through the striato-nigral direct pathway. These are very likely to be 5-HT_{2A} receptor-mediated effects that require mobilisation of the endogenous 5-HT system. These findings provide evidence about the specific signature of 5-HT_{2A} receptors on the dynamic regulation of BG circuits.

3.1. Material and methods

All animal procedures described in this part were conducted in accordance with the European Community Council Directive on “The Protection of Animals Used for Scientific Purposes” (2010/63/EU) and the Spanish Law (RD 53/2013). The experimental protocols were reviewed and approved by the Local Ethical Committee for Animal Research of the University of the Basque Country (UPV/EHU, CEEA, Ref. ES48/054000/6069). Every effort was made to minimise animal suffering and to use the minimum number of animals per group and experiment.

3.1.1. Animals

Experiments were performed on adult male Sprague–Dawley rats (280–330 g). Rats were housed collectively (five per cage) under standard laboratory conditions ($22 \pm 1^\circ\text{C}$, $55 \pm 5\%$ relative humidity, and 12:12 hr light/dark cycle) with food and water provided *ad libitum*.

A total of 127 rats were used for the characterisation of the spontaneous and cortically evoked activity of SNr neurons, and these were further subdivided into two subgroups for recording either in motor or mPF circuits. The experimental groups used in this study are detailed in the following section.

3.1.2. Pharmacology

These drugs were used in the present study: the 5-HT_{2A} receptor agonist TCB-2, the preferential 5-HT_{2A} receptor antagonist MDL11939 (α -phenyl-1-(2-phenylethyl)-4-piperidinemethanol) and, the non-selective 5-HT receptor antagonist methiothepin were obtained from Tocris Bioscience (Spain); the tryptophan hydroxylase inhibitor 4-chloro-DL-phenylalanine methyl ester hydrochloride (pCPA) and chloral hydrate from Sigma-Aldrich Quimica (Spain); the selective 5-HT reuptake inhibitor (SSRI) fluoxetine, from Biotrend (Germany) (Table 3.1). All drugs, TCB-2, MDL11939, methiothepin, pCPA, fluoxetine, and chloral hydrate, were freshly prepared in physiological saline (NaCl 0.9%) before immediate use on the day of the experiment.

Table 3.1. Used drugs and their pharmacological activity

DRUGS	ACTIVITY	PURCHASE
Chloral hydrate	anesthetic	Sigma-Aldrich Quimica (Spain)
4-chloro-DL-phenylalanine methyl ester hydrochloride (pCPA)	tryptophane hydroxylase inhibitor	Sigma-Aldrich Quimica (Spain)
Fluoxetine	selective 5-HT reuptake inhibitor (SSRI)	Biotrend (Germany)
TCB-2	5HT _{2A} receptor agonist	Tocris Bioscience (Spain)
MDL 11,939	selective 5HT _{2A} receptor antagonist	Tocris Bioscience (Spain)
Methiotepin maleate	non-selective 5HT receptor antagonist	Tocris Bioscience (Spain)

TCB-2 was chosen for its high affinity for 5-HT_{2A} receptors because, to the best of our knowledge, no selective agonist for this receptor subtype has been synthesised to this date.

MDL11939 was selected for being one of the most selective 5-HT_{2A} receptor antagonists available for research use. Doses were selected based on previous electrophysiological studies reporting their efficacy and selectivity (Delicata et al., 2018; Venzi et al., 2016).

pCPA and fluoxetine were used to address the role of endogenous 5-HT in the effects triggered by TCB-2. pCPA-treated animals (n=39; n=21 for motor and n=18 for mPF circuits) were injected intraperitoneally with the tryptophan hydroxylase inhibitor for three consecutive days at a daily dose of 300 mg/kg and recorded 24 h after the last administration. This pCPA dosage regimen has been shown to cause an almost complete depletion of 5-HT throughout the brain while leaving catecholamine levels intact (Edén et al., 1979; Miczek et al., 1975; Naslund et al., 2015; Näslund et al., 2013; Pettersson et al., 2016).

For the control group, we used vehicle-treated animals, which received intraperitoneal daily injections of 0.9% saline for three consecutive days.

The fluoxetine-treated rats (n=18; n=9 for motor and n=9 for mPF circuits) received an acute administration of the SSRI (10 mg/kg, i.p.). This acute dose of fluoxetine has been reported as being capable of inducing elevated brain levels of 5-HT that remain stable for at least 6 h following the injection (Volle et al., 2018). For this reason, animals were recorded between 1 and 6 h following the fluoxetine administration. Taking into account that data from vehicle-treated rats did not differ from those of control animals, this group was also used as a control group for a group acutely injecting with fluoxetine.

3.1.3. Electrophysiological procedures

3.1.3.1. Animal preparation and surgery

Animals were anaesthetised with chloral hydrate (420 mg/kg i.p. for induction followed by continuous administration of chloral hydrate at a rate of 115 mg/kg i.p. per hour using a peristaltic pump to maintain a steady level of anaesthesia). For additional drug administration, the right jugular vein was cannulated with a polyethylene cannula (Clay Adams, Becton Dickinson and Company Division, model PE-240). The rat was then placed in a stereotaxic frame with its head secured in a horizontal orientation, and the body temperature was maintained at ~37°C for the entire experiment with a heating pad connected to a rectal probe. The skull of each animal was exposed, and two 3-mm burr holes were drilled over the lateral or medial SNr and the ipsilateral motor cortex (MC) or mPF cortex (mPFC), respectively.

3.1.3.2. Recording electrode preparation

In vivo single-unit, extracellular recordings were performed by an Omegadot single glass micropipette, pulled with an electrode puller (Narishige Scientific Instrument Lab., PE-2, Japan), broken back to a tip diameter of 1-2.5 µm under a light microscope and filled with 2% pontamine sky blue in 0.5% sodium acetate. This electrode was lowered into the motor (lateral) or mPF (medial) SNr region following coordinates specified in **Table 3.2**.

Table 3.2. Stereotaxic coordinates of electrophysiological recordings and stimulation electrodes.

	STRUCTURE	TYPE OF ELECTRODE	COORDINATES		
			AP	ML	DV
Recording	SNr medial part	Glass micropipette	-5.3 mm	- 1.7 mm	~ - 7.5 mm
Stimulation	Motor cortex (MC)	Stainless-steel electrode	- 3.5 mm	- 3.2 mm	- 1.6 mm
Recording	SNr lateral part	Glass micropipette	- 5.6 mm	- 2.2 mm	~ - 7.5 mm
Stimulation	medial prefrontal cortex (mPFC)	Stainless-steel electrode	- 2.9 mm	- 0.6 mm	- 1.7 mm

3.1.3.3. Electrical stimulation of the cortex

The MC or the mPFC (see the specific coordinates in **table 3.2**) ipsilateral to the recording site was electrically stimulated (pulse width 600 μ s; frequency 1 Hz; intensity 1 mA) using coaxial stainless-steel electrodes (diameter, 250 μ m; tip diameter, 100 μ m; tip-to-barrel distance, 300 μ m; Cibertec S.A.). Our previous electrophysiological and histological verifications demonstrated no cortical tissue damage or plasticity phenomena after this stimulation protocol (Antonazzo et al., 2019).

3.1.3.4. Recording and neuronal identification

For single-unit extracellular recording, the electrode was lowered in the above-described SNr coordinates by a hydraulic microdrive (David Kopf® Instruments, Tujunga, California, EEUU, model 640). The electrical extracellular signal from the electrode was first pre-amplified (10x) and after amplified (10x) with a high-input impedance amplifier (Cibertec S.A., model amplifier AE-2), and then simultaneously monitored on an oscilloscope (HAMEG® analog digital scope HM407-2) and on an audio monitor (Cibertec S.A., model AN-10). Next, the signal was bandpass filtered at 30-5000 Hz in a second amplifier (Cibertec S.A., model amplifier 63AC) and finally, neuronal action potentials or “spikes” were digitised using a computer software (CED micro 1401 interface and Spike2 software, Cambridge Electronic Design, UK).

All SNr neurons were identified as GABAergic by their classically defined electrophysiological properties: spike width < 2 ms and the ability to present relatively high-frequency discharges without a decrease in spike amplitude (as described in Antonazzo et al., 2019). After identifying a stable baseline of the frequency of discharge of an SNr neuron (variation of the firing rate $\leq \pm 10\%$), the basal firing rate was recorded for 3-5 min. Then, the protocol of stimulation was performed (Figure 3.1)

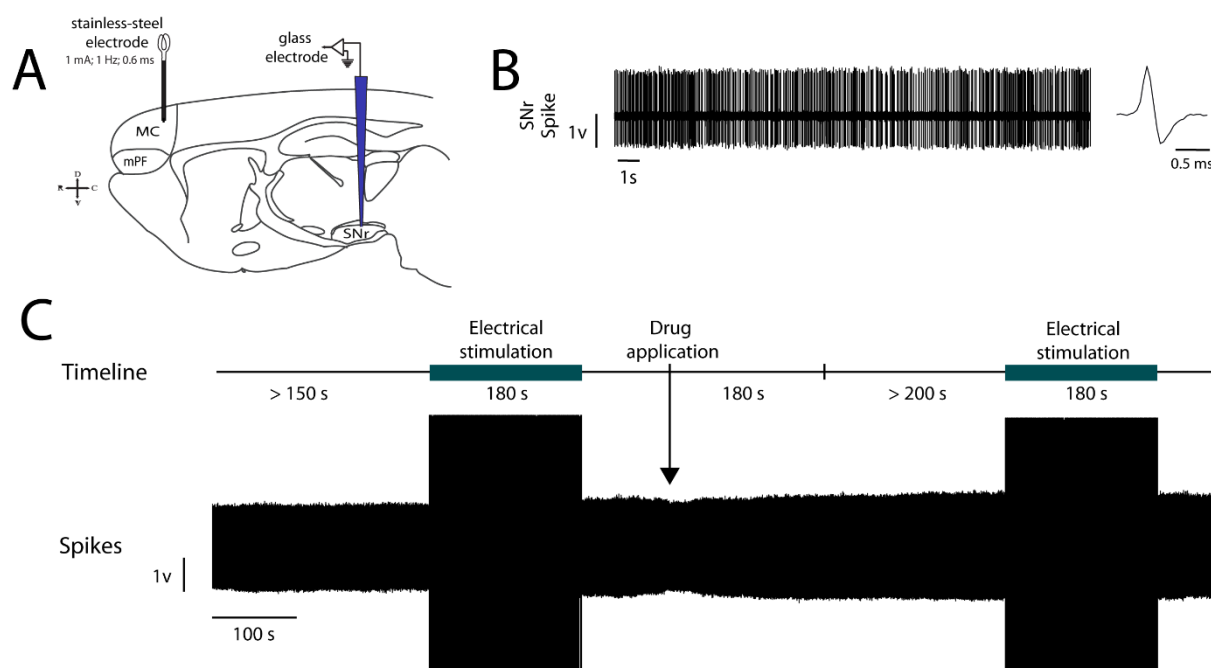


Figure 3.1. Schematic representation of the experimental design. **A**, Schematic representation of the experimental paradigm using Sprague Dawley rats. Stimulation electrodes were placed into the MC or mPF following the circuit studied, the glass pipette was placed into the medial or the lateral part of the SNr. Glass pipette contained Pontamine Sky Blue. **B**, Spontaneous activity of SNr neurons. **C**, Timeline example for the recording of a single SNr neuron.

Cortical stimulation evoked triphasic responses in SNr neurons consisting of a combination of early excitation (EE), inhibition (I), and/or late excitation (LE) (Aliane et al., 2009; Kolomiets et al., 2003; Maurice et al., 1999). Only SNr neurons responding to cortical stimulation were analysed in this study. The cortically evoked response was recorded for 3 min.

Thereafter, in the pharmacological assays, the outcome of the spontaneous and cortically evoked response of the SNr neuron was studied before and after the administration of the corresponding drug (TCB-2, MDL11939 or methiothepin). For this purpose, after the initial baseline characterisation, the drug was administered intravenously and, after 5 minutes, the spontaneous and stimulation-evoked activity were recorded again (for 5 and 3 min,

respectively). This protocol was repeated for different doses of the same drug or for consecutive administration of different drugs (MDL11939 + TCB2). Multiple neurons were recorded in each animal to characterise spontaneous and cortically evoked activity in both motor and mPF circuits, however, only one SNr cell responding to cortical stimulation was pharmacologically studied per animal. When possible, drugs were tested on neurons presenting a triphasic response, to fully characterise the effects of the drugs over cortico-nigral transmission.

3.1.4. Electrophysiological data analysis

Firing parameters of SNr neurons were analysed offline using the Spike2 software (version 7). The following parameters were evaluated:

Firing rate (FR): It is defined by the number of action potentials per second (expressed in Hz). The mean FR at baseline and after drug administration was quantified for at least 200 s.

Coefficient of Variation (CV): it consists of the ratio, expressed as a percentage, between the standard deviation and the mean of the neuron's interspike interval histogram. This histogram was made with 1 ms bins and considering all the inter-spike intervals below 0.5 s given the relatively high firing rate of SNr neurons.

Burst firing pattern: The existence of burst firing in neurons was determined through a Spike2 script ("surprise.s2s"), based on the Poisson surprise algorithm. Burst-related parameters (number of bursts, duration of bursts, number of spikes per burst, recurrence of bursts, and intra-burst frequency) were analysed during time epochs of 150 seconds under basal conditions, or for 120 seconds once the drug was administered. This was done using a script written for the Spike2 software. Briefly, this analysis evaluates how improbable any given burst that contains n spikes in a time interval T , occurred by chance and computed as follows: $S = -\log p$, where p is the probability that, in a random (Poisson) spike train having the same average spikes rate r as the spike train studied, a given time interval of length T contains n or more spikes. p is given by Poisson's formula. S refers to the Poisson Surprise of the burst (the degree to which the burst surprises a person who expects the spike train to be a Poisson process). In this study, only spike trains with $S \geq 3$ were considered to be bursting.

To analyse the cortically evoked responses in the SNr neurons, peristimulus time histograms (PSTHs) were generated from 180 stimulation trials using 1 ms bins. The criterion used to determine the existence of an excitatory response was a two-fold increase of the standard

deviation plus the mean number of spikes in the pre-stimulus period, for at least three consecutive bins. The amplitude of excitatory responses was quantified by calculating the mean number of spikes evoked within the excitation time window, with the mean number of spikes occurring spontaneously before the stimulation. The duration of an inhibitory response corresponded to the time interval without spikes for at least three consecutive bins (Figure 3.2).

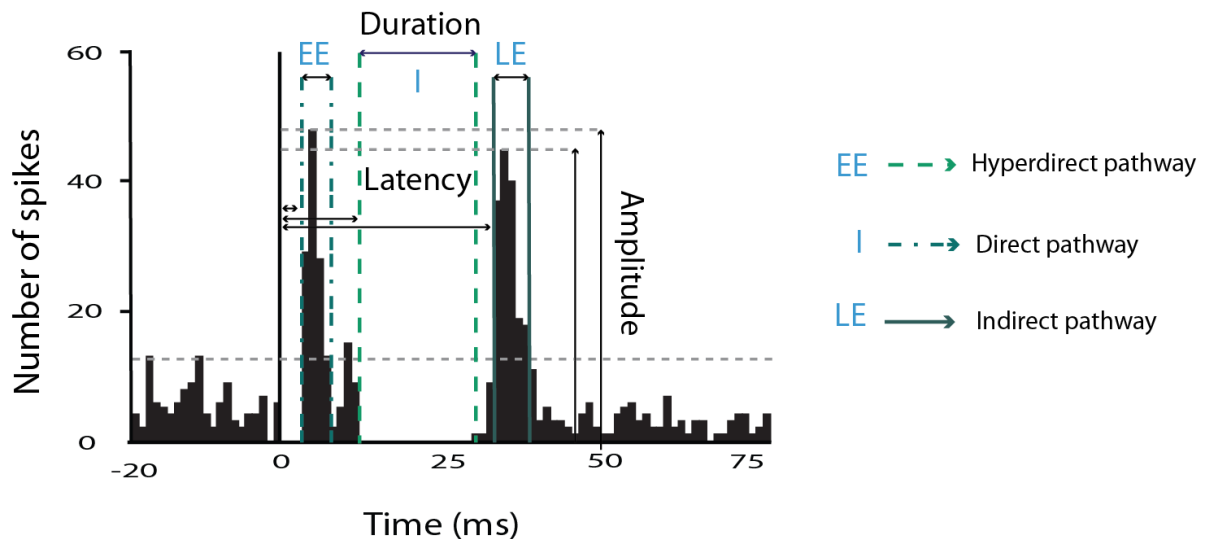


Figure 3.2. Peristimulus time histogram showing the characteristic triphasic response evoked in a SNr neuron after MC or mPFC stimulation. Peristimulus time histogram showing the characteristic cortically evoked triphasic response in SNr neurons. EE: Early Excitation corresponds to the activation of the hyperdirect pathway (cortex-STN-SNr). I: Inhibition corresponds to the activation of the direct pathway (cortex-STR-SNr). LE: Late excitation corresponds to the activation of the indirect pathway (cortex-STR-GPe-STN-SNr). The vertical black line at 0 ms represents the time when the stimulus was applied. The horizontal dashed lines in grey show the threshold above which a response was considered excitatory. Other lines and arrows show the parameters for the analysis of different epochs. Duration indicates how long a response occurred, latency represents the time from the stimulation to the response and amplitude indicates the magnitude of the excitatory responses.

3.1.5. Statistical analysis

Experimental data proceeding only from stimulation-responding neurons were analysed using the computer program GraphPad Software (v. 5.01, GraphPad Software, Inc; RRID: SCR_002798). To explore differences in pCPA- and fluoxetine-treated groups in the firing rate, CV and cortically evoked responses in lateral and medial SNr neurons, one-way analysis of variance (ANOVA), followed by *post hoc* comparisons using Bonferroni's *post hoc* test, was used. The chi-squared (χ^2) test was used to determine differences in neurons exhibiting burst firing patterns and changes in the occurrence of cortically evoked responses, as well as in the

different patterns occurring after cortical stimulation. Burst-related parameters were analysed using the Kruskal-Wallis test, except for the intra-burst frequency, which was analysed using ANOVA, followed by Bonferroni's *post hoc* test.

To assess the effect of TCB-2, MDL11939 and methiothepin in motor and mPF circuits, repeated measures one-way ANOVA was used followed by Bonferroni's *post hoc* test to compare the mean values of the firing rate, CV, and parameters related to cortically-evoked responses before and after drug application. To evaluate the effect of a single dose of TCB-2 (100 µg/kg, i.v.) on cortically evoked responses, a paired two-tailed Student's *t* test was used. Chi-squared (χ^2) tests before and after drug application were also used to study the effects of these drugs on burst activity. The level of statistical significance was set at $p < 0.05$. Data are presented as group means \pm standard error of the mean (SEM) of *n* neurons.

3.1.6. Verification of the recording and stimulation sites

In a set of experiments, at the end of SNr recordings, histological verifications of the cortical stimulation site (MC or mPFC) and of the recording place within lateral or medial SNr were carried out (Figure 3.3). A 10 µA cathodic current was constantly applied through the recording electrode for 10 minutes to allow the formation of a Pontamine Sky Blue deposit on the recording site. In these cases, animals were deeply anaesthetised with chloral hydrate (1 g/kg, i.p) and transcardially perfused with phosphate buffer saline (PBS; 0.1M, pH=7.4), followed by 4% ice-cold paraformaldehyde in PBS. Brains were removed and post-fixed in paraformaldehyde for at least 24h at 4°C. Afterward, brains were transferred to a 30% sucrose solution until they sank. Brains were cut in 40-µm coronal sections using a freezing microtome (HM 430, Microm®), and slices were conserved in a cryoprotectant solution (30% ethylene glycol and 26% glycerol in PBS) at -20 °C until further processing. Coronal brain sections containing the SNr were mounted on gelatinised glass slides, stained with 1% Neutral Red for 10 minutes, washed in distilled water, dehydrated in an ascending series of alcohol, cleared with xylene, and coverslipped with DPX (Sigma-Aldrich) mounting medium. A blue dot on the lateral or medial portion of the SNr, examined under a microscope, determined the correct placement of the recording electrode.

To check the correct placement of the stimulation electrode, a 1 mA cathodic current was passed through the electrode for 10 minutes to allow the deposition of iron at the tip of the electrode. Brains removed after perfusion were post-fixed in a solution containing 80% of a 4% paraformaldehyde solution, 20 % of ethanol containing 2% acetic acid, and 1% (w/v) of potassium ferricyanide. This stained the iron deposit of the electrode in blue, showing the stimulation site. Coronal sections containing the MC or ACC were mounted on gelatinised

glass slides, and if the blue point was apparent, sections were counterstained with Neutral red as described above.

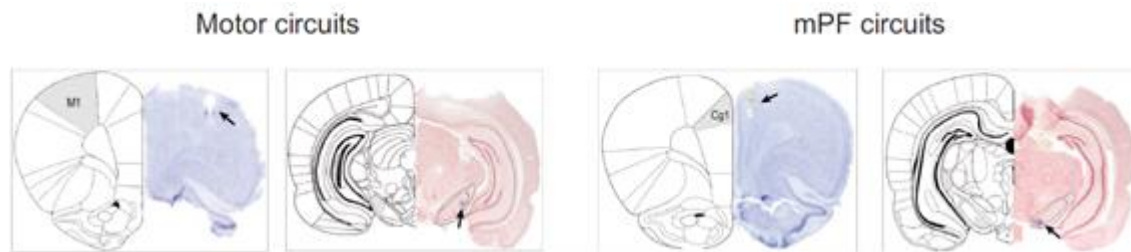


Figure 3.3. Representative coronal brain slices showing the placement of the stimulation and recording electrodes. Left, when studying the motor circuits the stimulation electrode was placed in the MC (M1) and the recording site was in the lateral SNr, as shown by the deposition of Pontamine Sky Blue. Right, when studying the medial prefrontal (mPF) circuits, the stimulation electrode was placed in the mPFC (Cg1) and the recording site was in the medial SNr, as shown by the deposition of Pontamine Sky Blue. Arrowheads indicate the place where these electrodes were placed.

3.2. Results

3.2.1 Modulatory action of 5HT_{2A} receptor on spontaneous and cortically evoked activity of SNr neurons

3.2.1.1. Effect of the 5-HT_{2A} receptor agonist TCB-2 on spontaneous and cortically evoked activity of SNr neurons

To study the functional role of the 5-HT_{2A} receptor on SNr neuron activity, we first examined the effect of the 5-HT_{2A} receptor agonist TCB-2 on the electrical activity of lateral and medial SNr neurons from vehicle-treated animals. As already mentioned, SNr neurons were separately recorded from lateral and medial territories (Figure 3.4A) in 16 rats (n=7 for the motor circuit and n=6 for the mPF circuit). To ensure the SNr cells belong to their corresponding BG circuit, only those responding to cortical stimulation were used in the analysis (success rate: 98.7% and 48.6% for motor or mPF circuits, respectively). Data on spontaneous and cortically evoked activity did not differ from those obtained in control animals of this study.

The systemic administration of TCB-2 (50-200 µg/kg, i.v, doubling doses) did not modify the basal firing rate, coefficient of variation, nor the firing pattern of lateral SNr neurons (Figure 3.4B-D, green). In contrast, in medial SNr neurons, TCB-2 administration produced a significant increase, in the basal firing rate in a dose-dependent manner (maximal increment of the firing rate was 32% of the basal value) ($F_{(3,20)}=12.33$, $p=0.0003$, repeated measures one-way ANOVA; Figure 3.4B, blue), while the regularity and the firing pattern remained unaltered (Figure 3.4C-D).

We next investigated the effect of the 5-HT_{2A} receptor activation on cortically evoked responses of lateral and medial SNr neurons. According to previous studies, stimulation of the MC or mPFC evoked characteristic triphasic responses in SNr neurons (30.1% of the recorded cells in the lateral SNr and 29.0% in the medial SNr) that consisted of an early excitation (EE) followed by an inhibition (I) and a late excitation (LE). As illustrated in Figure 3.4A, EE is attributable to the activation of the “hyperdirect” cortico-subthalamo-nigral pathway, I to the activation of the “direct” cortico-striato-nigral pathway, and LE to the activation of the “indirect” cortico-striato-pallido-subthalamo-nigral pathway (Maurice et al. 1999). Furthermore, different patterns of responses could be observed in both SNr territories. In addition to triphasic responses, biphasic and monophasic cortically evoked responses were recorded in both SNr territories from the activation of the different pathways along the circuits (Figure 3.10A-C). The percentage of occurrence of such patterns of responses in lateral and medial SNr neurons is shown in Figure 3.10D-G.

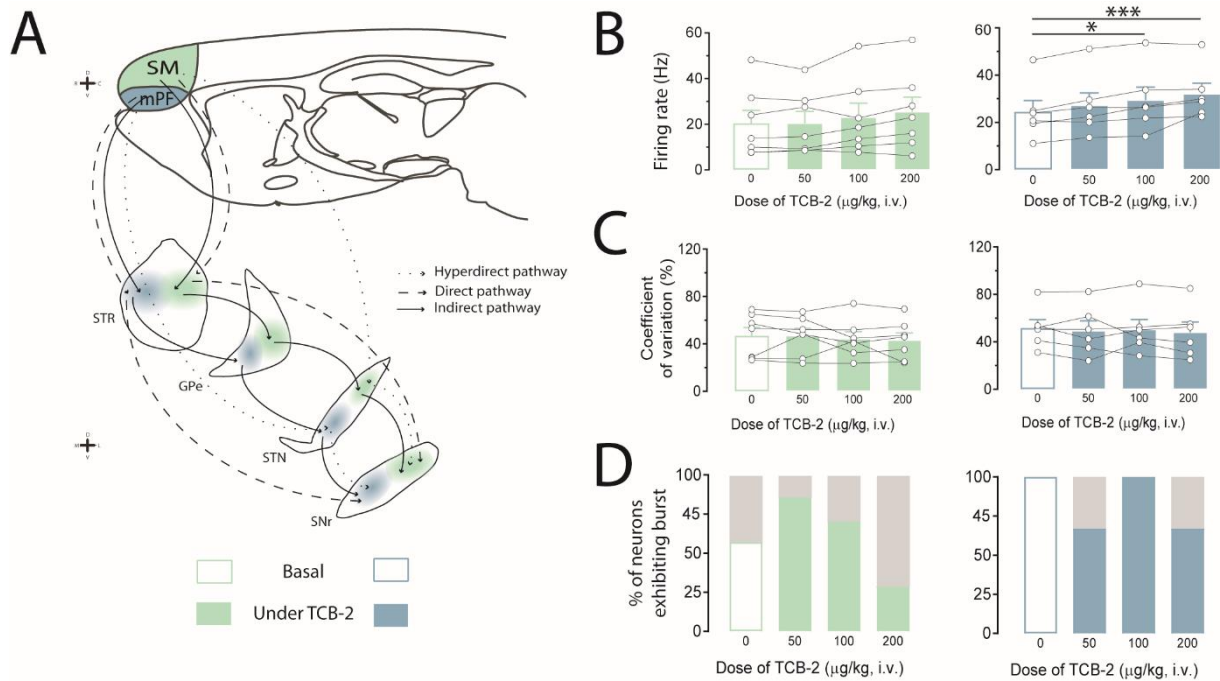


Figure 3.4. Effect of systemic administration of cumulative doses of the selective 5-HT_{2A} receptor agonist TCB-2 on spontaneous activity of lateral and medial *substantia nigra pars reticulata* neurons. **A**, Schematic sagittal section of the rat brain showing cortico-nigral information transmission through the motor (in green) and medial prefrontal (mPF) (in blue) basal ganglia circuits. Additional coronal sections of the different BG nuclei show their involvement in the different pathways. Cortical information is transferred through the hyperdirect pathway (cortex-STN-SNr, dotted line), the direct pathway (cortex-STR-SNr, dashed line), and the indirect pathway (cortex-STR-GPe-STN-SNr, solid line). **B-C-D**, Histograms illustrating the effect of cumulative doses of TCB-2 (50 - 200 µg/kg, i.v., doubling doses) on the firing rate, mean of coefficient of variation, and firing pattern (% of bursting (colour) vs. non-bursting (grey)) of SNr neurons from the motor (B, C, D in green) and from the mPF (B, C, D in blue) circuits recorded in anesthetised rats 24 h after the last vehicle injection. Each bar represents the mean \pm SEM of n neurons. Each dot represents a single neuron. * $p < 0.05$, *** $p < 0.001$ vs. basal. Bonferroni's *post hoc* test.

To accurately analyse cortically evoked responses, the dose of TCB-2 was carefully selected from the above-described results with the view to minimise any effect on the firing activity of SNr neurons, which could make the analysis of the cortically evoked responses difficult. In lateral SNr neurons, systemic administration of TCB-2 (100 µg/kg, i.v.) diminished the duration of the late excitation ($t_{(6)}=3.118$, $p=0.0206$, paired Student's t -test) without changing early excitation or inhibition (Figure 3.5A, B). In medial SNr neurons, TCB-2 significantly increased the duration of the inhibition ($t_{(4)}= 3.352$, $p=0.0285$, paired Student's t test), whereas it reduced the duration of the late excitation ($t_{(4)}= 3.206$, $p=0.0327$, paired Student's t test) (Figure 3.5C,D).

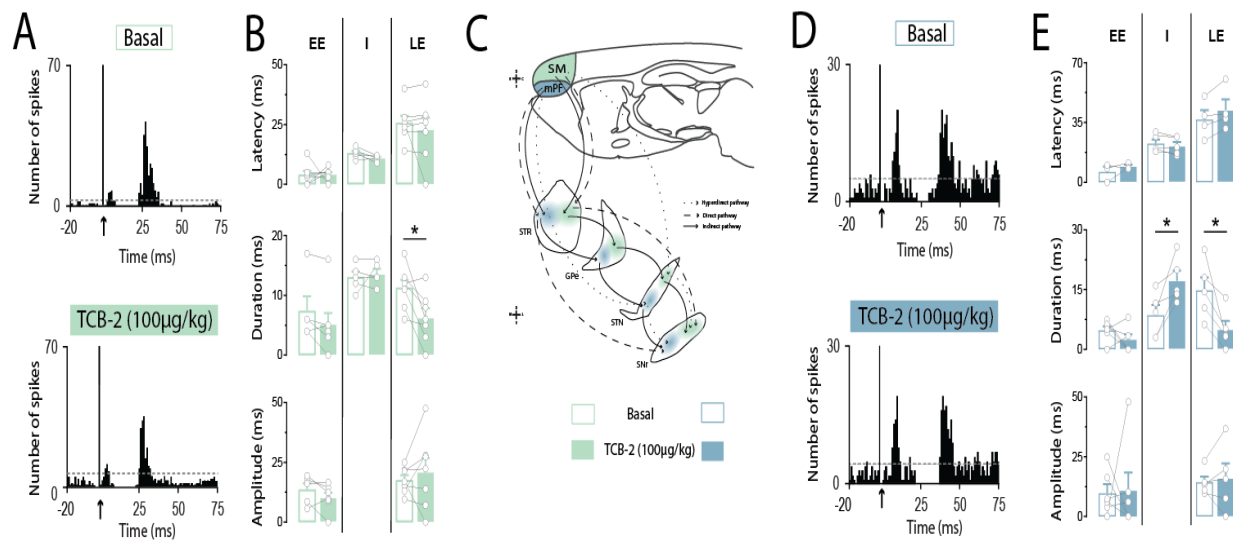


Figure 3.5. Effect of systemic administration of TCB-2 on cortically evoked responses in lateral and medial *substantia nigra pars reticulata* neurons. Representative peristimulus time histogram showing a triphasic response in a SNr neuron by stimulation of the MC (**A**) or mPFC (**D**) in basal condition (top) and after administration of TCB-2 (100 µg/kg, i.v.) (Bottom). Bar graphs illustrate the effect of TCB-2 on cortically evoked responses in SNr neurons ($n \geq 5$ for each epoch) from motor (**B**) or medial prefrontal (**E**) circuits. Arrows indicate the stimulation artefact. Dashed lines indicate the threshold for excitatory responses. EE: early excitation, I: inhibition, and LE: late excitation. Each bar represents the mean \pm SEM of n neurons. Each dot represents a single neuron. * $p < 0.05$, vs. basal. Bonferroni's *post hoc* test.

3.2.1.2. Effect of the 5-HT_{2A} receptor blockade on spontaneous and cortically evoked activity of SNr neurons

In order to confirm the 5-HT_{2A} receptor implication in the observed effects, changes in SNr neuron activity induced by TCB-2 after the administration of the preferential 5-HT_{2A} receptor antagonist MDL11939 were evaluated. Thus, in medial SNr neurons, the effects induced by TCB-2 on the firing rate were effectively blocked by the previous administration of MDL11939 (200 µg/kg, i.v.) ($p > 0.05$, repeated-measures one-way ANOVA). Additionally, no changes in the spontaneous activity of medial or lateral SNr cells were found after the selective 5-HT_{2A} antagonist at the administered dose (Figure 3.6).

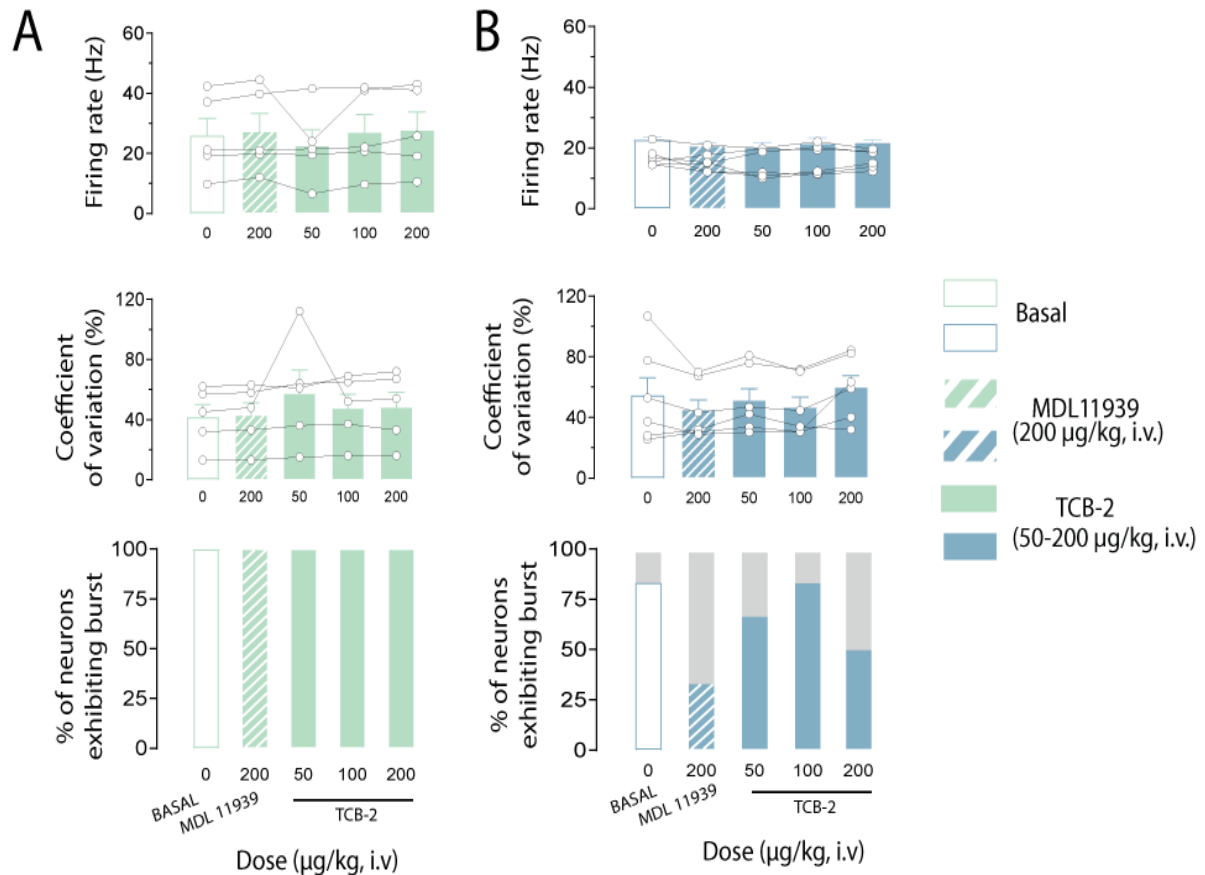


Figure 3.6. Blockade of the effects of TCB-2 by the previous administration of the preferential 5-HT_{2A} receptor antagonist MDL11939 on the spontaneous activity of lateral and medial *substantia nigra pars reticulata* neurons. Administration of MDL11939 (200 µg/kg, i.v.) did not show any effect by itself in the mean firing rate, mean coefficient of variation and firing pattern (percentage of bursting (colour) vs. non-bursting (grey)) of SNr neurons from the motor (**A**) and the mPF (**B**) circuits. However, this dose of MDL11939 was able to block the effects observed after TCB-2 administration in the firing rate of medial SNr neurons. Each bar represents the mean \pm SEM of *n* neurons. Each dot represents a single neuron.

We next looked at cortical evoked responses. In all the lateral and medial SNr recorded neurons, the previous administration of the preferential 5-HT_{2A} antagonist MDL11939 (200 µg/kg i.v) blocked the effects induced by TCB-2 administration (100 mg/kg, i.v.) on the cortico-nigral transmission through the motor and mPF BG circuits. Moreover, MDL11939 did not alter the cortically evoked responses ($p > 0.05$, repeated-measures one-way ANOVA for early excitation, inhibition, and late excitation in both circuits) (Figure 3.7).

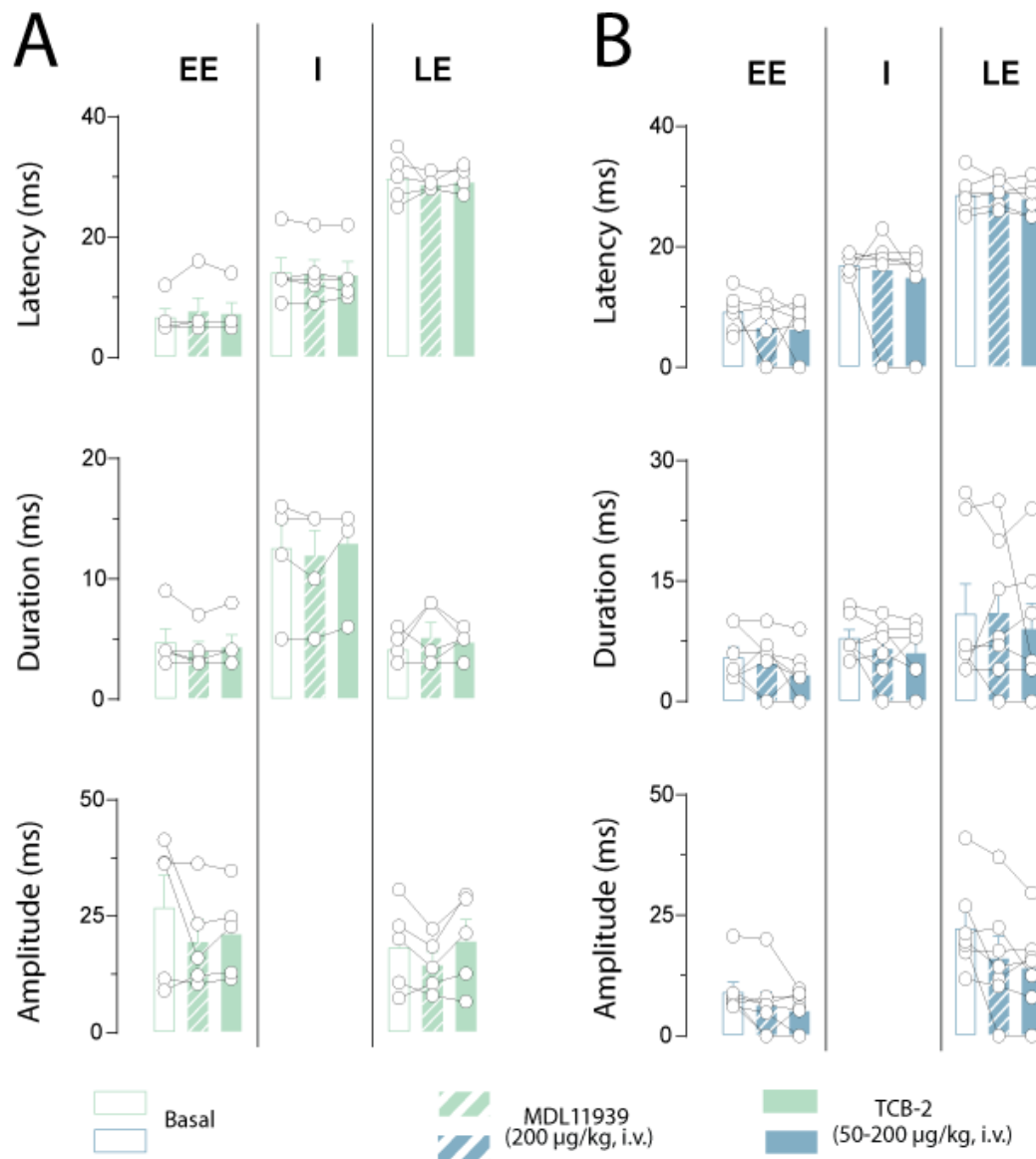


Figure 3.7. Blockade of the effects of TCB-2 by the previous administration of the preferential 5-HT_{2A} receptor antagonist MDL11939 on cortically evoked responses in lateral and medial *substantia nigra pars reticulata* neurons. Bar graphs showing the mean effect of MDL11939 (shaded bar) and TCB-2 (full bar) on cortically evoked responses in SNr neurons ($n \geq 5$ for each epoch) in motor (A) and mPF (B) circuits. MDL11939 caused no effect by itself on the cortically evoked activity of these neurons. EE: early excitation, I: inhibition, and LE: late excitation. Each bar represents the mean \pm SEM of n neurons. Each dot represents a single neuron.

In order to confirm the lack of effect of the 5-HT_{2A} antagonist MDL11939, presumably suggesting that endogenous 5-HT does not exert a tonic control on SNr neuron electrical activities via 5-HT_{2A} receptors, we studied the effect of the non-specific 5-HT receptor antagonist methiothepin on the spontaneous and cortically evoked activity of SNr neurons.

Systemic administration of cumulative doses of methiothepin (25-100 $\mu\text{g/kg}$, i.v.; doubling dose) did not produce any significant modification of lateral and medial SNr neuron activity or cortico-nigral transmission through the motor and mPF circuits (Figure 3.8).

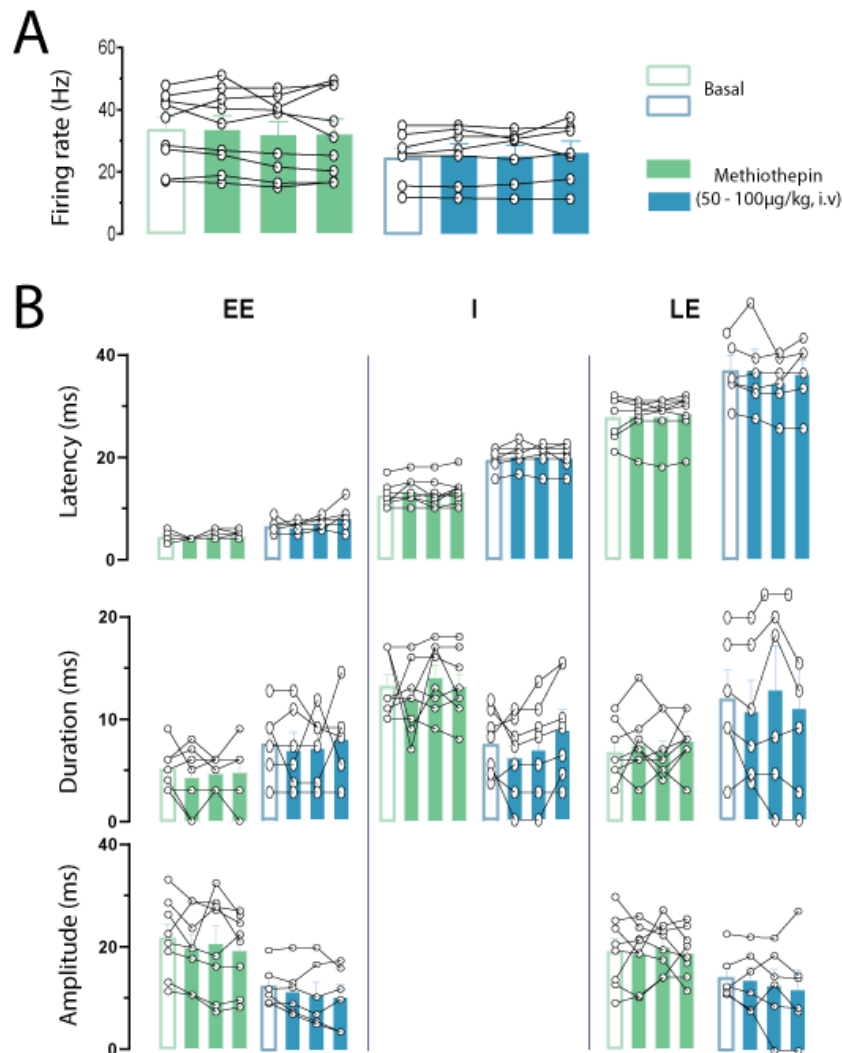


Figure 3.8. Effects of the systemic administration of a cumulative dose of the non-selective 5-HT antagonist methiothepin on the spontaneous and cortically evoked activity of lateral and medial *substantia nigra pars reticulata* neurons. **A**, Mean firing rate of lateral (green) and medial (blue) SNr neurons. Cumulative doses of the non-selective 5-HT receptor antagonist methiothepin (25-100 $\mu\text{g/kg}$, i.v.) induced no changes in either of the analysed spontaneous electrophysiological parameters. **B**, Histograms illustrating the effect of the administration of cumulative doses of methiothepin (25-100 $\mu\text{g/kg}$, i.v.) on the different components (i.e., EE, I and LE) of the cortically evoked activity of SNr neurons from the motor (green) and mPF circuits (blue), and the different electrophysiological parameters analysed (i.e., latency, duration and amplitude). Administration of methiothepin (25-100 $\mu\text{g/kg}$, i.v.) induced no changes in either of the electrophysiological parameters analysed regarding the cortically evoked responses observed in lateral and medial SNr neurons. EE: early excitation, I: inhibition, and LE: late excitation. Each bar represents the mean \pm SEM of n neurons. Each dot represents a single neuron.

3.2.2 Role of the endogenous 5-HT in the effects triggered by TCB-2

3.2.2.1 Effect of the 5-HT depletion on spontaneous activity and cortically evoked response of SNr neurons

Next, to study the contribution of the endogenous 5-HT in the TCB-2-mediated effects, we administered the drug to animals treated with the 5-HT synthesis inhibitor pCPA (300 mg/kg, i.p., for 3 days). To do so, we first characterised the spontaneous and cortically evoked activity of lateral and medial SNr neurons from pCPA-treated-animals (57 lateral neurons from n=15 rats and 46 medial SNr neurons from n=12 rats) and the results were compared with those obtained in their respective vehicle-treated animals (74 lateral neurons from n=20 rats and 35 medial SNr neurons from n=10 rats).

As illustrated in the Figure 3.9A, compared to the vehicle-treated group, the mean basal firing rate of lateral SNr neurons was significantly higher in pCPA-treated animals ($F_{(2,189)}=12.82$, $p<0.001$, one-way ANOVA), whereas it remained unchanged in medial SNr neurons from these animals (Figure 3.9B). Moreover, no differences were found in the rest of the analysed parameters.

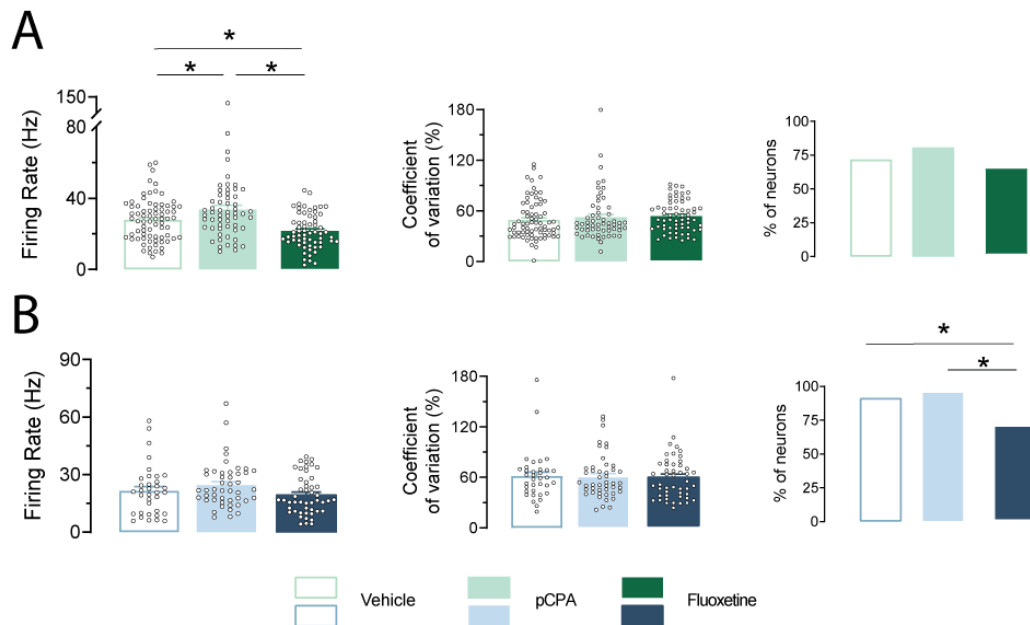


Figure 3.9. Effect of the administration of the 5-HT synthesis inhibitor pCPA (300 mg/kg/day, i.p. 3 days) or the selective 5-HT reuptake inhibitor fluoxetine (10 mg/kg, i.p.) on the spontaneous activity of lateral and medial *substantia nigra pars reticulata* neurons. Histograms illustrating the effect on the mean firing rate (left), mean coefficient of variation (middle) and firing pattern (right) (percentage of bursting (colour) vs. non-bursting (grey)) of the administration of vehicle or pCPA (300 mg/kg/day, i.p., 3 days) in lateral (**A**) and medial (**B**) SNr neurons recorded 24 h after the last injection, and of the acute dose of fluoxetine (10 mg/kg, i.p.) during the 6 following hours after its administration. Each bar represents the mean \pm SEM of n neurons. Each dot represents a single neuron. * $p<0.05$. Firing rate, Bonferroni's *post-hoc* test; neurons exhibiting burst firing pattern, Chi-square test.

Next, we analysed the cortically evoked responses of lateral and medial SNr neurons. pCPA treatment did not induce any changes in the percentage of neurons displaying different patterns of response in any of the SNr sub-territories studied (Figure 3.10). However, regarding the electrophysiological parameters of the cortically evoked responses in SNr neurons, in pCPA-treated animals, we observed an enhancement in the duration of the inhibition in medial SNr neurons (related to the direct pathway in mPF circuits) ($F_{(2,66)}=5.812$, $p=0.0047$, one-way ANOVA; Figure 3.11B).

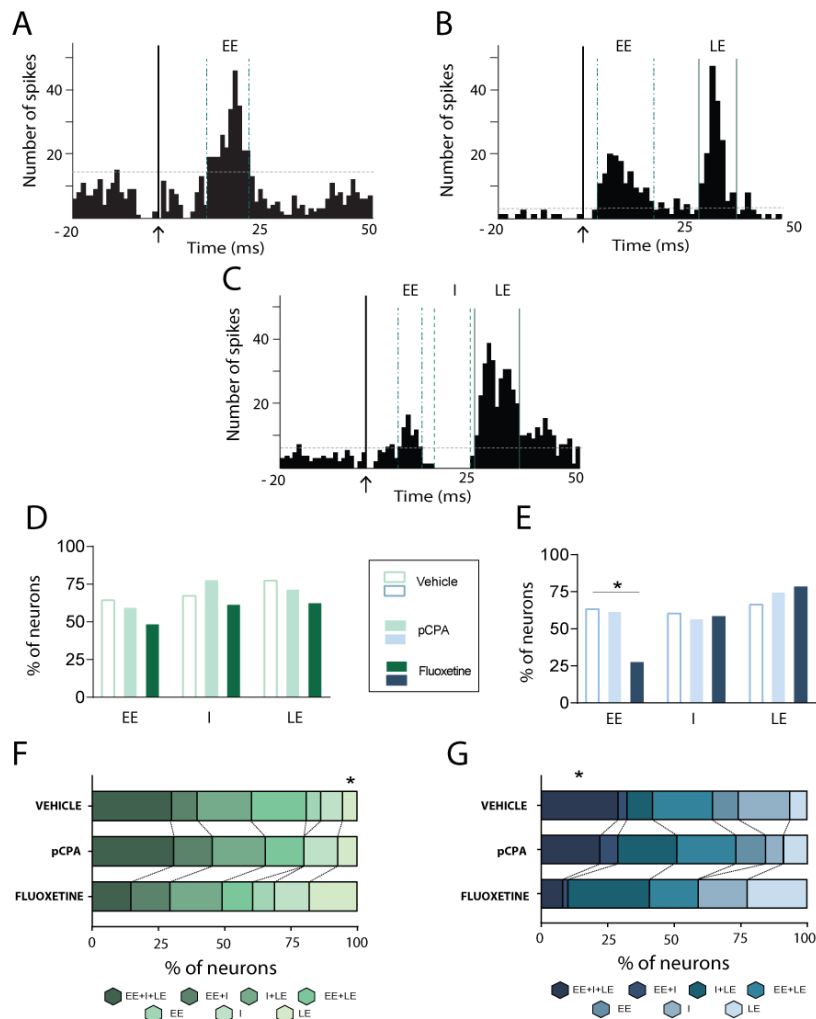


Figure 3.10. Patterns of response evoked in lateral and medial *substantia nigra pars reticulata* neurons by motor or mPF cortex stimulation. **A-C**, Peristimulus time histograms showing a representative example of a monophasic (**A**), biphasic (**B**) or triphasic (**C**) responses evoked in a SNr neuron from a vehicle-treated rat. Arrows indicate the cortical stimulation artefact. Dashed lines indicate the threshold for excitatory responses and vertical dashed, dotted, and solid lines highlight the separation of EE, I, and LE epochs. **D-E**, Percentage of SNr neurons displaying EE or LE, or I after motor (**D**) or mPF (**E**) cortical stimulation in vehicle-, pCPA- (300 mg/kg/day, i.p., 3 days), and fluoxetine- (10 mg/kg, i.p.) treated rats. Fluoxetine administration caused a decrease in the number of medial SNr neurons displaying an EE; $*p < 0.05$, Chi-square test. **F-G**, Percentage of occurrence of the different patterns of responses evoked in SNr cells by motor (**F**) or mPF (**G**) cortical stimulation in vehicle-, pCPA- and fluoxetine-treated rats. Fluoxetine decreased the number of lateral SNr neurons displaying LE (**F**) and the number of medial SNr neurons displaying triphasic responses (EE+I+LE) (**G**) $*p < 0.05$, Chi-square test. EE: early excitation, I: inhibition, and LE: late excitation.

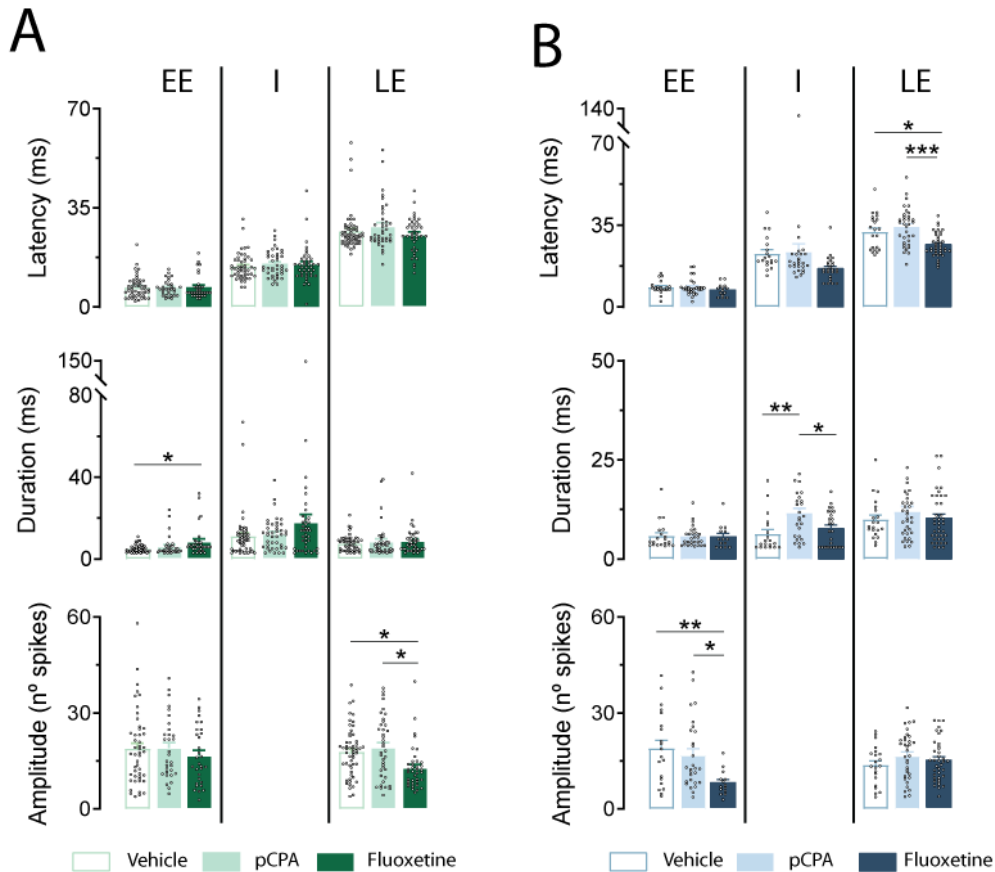


Figure 3.11. Effect of the treatment with vehicle, pCPA and fluoxetine on the cortically evoked responses in lateral and medial *substantia nigra pars reticulata* neurons. A-B, Histograms illustrating the effect of the treatment with vehicle, pCPA (300 mg/kg/day, i.p., 3 days) or fluoxetine (10 mg/kg, i.p.) on the electrophysiological parameters analysed from cortically evoked responses in lateral (A) and medial (B) SNr neurons. In lateral SNr neurons, fluoxetine was able to increase the duration of the EE and decrease the amplitude of the LE. Fluoxetine was also able to decrease the latency of the LE and the amplitude of the EE in neurons recorded in the medial SNr. In these neurons, pCPA increased the duration of the I. EE: early excitation, I: inhibition, and LE: late excitation. Each bar represents the mean \pm SEM of n neurons. Each dot represents a single neuron. * $p < 0.05$, ** $p < 0.01$, *** $p < 0.001$. Bonferroni's *post-hoc* test.

3.2.2.2 Effect of the 5-HT_{2A} receptor agonist TCB-2 in pCPA-treated animals

Once the impact of pCPA treatment on spontaneous and cortically evoked activity in SNr neurons was characterised, we investigated the contribution of the endogenous 5-HT in the TCB-2-mediated effects. In pCPA-treated animals, the systemic administration of TCB-2 (50-200 μ g/kg, i.v.) did not modify the firing rate, coefficient of variation or firing pattern of lateral SNr neurons ($n=6$) (Figure 3.12A). In medial SNr neurons from these animals ($n=6$), TCB-2 (50-200 μ g/kg, i.v.) also did not induce any changes in the basal firing rate nor the coefficient of variation, but the minimal dose of 5-HT_{2A} receptor agonist (50 μ g/kg, i.v.) significantly

reduced the number of neurons exhibiting a burst firing pattern ($\chi^2=8.0$, $p=0.0460$, chi-square test; Figure 3.12B). In addition, in contrast to the outcome observed in the vehicle-treated group, the administration of TCB-2 (100 $\mu\text{g/kg}$, i.v.) to pCPA-treated rats did not modify any of the studied parameters of the cortically evoked responses of lateral or medial SNr neurons (Figure 3.12C,D).

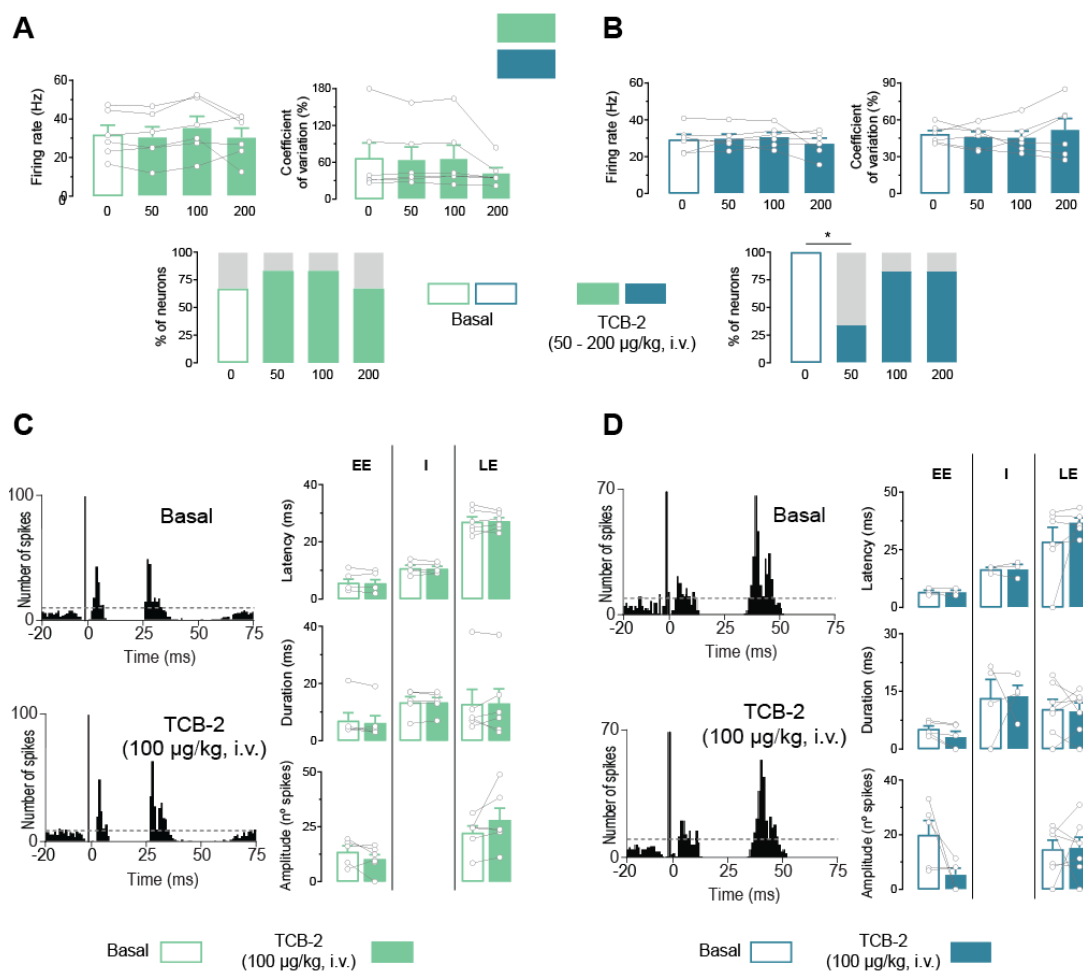


Figure 3.12. Effect of the systemic administration of cumulative doses of the 5-HT_{2A} receptor agonist TCB-2 on the spontaneous activity and cortically evoked responses of lateral and medial *substantia nigra pars reticulata* neurons from pCPA-treated rats. A-B, Histograms illustrating the effect on the mean firing rate, mean coefficient of variation and firing pattern (percentage of bursting (colour) vs. non-bursting (grey)) of the administration of TCB-2 (50-200 mg/kg, i.v.) in lateral (A) and medial (B) SNr neurons recorded in pCPA-treated rats (300 mg/kg/day, i.p., 3 days) 24 h after the last injection. In neurons from the medial SNr administration of TCB-2 at the lowest dose (50 mg/kg, i.v.) was able to reduce the percentage of bursting neurons with no effect at higher doses (100-200 mg/kg, i.v.). Histograms illustrating the effect on the electrophysiological parameters analysed from cortically evoked responses in lateral (C) and medial (D) SNr neurons of the administration of TCB-2 (50-200 mg/kg, i.v.) in pCPA-treated rats (300 mg/kg/day, i.p., 3 days) 24 h after the last injection. In pCPA-treated rats, TCB-2 (100 mg/kg, i.v.) was unable to alter cortico-nigral information transmission through any of the pathways that constitute the motor and mPF circuits. EE: early excitation, I: inhibition, and LE: late excitation. Each bar represents the mean \pm SEM of n neurons. Each dot represents a single neuron. * $p<0.05$ vs basal neurons exhibiting burst firing pattern. Chi-square test.

3.2.2.3 Effect of endogenous 5-HT brain levels elevation on spontaneous and cortically evoked activity of SNr neurons

The absence of modulation of the SNr activity observed in pCPA-treated animals following 5-HT_{2A} receptor activation suggests that the effects triggered by TCB-2 could require the contribution of endogenous 5-HT. To test this hypothesis, we used an acute administration of the SSRI fluoxetine (10 mg/kg, i.p.) in order to elevate the endogenous 5-HT brain levels and study if under these conditions, we could mimic the TCB-2-induced effects. Thus, lateral and medial SNr neurons were recorded in fluoxetine-injected animals (62 lateral SNr neurons from n= 9 rats and 48 medial SNr neurons from n=9 rats) from 1 to 6 hours after the administration.

In comparison with the vehicle-treated group, the SNr neurons recorded in the lateral territory in fluoxetine-injected rats showed a significantly reduced mean basal firing rate while displaying no differences in their firing pattern ($F_{(2,189)}=12.82$, $p<0.001$, one-way ANOVA; **Figure 3.9A**). In medial SNr cells, fluoxetine did not modify the basal firing rate but reduced the number of neurons exhibiting a burst firing pattern ($\chi^2= 16.57$, $p=0.0003$, chi-square test, **Figure 3.9B**).

Next, we studied the cortically evoked SNr activity. Administration of fluoxetine increased the number of monophasic responses consisting of a late excitation in lateral SNr neurons ($\chi^2=6.455$, $p=0.0397$, chi-square test; **Figure 3.10F**). Moreover, fluoxetine reduced the proportion of medial SNr neurons displaying triphasic responses ($\chi^2=6.076$, $p=0.0479$, chi-square test; **Figure 3.10G**) and greatly reduced early excitation occurrence ($\chi^2=6.192$, $p=0.0452$, chi-square test; **Figure 3.10E**). Regarding the electrophysiological parameters of the cortically evoked responses in SNr neurons, fluoxetine modified the characteristics of the early and late excitatory responses in both territories (**Figure 3.11**). Lateral SNr cells from fluoxetine-treated animals showed an increase in early excitation duration ($F_{(2,106)}=4.859$, $p=0.0096$, one-way ANOVA) and a diminished late excitation amplitude ($F_{(2,127)}=6.703$, $p=0.0017$, one-way ANOVA) (**Figure 3.11A**). In medial SNr neurons, fluoxetine decreased early excitation amplitude ($F_{(2,58)}=5.822$, $p=0.0049$, one-way ANOVA) and decreased late excitation latency ($F_{(2,89)}=11.20$, $p<0.0001$, one-way ANOVA) (**Figure 3.11B**).

3.3. Discussion

The present study tested the hypothesis that the stimulation of 5HT_{2A} receptors could have a specific signature on the dynamic regulation of BG circuitry, preferentially acting on associative/limbic territories of the nuclei conforming those networks. In accordance with this hypothesis, here we show a topographical-dependent dissociation in the effects triggered by the 5HT_{2A} agonist TCB-2, which specifically increases the medial SNr neuron activity and is able to enhance the mPF-BG transmission through the direct pathway. These are very likely to be 5-HT_{2A} receptor-mediated effects that require the mobilisation of the endogenous 5-HT system.

Data from positron emission tomography (PET) studies performed with specific radioligands ([¹¹C]-MDL100907, [¹²⁵I]-(±) DOI, [³H]-ketanserin or [¹⁸F]-altanserin), and those from autoradiography or immunohistochemical assays, agree on the topographical differences in the distribution of 5-HT_{2A} receptors among BG nuclei (Appel et al., 1990; Ito et al. 1998; López-Giménez et al. 1997; Miczek et al. 1975; Morilak and Ciaranello 1993; Pinborg et al. 2003; Riad et al. 1999; Riss et al. 2011). These studies describe relatively moderate levels of expression in associative/limbic structures, such as the medial striatum and the ventral pallidum, (with the exception of the *nucleus accumbens*, which has the highest expression of these receptors), and a lower expression in most of the BG nuclei. In agreement with this distribution, the present *in vivo* electrophysiological study provides evidence that 5-HT_{2A} receptors have preferential regulatory action on limbic/cognitive territories of the SNr and on mPF BG circuitry.

In vehicle-treated animals, systemic administration of TCB-2 dose-dependently stimulated medial SNr neuron activity but did not modify lateral SNr neuronal electrical parameters. The increased firing rate of medial SNr neurons induced by TCB-2 was completely blocked by the previous administration of MDL11939, thus indicating that it was mediated by 5-HT_{2A} receptors. The fact that neither this preferential antagonist nor the non-selective antagonist methiothepin caused any changes in the basal activity of SNr neurons additionally suggests that 5-HT_{2A} receptors do not exert any tonic control upon them. Previous *in vitro* electrophysiological data had reported mixed results, showing that 5-HT_{2A} receptor activation had no effect (Rick et al., 1995) or participated in the inhibitory effect produced by 5-HT on SNr neurons (Góngora-Alfaro et al., 1997). The discrepancies between *in vitro* and *in vivo* studies may be due to the participation of 5HT_{2A} receptors located in other nuclei that project to the SNr when the agonist is systemically applied, or may reflect the different selectivity of the drugs applied.

Our data are in agreement with behavioural studies performed in rodents showing that the acute or chronic administration of TCB-2 does not produce changes in locomotor activity, sensorimotor gating nor exploratory/stereotyped behaviour, but is able to induce other behavioural abnormalities, such as the suppression of feeding in food-deprived animals (Fox et al., 2010; Tsybko et al., 2020). Food motivation and intake are associated with the anatomical circuit involving the mPFC and limbic parts of the BG (Sgambato-Faure et al., 2016), and dysfunctions of this circuit could be related in eating disorders (Stefano et al., 2013). Thus, the medial distribution of TCB-2's could be involved in the observations at the behavioural level.

According to the described effects on SNr spontaneous activity, we observed that mPFC-nigral transmission was also more affected by the TCB-2 administration than the cortico-BG information processing through the motor circuits. Thus, in mPF circuits, activation of 5-HT_{2A} receptors resulted in a notable imbalance between the direct and indirect trans-striatal pathways, with an enhancement in information transfer through the direct pathway (increased inhibition) accompanied by a reduced transmission via the indirect pathway (decreased late excitation). Effects triggered by TCB2 on cortico-BG transmission were blocked by the previous administration of MDL11939, confirming once again the implication of 5-HT_{2A} receptors. Intracellular recordings performed in rat brain slices have demonstrated that 5-HT depolarises *nucleus accumbens* neurons via a 5-HT_{2A} receptor-mediated mechanism, as this effect was blocked by the antagonists ketanserin and mianserin, but not by other 5-HT receptor subtype antagonists (North & Uchimura, 1989). This stimulatory effect may explain the favoured transmission through the direct pathway in mPF circuits, since this receptor is also present in the dorsomedial striatum. Furthermore, this receptor does not seem to participate in STN excitability (Xiang et al., 2005), which would explain why the hyperdirect pathway was not affected.

To the best of our knowledge, this work is the first demonstration that 5-HT_{2A} receptors have a specific regulatory role on BG circuit functionality, which differs from the previously reported role of 5-HT_{2C} receptors. Beyeler and colleagues demonstrated that the 5-HT_{2C} agonist Ro-60-0175 also did not affect the spontaneous or cortically activated lateral SNr activity, but was able to increase the late excitatory response (indirect pathway transmission) of medial SNr neurons (Beyeler et al., 2010). More recently, it has been shown that the 5-HT_{2C} antagonists SB243213 and SB242084 are able to abolish the enhancement in the cortico-nigral transmission through the hyperdirect pathway (early excitatory response) in medial SNr neurons induced by D2/3 receptor agonist quinpirole (Lagière et al., 2020). Although activation of both receptor subtypes acts preferentially on the associative/limbic territories of the BG, the

5-HT_{2C} receptor appears to regulate cortico-BG information processing via trans-subthalamic pathways, whereas 5-HT_{2A} does so through trans-striatal pathways. This hypothesis would be in agreement with the high expression of 5HT_{2C} receptors and the very low expression of 5HT_{2A} receptors in the STN (Pompeiano et al., 1994; Reznitsky et al., 2016).

The absence of modulation of the SNr neuron activity following TCB-2 administration in pCPA-treated animals highlights the participation of endogenous 5-HT in the observed effects. In mPF circuits, 5-HT depletion induced by pCPA treatment enhanced the cortico-BG transmission through the direct pathway by itself, i.e. it produced the same effect elicited by TCB-2 administration. Therefore, this effect could be indirectly related to the decrease in 5-HT neuron activity, as it has been already reported for the 5-HT_{2A} agonists LSD and DOI (Aghajanian *et al.*, 1970; Martín-Ruiz et al. 2001; De Montigny and Aghajanian 1977). Supporting this idea, we recently have shown that the activation of the inhibitory 5-HT_{1A} receptors by buspirone induces an increase of the inhibitory component of the triphasic response in SNr neurons (Vegas-Suárez et al., 2022).

In addition, we further investigated if the mobilisation of the endogenous 5-HT system was able to mimic the specific effects triggered by TCB-2, by injecting the SSRI fluoxetine. However, the acute challenge of fluoxetine specifically decreased the basal firing rate of lateral SNr neurons and consistently induced an increase in early excitation, together with a reduction in late excitation in lateral SNr neurons, while inducing a decrease in early excitation in neurons from the medial SNr. The discrepancies between the TCB-2 and fluoxetine-induced effects could be explained by the activation of 5-HT receptor subtypes (other than 5-HT_{2A} receptors, located in the BG circuitry) after the elevation of 5-HT levels, such as the 5-HT_{1B} receptors in striato-pallidal and sub-thalamo-nigral synapses (Ding et al., 2013; Querejeta et al., 2005; Rav-Acha et al., 2008) or the 5-HT_{1A} receptors located in *globus pallidus* neurons (Rav-Acha et al., 2008).

There are some limitations in the present study. Firstly, the off-targets of the used drugs. For instance, it should be noted that the full pharmacological profile of TCB-2 is unknown and recent evidence indicates some affinity to 5-HT_{2C} and 5HT_{1A} receptors (Di Giovanni & De Deurwaerdère, 2018). Furthermore, although it has a preferential action for 5-HT_{2A} receptors, MDL11939 can also behave as an antagonist of 5HT_{2C} receptors. Similarly, fluoxetine, in addition to being non-selective SERT blocker, can also act as a 5-HT_{2A}, 5-HT_{2B} or 5-HT₆ receptors antagonist, a norepinephrine reuptake blocker and a sigma 1 receptor ligand. Secondly, although the acute dose of fluoxetine used in our experimental design has been reported as being able to induce stable elevated brain 5-HT levels for at least 6 h after injection (Volle et al., 2018), this finding has not been evidenced by other authors (Rogóz & Gołmbiowska, 2010). Finally, we restricted the study to male animals; however, sex

differences have been evidenced in BG and cortical activities (Nikulin & Brismar, 2005; Wilson, 1993). Further experiments in female rats would therefore be required to assess a possible sexual dimorphism in the modulatory role of 5HT_{2A} on the functionality of BG circuits.

In summary, the present study allows us to better understand the role of the 5-HT_{2A} receptor on the dynamic regulation of BG circuits and highlights its preferential modulatory action enhancing mPF information processing through the direct pathway. In addition, these findings point out a therapeutic potential of the 5-HT_{2A} receptor in the treatment of disorders linked to abnormal activity on the associative/limbic BG circuits.

4. STUDY II

Contribution of arkypallidal neurons during levodopa-induced dyskinesia

In this chapter, we will discuss the results obtained in the second part of my PhD, under the supervision of Dr. Boraud and Dr. Mallet. Results on this part are focused on the GPe GABAergic transmission in healthy and pathological conditions. More precisely, we aimed to characterise the role of Arky-GPe neuron activity in the establishment of the parkinsonian and dyskinetic states. We will first develop our methodological approaches, then present the results, and finally discuss them with their limitations and perspectives of future works.

Summary

The external globus pallidus (GPe) integrates striatal inputs and is an important hub nucleus that orchestrates BG network activity. In addition, a subpopulation of GPe neurons, the Arky-GPe neurons, directly form a negative feedback loop to the striatum that powerfully controls action inhibition in normal condition. However, the functional importance of Arky-GPe neurons in pathological conditions, such as LID generation, is totally unknown. The goal of this work was to investigate the contribution of GPe Arky-GPe neurons across different pathological motor states of PD and LID. To do so, we employed optical methods (i.e. fiber photometry and miniscope) to monitor the change of calcium activity of Arky-GPe neurons upon transition from healthy condition to the pathological state of PD and LID. Having characterised the abnormal activity change of Arky-GPe neurons during LID, we then used optogenetic manipulation to restore their activity and test their contribution to LID generation. These findings shed light on the role of this neuronal population in the mechanisms involved in LID maintenance.

4.1. Material and methods

All animal procedures described in this part were conducted following the European Community Council Directive on “The Protection of Animals Used for Scientific Purposes” (2010/63/ EU) and the French ministry of higher education and research. The Local Ethical Committee for Animal Research of CNRS, Aquitaine Region reviewed and approved the experimental protocols (DAP 25001).

4.1.1. Animals

In this study, we used both male and female adult mice with C57BL6 genetic backgrounds. Arky-GPe neurons were specifically targeted using the FoxP2-Cre mouse line and Proto-GPe neurons were targeted using the PV-Cre or Nkx2.1-Cre mouse lines. Mice were housed collectively (two to five per cage) under standard laboratory conditions ($22 \pm 1^\circ\text{C}$, $55 \pm 5\%$ relative humidity, and 12:12 hr light/dark cycle) with food and water provided *ad libitum*. All behavioural manipulations were performed during the light phase.

A total of n=39 mice were used to study the contribution of Arky-GPe neurons during LID:

- n=19 FoxP2-Cre mice to record the calcium activity (n=6 were included in the analysis for the fiber photometry recordings and n=4 included for the mini-endoscope-used study).
- n=11 FoxP2-Cre were used for the optogenetic manipulation of Arky neurons during behaviour.
- Finally, n=3 Nkx2.1-Cre and n=6 PV-Cre mice were used for the optogenetic inhibition of Proto-GPe during dyskinesias.

4.1.2 Drugs

The following table shows the list of drugs used (Table4.1). Except for urethane, all drugs used in this study were freshly prepared on the injection day. 6-OHDA was diluted in a solution of NaCl 0.9% + Acid Ascorbic 0.01% and all other drugs: l-3,4-dihydroxyphenylalanine (L-DOPA), CNO, desipramine, and benserazide were prepared in physiological saline (NaCl 0.9%). Exagon and lidocaine were mixed and prepared in physiological saline before the euthanasia. For *in vivo* electrophysiological recordings, we used urethane as an anesthetic.

Table 4.1: Used drugs and their pharmacological activity

DRUGS	ACTIVITY	DOSAGE	PURCHASE
6-hydroxydopamine (6-OHDA)	Catecholaminergic neurotoxin	4 µg/µl (i.c)	Sigma-Aldrich
L-3,4-dihydroxyphenylalanine (L-DOPA)	Precursor of dopamine	6 - 12mg/kg (i.p)	Sigma-Aldrich
Clozapine N-oxide (CNO)	DREADD agonist	1 mg/kg (i.p)	Sigma-Aldrich
Desipramine	Norepinephrine reuptake inhibitor	25 mg/kg (i.p)	Sigma-Aldrich
Benserazide	Inhibitor of AADC	12 mg/kg (i.p)	Sigma-Aldrich
Urethane	Anesthetic	1.3 g/kg (i.p)	Sigma-Aldrich
Pentobarbital (Exagon)	Barbiturate	300 mg/kg (i.p)	Axience
Lidocaine	Local anesthetic	30 mg/kg (i.p)	Axience

4.1.3 Viral vectors

The general characteristics of the viral vectors employed and their volumes are summarised in Table 4.2. All viruses were injected in the GPe at stereotaxic coordinates detailed in Table 4.3.

All viruses were injected in the right hemisphere, with the exception for the fiber photometry technique, where we injected in the GPe of both hemispheres.

Table 4.2: List of viral vectors used and their properties

Serotype	Transgene	Titre	Vector core	Volume
AAV5	EF1 α -DIO-hChR2(H134R)-eYFP	4×10^{12}	UNC	60 nl
AAV5	hSyn-CTL-eYFP	6.6×10^{12}	UNC	60 nl
AAV5	CAG-Flex-ArchT-tdTomato	3.1×10^{12}	UNC	60 nl
AAV9	hSyn-Flex-jGCaMP8f-WPRE.SV40	2.4×10^{13}	Addgene	60 or 110 nl
AAV9	Syn-Flex-jGCaMP6s-WPRE.SV40	10^{13}	Addgene	250 nl
AAV2	hSyn-DIO-hM4D(Gi)-mCherry	3×10^{12}	Addgene	60 nl

4.1.4 Stereotaxic surgery

All the coordinates used for the injection of viruses or fiber implantation are resumed in Table 4.3.

Table 4.3: Coordinates for all structures injected or implanted

STRUCTURE	INTERVENTION	COORDINATES		
		AP	ML	DV
Globus Pallidus	Injection	-0.4 mm	1.9 mm	- 3.6 mm
Globus Pallidus	Implantation	-0.4 mm	1.9 mm	-3.4 mm
Striatum	Implantation	+ 0.9 mm	2.05 mm	- 2.25 mm
Medial Forbrain Bundle	Injection	- 1.3 mm	- 1.2 mm	- 4.75 mm
Substantia nigra <i>pars compacta</i>	Implantation	- 4.45 mm	1.4 mm	- 3.25 mm
Substantia nigra <i>pars compacta</i>	Infusion	- 4.45 mm	1.4 mm	- 4.25 mm

4.1.4.1 Injection of viral vectors

In order to optogenetically manipulate Arky-GPe or Proto-GPe neurons, we directly injected an 'AAV-DIO/Flex-opsin-Tag'-type adenovirus (Table 4.2) into the GPe in FoxP2-Cre, Nkx2.1-Cre, or PV-Cre mice.

We designed excitatory and inhibitory optogenetic approaches using channelrhodopsin (ChR2) or archaerhodopsin (ArchT3), respectively.

Channelrhodopsins are nonspecific cation channels that depolarise the membrane of targeted neurons upon blue light illumination (470nm), while archaerhodopsin proteins are proton pumps that open up with a green light illumination (561nm).

The specificity of this approach on Arky-GPe or Proto-GPe neurons lies in the inversion of the opsin reading frames. Indeed, only neurons expressing the Cre recombinase protein will be able to express the opsin. Consequently, it will be possible to manipulate the electrical activity of these neurons by emitting blue or green light with a very high spatial and temporal resolution (of the order of a millisecond).

The following paragraph describes the surgery steps.

First, mice were deeply anesthetised with isoflurane, used at 4% for the induction and 1.5% for the maintenance, and placed in a stereotaxic frame with their head secured in a horizontal orientation. The body temperature was maintained at ~37°C for the entire experiment with a heating pad connected to a rectal probe.

The skull of the animal was exposed, and one burr hole was drilled over the GPe injection site at anteroposterior (AP): -0.4, mediolateral (ML): 1.9, dorsoventral (DV): -3.6).

Depending on the experiment, the viral vector was delivered unilaterally or bilaterally with a calibrated thick-walled micropipette that had its tip broken to a diameter of 30-25 µm. We used air pressure pulses delivered by a Picospritzer® to eject the virus in the GPe

Due to the high expression of the protein FoxP2 in the STR and to minimise virus diffusion in that nucleus (and thus a specific opsin expression outside the GPe), we injected a relatively small volume of virus (i.e. 60nl) for all our optogenetic/fiber photometry experiments.

For the calcium imaging experiments using miniature miniscope (Inscopix®), we injected a higher volume (110-250nl), to maximise the chances of having transfected FoxP2-Cre neurons below the GRIN lens in the GPe.

After the injection, the micropipette was left on the site for an additional 2-3 minutes to allow the diffusion of the virus.

At the end of the surgery, mice received an analgesic treatment (Buprenorphine, 0.05 mg/kg, s.c) and were allowed to recover for at least two weeks for the correct expression of opsins.

4.1.4.2 Dopaminergic lesion with 6-hydroxydopamine

In this study, we used a neurotoxic unilateral model of Parkinson's disease in mice. Thirty minutes before the surgery, mice were pretreated with desipramine (25mg/kg, i.p) in order to preserve the integrity of the noradrenergic system.

Two models of 6-OHDA-unilesioned mice were used depending on the site of the 6-OHDA injection: either in the MFB (model 1) or in the SNc (model 2).

Model 1: two weeks after the opsin injection, we injected 1µl of 6-OHDA (concentration of 4µg/µl) into the MFB (AP: -1.3, ML: 1.2, DV: -4.75) following a traditional surgery using a glass micropipette (described in section 4.1.4.1),

Model 2: This model was developed because the size of the inscopix miniscope did not give access to the stereotaxic coordinates of the MFB. We thus decided to implant a cannula above the SNc (AP: -4.25, ML: 1.2, DV: -3.25) and fix it permanently in place using bone cement (Super-bond C&B, Sun medical). The cannula had a 20° angle in the AP direction so it would not interfere with the connection to the miniscope or the optic fiber. This gave us the possibility to infuse 2µl of 6-OHDA (concentration of 4µg/µl) using a 10 µl-Hamilton syringe (AP: -4.25, ML: 1.2, DV: -4.25).




Mice were allowed to recover at least two weeks after the 6-OHDA lesion.

To prevent dehydration, mice received 20% sterile glucose–saline (0.1 ml/10 g body weight, i.p.) immediately after surgery and then once a day during the first post-operative week. In addition, they received a saline injection (0.9% NaCl, 0.5 ml/20 g body weight, i.p) every morning until weight loss stopped.

4.1.4.3 Implantation of optic fibers and GRIN lens

Mice were deeply anesthetised with isoflurane, used at 4% for the induction and 1.5% for the maintenance, and then placed in a stereotaxic frame with their head secured in a horizontal orientation. Their body temperature was maintained at $\sim 37^{\circ}\text{C}$ for the entire surgery with a heating pad connected to a rectal probe. The skull of the animal was exposed, and one burr hole was drilled above the site of implantation. GRIN lens, optic fiber for the fiber photometry, or optogenetic manipulation were supplied by different manufacturers (Table 4.4), but the implantation procedures were similar. A pre-track using an 20G needle was carefully made until it was 3.4 mm deep and then was left in place for 10 min. Then, the lens or optic fiber was slowly lowered to its final DV coordinates and fixed permanently using bone cement (Sun medical).

Table 4.4: Different manufacturers used for the optic fibers and GRIN lens

Technical used	Manufacturer	Core	Diameter	
Optogenetic manipulation	Home custom	0.22 NA	100 μm	
Calcium imaging	Inscopix	—	500 μm	
Fiber photometry	RWD	0.5 NA	200 μm	

4.1.5 Behavioural studies

The aim of this study II was to measure the motor behaviour of mice at different physiological and pathological stages. We therefore used different behavioural tests as explained in the following section.

All behavioural studies were conducted between 8:00 a.m and 7:00 p.m. Motor activity of mice was evaluated in a glass Openfield, thoroughly cleaned before each recording session to remove odour traces. The behavioural test started 1 week after the 6-OHDA lesion, to allow complete recovery of the animal. Experimental designs are summarised in Figure 4.1.

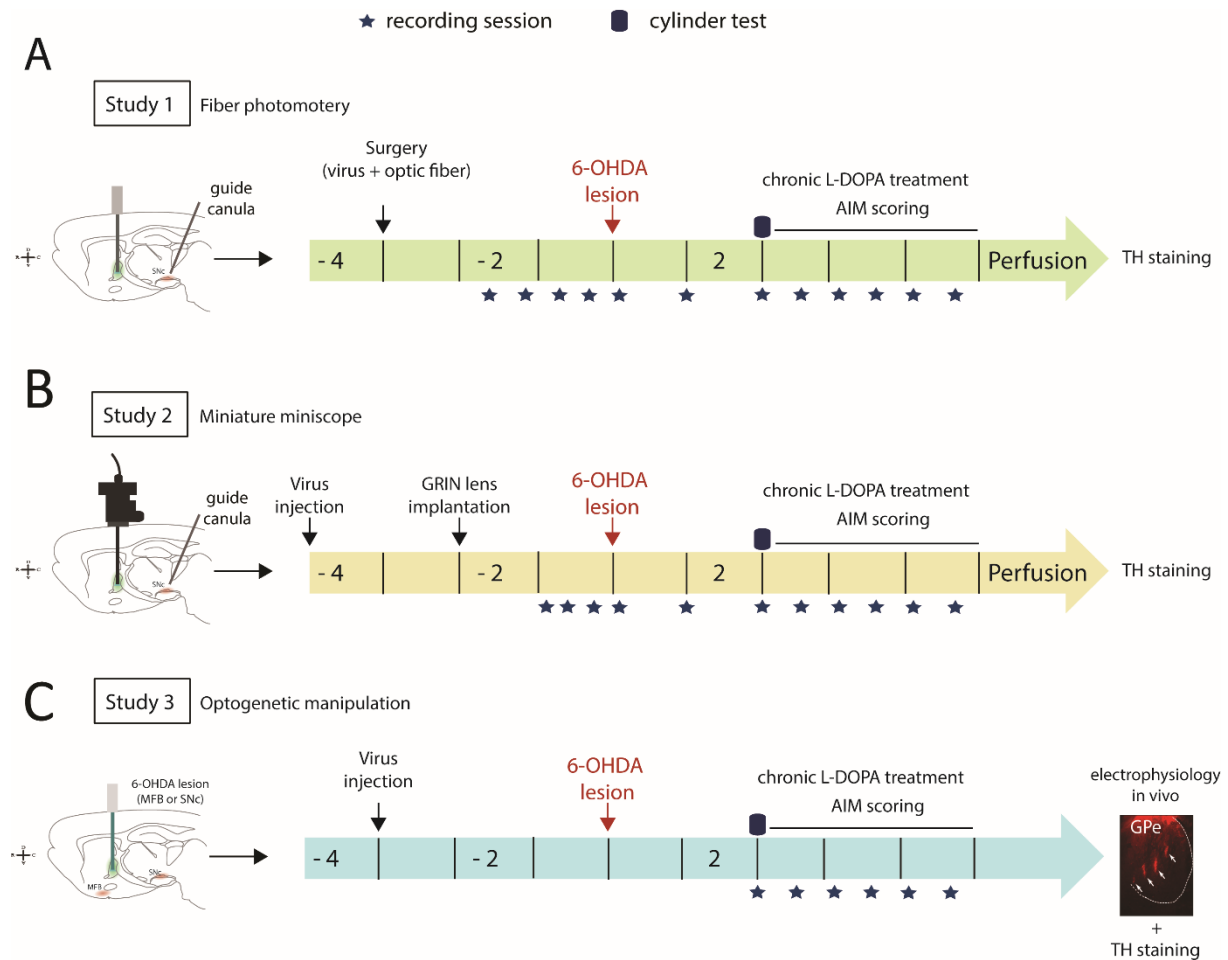


Figure 4.1. Experimental designs of the three studies developed. **A**, Study 1: calcium imaging of Arky-GPe neurons using a miniature miniscope. **B**, Study 2: fiber photometry of Arky-GPe neurons. One optic fiber per hemisphere was implanted. **C**, Study 3: optogenetic manipulation of GPe neurons.

4.1.5.1 Cylinder test

The cylinder test was used to assess the degree of motor impairment produced by DA loss and the screening of the lesion was evaluated 2 weeks after surgery when the DA depletion was considered stabilised (Dekundy et al., 2007).

The cylinder test evaluates the forelimb use asymmetry by determining the animal's ability to support its own body weight against the wall of a glass cylinder during explorative behaviour (Figure 4.2A).

Briefly, mice were individually placed in a transparent glass beaker (1L) for 5 minutes, with two mirrors positioned at a 90° angle behind the cylinder to allow a complete view of the exploratory activity. We calculated the percentage of contralateral or ipsilateral forelimb use with respect to the total number of touches.

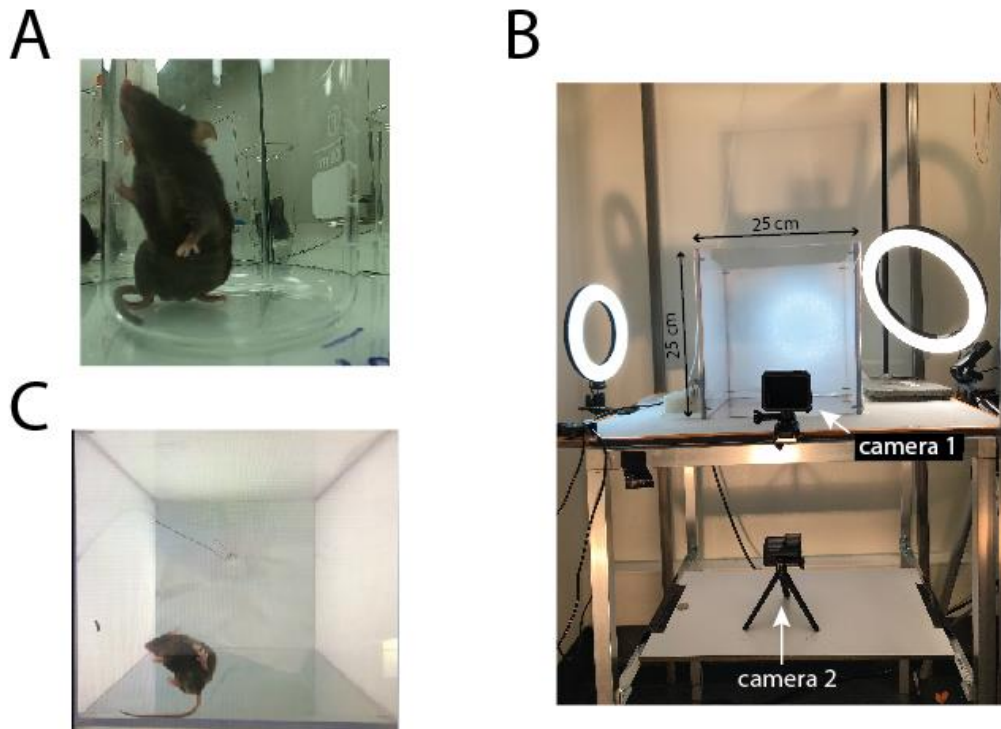


Figure 4.2. Behavioural test setup. **A**, The cylinder test evaluates the ability to perform explorative behaviour and allows the calculation of spontaneous forelimb use. **B**, Set up used for recording behaviour with two cameras placed around the glass Openfield. **C**, Bottom view of parkinsonian mice. We used this view to count the number of ipsilateral and contralateral rotations.

4.1.5.2 Motor activity

Motor activity in mice was evaluated in a transparent Openfield for at least 10 min and recorded using two GoPro cameras: Hero 8 and 9. One was placed to record mice from a side view in the Openfield and the other, to film from a bottom view (Figure 4.2B).

The number of ipsilateral or contralateral rotations were manually counted. The tracking of the mice was performed using the supervised algorithm DeepLabCut (Mathis et al., 2018).

To allow precise tracking of the mouse's features across different conditions, the camera settings were set as follows: 60FPS, 1080 RES, 800 ISO min, 1600 ISO max.

4.1.5.2 Levodopa-induced dyskinesia scoring

Two weeks after the 6-OHDA lesion, the cylinder test was used to evaluate the degree of motor impairment. At that moment, chronic L-DOPA treatment was initiated.

L-DOPA methyl ester (6 mg/kg i.p.) plus benserazide (12 mg/kg i.p.) were given intraperitoneally (Mela et al., 2007). This dose of benserazide is within the range required to ensure a sufficient duration (>2 h) of the biochemical and motor effects of single L-DOPA doses in rodents (Da Prada et al., 1987).

Every day, immediately after L-DOPA administration, mice were placed in separate cages for at least 2 hours. Two times a week mice were put in the Openfield, and AIMs were rated as previously described (Dekundy et al., 2007).

Each mouse was observed individually for 1 min every 5 min for a 90 min time period, starting 5 min after the L-DOPA/benserazide administration, in order to generate the establishment curve of dyskinesias. This quantification was then used to define the time at which AIMs were maximal and to determine when to manipulate Arky-GPe activity with optogenetic stimulations.

Only the hyperkinetic and dystonic movements that could be clearly distinguished from naturally occurring behaviours (i.e. grooming, sniffing, rearing, and gnawing) were considered in the ratings. The AIMs were classified into three different subtypes based on their topographic distribution:

- (i) **Axial AIMs**, i.e. Lateral flexion of the neck or torsional movements of the upper trunk towards the side contralateral to the lesion;
- (ii) **Forelimb AIMs**, i.e. Hyperkinetic, jerky stepping movements of the forelimb contralateral to the lesion, or small circular movements of the forelimb to and from the snout;
- (iii) **Orolingual AIMs**, i.e. These are recognisable as bursts of empty masticatory movements, accompanied to a variable degree by jaw opening and tongue protrusion.

Each AIM subtype was scored on a severity scale ranging from 0 to 4:

0, absent; **1**, present during less than half of the observation time; **2**, present during more than half of the observation time; **3**, present all the time but suppressible by external stimuli; **4**, continuous, severe and not suppressible.

Examples of the three subtypes of dyskinetic behaviours and scheme depicting the experimental procedure are shown in Figure 4.3.

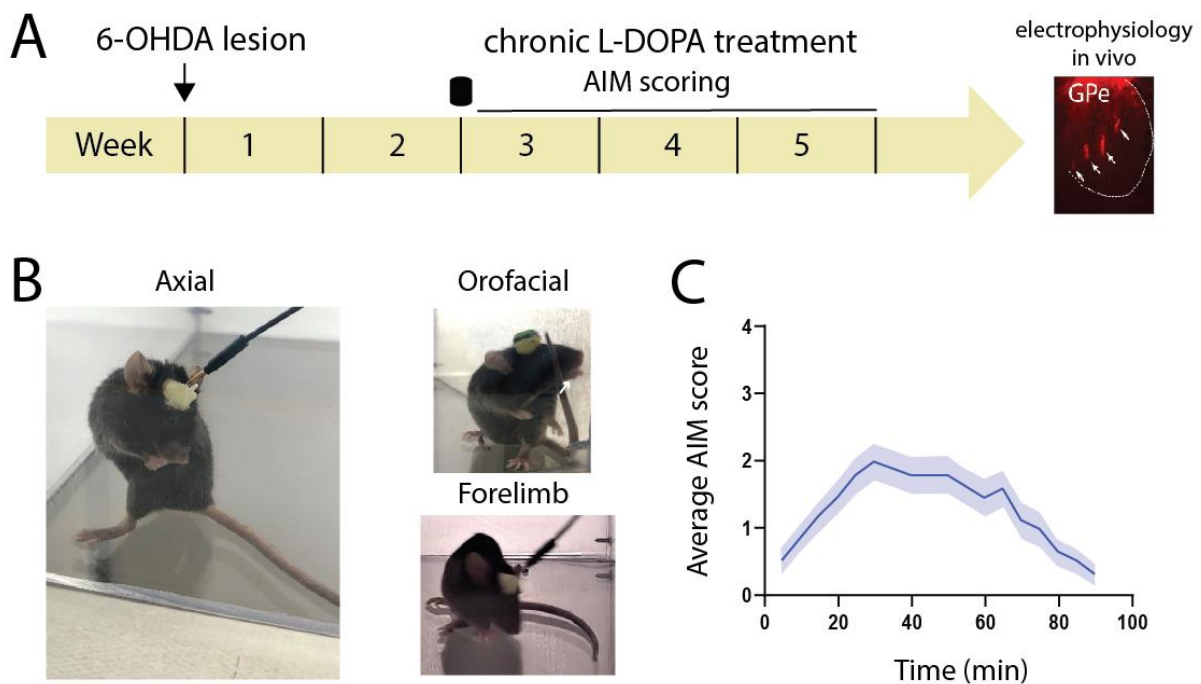


Figure 4.3. L-DOPA-induced dyskinesia in mice with a unilateral 6-OHDA lesion. A, Chronology of the experimental procedure. **B,** Images of different AIM subtypes. Abnormal movements of the jaw was shown by the white arrow. **C,** Graph representing the overall AIM score across time, $n = 5$ mice recorded during the 90 min time period. Note that the peak LIDs appear 25 min after L-DOPA administration and plateaued until 55-60 min.

4.1.6 Protocols of optogenetic stimulations

Prior to optogenetic stimulation experiments, mice were habituated to tethering with lightweight patch cables coupled to an optical commutator (ThorLabs). Light stimulations were performed through optical fibers (0.22NA, core diameter: 105 μ m, Thorlabs) implanted into the right GPe. Optical stimulation experiments consisted of at least 1 min baseline followed by 30s light ON/30s light OFF, repeated 5x. The opto-excitation protocol was delivered in pulse train (wavelength: 473nm, ON stim: 10ms, frequency: 20Hz, intensity: 2.5mW), while the opto-inhibition protocol was delivered continuously during the 30s (wavelength: 563 nm, intensity: 5mW)(Figure 4.4). The inhibitory protocol was chosen based on previous work in the field

(Girasole et al., 2018), while the excitatory one was tested during our *in vivo* electrophysiological recordings (See Figure 4.12 A-C). The laser bench (Errol laser) was controlled by analog signals sent by a Power1401-3 (Cambridge Electronic Design) connected to a computer equipped with the Spike2 software (version 8).

For each stimulation experiment, we calculated all the behavioural measurements (AIMs and number of rotations) during three periods, designed: 'OFF', 'ON', and 'Post-ON'. The 'OFF' period was the 15s preceding the laser. The 'ON' period was the period of the illumination of the laser (30s long). The 'Post-ON' period was 15s after the end of the laser illumination.

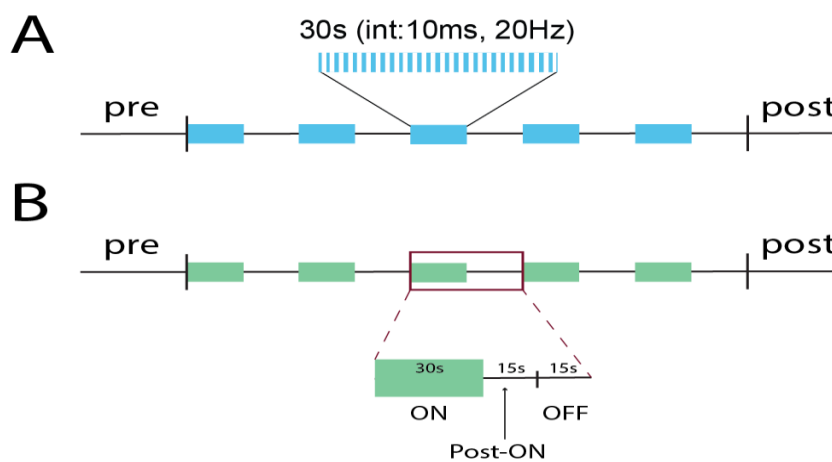


Figure 4.4. Protocols of optogenetic manipulations. **A**, Protocol of optogenetic stimulation: pulsed light (473nm, 10ms, 20Hz, 2.5mW). **B**, Protocol of optogenetic inhibition: continuous light (520nm, 30s, 5mW). Example of three periods of analysis: ON, Post-ON and OFF.

4.1.7 Histological procedures

At the end of the behavioural session, mice were sacrificed with an overdose of pentobarbital/lidocaine mix (300mg/kg pentobarbital + 30 mg/kg lidocaine, i.p). Intracardiac perfusion (PBS 0.01mM) was performed for further histological validations. Brains were kept for 24h in a solution of paraformaldehyde 4% and then cut in 50 μ m slices with a vibratome (VT1000, Leica Microsystems). Slices conserved in PBS-azide (0.01%, 4°C) were first rinsed (3 washes for 5 min) in PBS 0.1mM and then incubated with the primary antibody anti-TH (1:4000) with gentle agitation overnight at room temperature.

The next day, we rinsed the slices (3 washes for 5 min) and then, the sections were incubated with the secondary antibody (1:500 donkey anti-rabbit IgG, 647nm) for 4h at room temperature.

In order to visualise the ChR2 opsin, we performed an eYFP amplification. The same step was carried out with incubation in the primary antibody anti-GFP (1:1000) and then in the secondary antibody (1:500 anti-chicken, 488nm). Finally, slices were washed in PBS 0.1mM and mounted onto slides in a clear liquid medium (Fluoromount-G [™], Invitrogen, 00-4958). The low magnification images were acquired with an epifluorescence microscope (Axio Imager 2, Zeiss).

Table 4.4: List of primary and secondary antibodies used for immunohistochemistry.

ANTIGEN	HOST	REFERENCE	MANUFACTUER
Tyrosine Hydroxylase	Rabbit	137869	abcam
Rabbit IgG (647nm)	Donkey	A31573	Life Tech
Anti - GFP	Chicken	GFP - 1020	Aves
Chicken IgG (488nm)	Donkey	703-545-155	Alexa Fluor®

4.1.8 Electrophysiological procedures

At the end of the behavioural session, electrophysiological recordings were conducted under urethane anesthesia. Urethane was directly applied in order to induce and maintain anesthesia (i.p., 1.3g/kg; CAT#U2500, Sigma-Aldrich). Animals were then secured in a stereotaxic frame (Unimécanique, M2e) and placed on a heating blanket.

The optic fibers implant previously cemented was drilled out and removed. Craniotomies were enlarged to enable the descent of the recording electrode.

In each mouse, an electrocorticogram (ECoG) of the SM cortex was performed (AP:+2.5 mm, ML:2.1mm) with a 1mm screw juxtaposed to the dura mater. All along the recording, the anesthesia level was frequently controlled by examining the ECoG and by testing the response of gentle sensory stimuli (tail pinch).

In vivo extracellular recordings were performed using a multisite silicon probe (Tetrode 64channels A4x4tet B441, NeuroNexus) paired with an optic fiber (0.22NA, core diameter:

105µm,). This method allowed us to combine extracellular recordings with optogenetic manipulations. *In vivo* extracellular recordings were performed using a multisite silicon probe (Tetrode 64channels A4x4tet B441, NeuroNexus) paired with an optic fiber (0.22NA, core diameter: 105µm). This method allowed us to combine extracellular recording and optogenetic stimulation. When the silicon probe was implanted in the brain, the electrophysiological signals were connected and amplified using a 32 channel multiprocessor and raw data were digitised at 22 kHz using an AlphaLabSNR (ALPHA Omega). Spike activity was also recorded separately for each channel by filtering the raw data at 300 Hz-10 kHz. Data were visualised through a connection with a PC running the Alpha SNR software (version 1.3.3). Spike sorting of the electrophysiological data was performed using the Spike2 software (version 8, CED). Putative single-unit activity was isolated according to standard procedures including template matching, principal component analysis, and supervised clustering. The isolation of single units was verified by the presence of a refractory period in the interspike interval histograms. The mean firing rate of each neuron was calculated as well as the coefficient of variation (CV). Optotagging responses of putative Arky-GPe neurons to a laser stimulation were identified based on peri-stimulus time histograms or PSTH (width: 100 ms, offset: 25 ms, bin size: 1 ms) computed on the laser events. A neuron was considered optotagged if the spike count values of 3 consecutive bins in response to light stimulation was greater than 2 standard deviation, calculated on the baseline epoch.

To identify the location of the recorded electrode, we previously covered the shank of the electrode with a dil fluorescent solution (DiLC18(3), 1mg/kg, Invitrogen).

4.1.9 Calcium imaging procedures

4.1.9.1 Calcium imaging using fiber photometry

Fiber photometry is an adaptable method for the measurement of neuronal population global calcium signal (using GCaMP protein) measured in real-time and in freely behaving animals (Calipari et al., 2016). Briefly, two diodes emit light at 470nm (GCaMP stimulation wavelength) and 410nm (control for artefactual fluorescence, isosbestic) using a 200 µm x 0.5NA optical fiber connected to a microscope objective and fiber launch (R810 dual colour multichannel, RWD). Light emission is collected by the same optical fiber and extracted by the RWD software analysis.

Data are analysed using a custom-written script in Python. We normalised data using $\Delta F/F$ as shown below.

$$\Delta F/F = (GCaMP\ signal - isobestic\ signal) / isobestic\ signal$$

For peak detection, we adapted our methods from analyses previously performed (Muir et al., 2018; Sherathiya et al., 2021):

We first transformed our data to z-score:

$$score = \Delta F/F - (mean\ of\ \Delta F/F) / Standard\ deviation\ of\ \Delta F/F$$

Then, the z-score data was processed as follows:

Since some data contained high amplitude events that represented artefactual signals, these outliers were removed if the local maxima was above two median absolute deviation (MAD) of the median value. The median of the resultant trace was calculated. The peak detection threshold was set at three times this median.

Then, the resultant average peak amplitude and peak frequency were compared across the group's conditions.

Last, we also calculated the area under the curve (AUC) computed using the trapezoidal method.

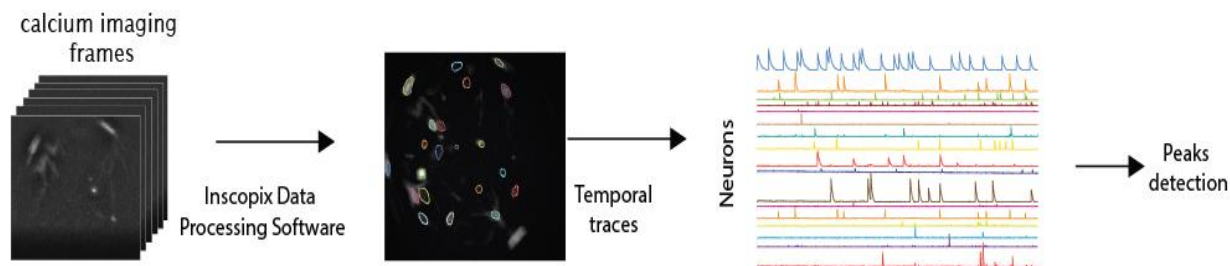
4.1.9.2 Calcium imaging using a miniature miniscope

In addition to the fiber photometry technique, we used a miniature miniscope connected to a GRIN lens (size: 0.5mm, length: 6.1mm) allowing us to access variations of calcium signal (using GCaMP) in individual neurons (Ghosh et al., 2011; Stamatakis et al., 2021; Yang et al., 2016).

One week after GRIN lens implantation, mice were habituated to the Openfield and to the tethering with the nVista microscope (Inscopix), attached to the fixed baseplate.

The fluorescence level was recorded at 20 or 40 frames per second according to whether mice received the GCaMP6S or GCaMP8f virus, light-emitting diode intensities were 1.2 to 1.7 mW, and gain (5.3 to 6.4x).

Calcium traces were extracted using the Inscopix Data Processing Software (Figure 4.5). Raw data were cropped, spatially downsampled (2x), spatially filtered (cutoffs: low, 0.005 pixel; high, 0.500 pixel), and motion-corrected. Individual neurons were manually identified by the Manual ROIs option and then calcium signal traces were further deconvolved using an online active set method to infer spikes (OASIS). The peak detection was achieved using a custom-written script in Python as described previously.



0.500 pixel), and motion-corrected. Individual neurons were manually identified by the Manual ROIs option and then calcium signal traces were further deconvolved using an online active set method to infer spikes (OASIS). The peak detection was achieved using a custom-written script in Python as described previously.

Figure 4.5. Calcium imaging pipeline using the Inscopix Data Processing Software.

4.1.10 Analysis of data

4.1.10.1 Data analysis of locomotion

X-Y coordinates of the landmarks were extracted using DeepLabCut. This algorithm is based on a recognised image algorithm (ResNet), implemented with Python to estimate the position of different body parts.

In this study, we manually labelled 11 body parts (see figure 4.6). Before any further data processing, the DeepLabCut labelling output was checked for errors in detection. We then chose to use the base tail x-y for the analysis of locomotor activity. Finally, the velocity and distance travelled were calculated using a custom-written script in Python.

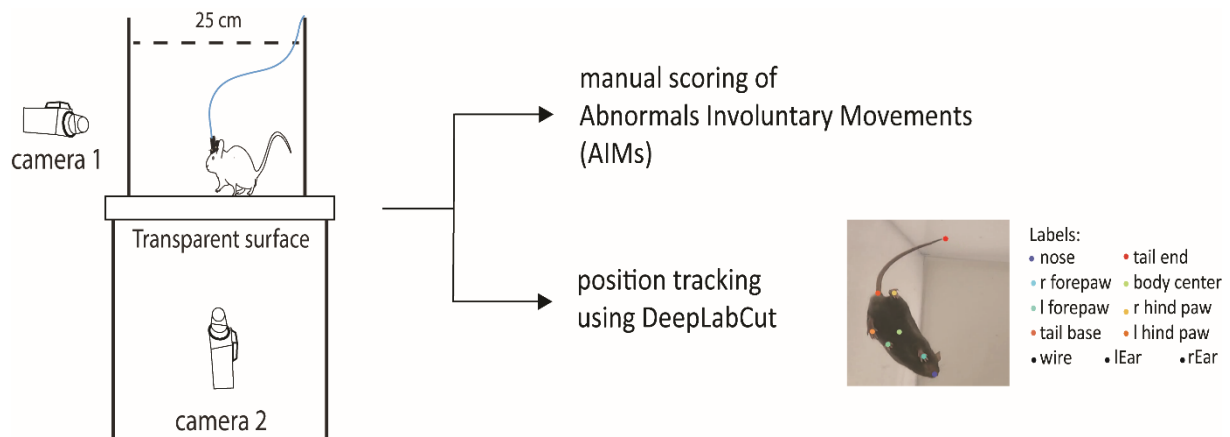


Figure 4.6. Experimental design of locomotor analysis. After the recording session, side view videos were used to manually score AIMs. Thus, the bottom view videos were analysed using the DeepLabCut algorithm.

4.1.10.2 Statistics

Experimental data were analysed using the computer program GraphPad Prism (v. 5.01, GraphPad Software, Inc; RRID: SCR_002798). Data in the figures are presented as the mean \pm standard error of the mean (SEM). Bar plots were used to illustrate sample distribution of AIM scores with individual mice values represented by grey lines. Violin plots and box were also used to illustrate sample distribution. For AIM averages and signal comparison across conditions, we used a two-way analysis of variance ANOVA followed by post hoc comparisons using Tukey's *post hoc* test. For hemisphere signal comparison, we used a paired Student's test. For electrophysiological comparison and group comparison (annex1) we used Wilcoxon matched-pairs signed rank test. The level of statistical significance was set at $p < 0.05$.

4.2 Results

4.2.1 Characterisation of Arkypallidal activity across healthy and pathological PD conditions

4.2.1.1 The SNc-lesioned mice reproduce the pathological features present in models of Parkinson's disease

In order to record the calcium activity of Arky-GPe neurons and compare its variation across different conditions (in healthy, Parkinsonian (PD), and dyskinetic (LID) conditions), we had to place a guide cannula that enabled us to inject the 6-OHDA toxin in animals previously implanted with GRIN lens fibers. To perform these experiments, we used a SNc-lesioned mouse model and as the miniscope's base plate was large, it prevented us from inserting the guide cannula into the MFB. Another advantage of targeting the SNc is that its location is sufficiently far enough from the GPe to avoid any changes in the focal plane of the miniscope that could occur as a result of the toxin infusion. For consistency purposes, we decided to also use this SNc-lesioned model in our fiber photometry experiments. The guide cannula were implanted at the same stereotaxic coordinates and configuration for all these sets of experiments was also the same (Figure 4.7A).

Two weeks after the 6-OHDA infusion, we tested the forelimb motor asymmetry of mice in the cylinder and excluded from analysis all the mice (5 mice out of 15) that presented an asymmetry score below 60% (Figure 4.7B). Such low asymmetry score was suggestive of a weak DA depletion as confirmed post hoc by the immunohistochemistry staining for the TH enzyme (Figure 4.7C). We tracked the locomotion of each mouse and calculated the distance travelled in each behavioural session. The plot in Figure 4.7E represents the mean distance travelled by mice, for those with a correct 6-OHDA lesion (included) or not (excluded). As expected, we observed a significant diminution in the distance travelled after the infusion of 6-OHDA, but only for the well-lesioned mice. After L-DOPA administration, we observed an increase in the distance travelled as compared to the PD condition, but also between healthy and LID states. For mice with no DAergic depletion no significant differences were observed (Figure 4.7E).

Altogether, these results show that SNc-lesioned mice can recapitulate the core motor deficits classically present following MFB lesion, as well as developed LID. Of note, both PD motor impairments and LID severity were not as pronounced in SNc-lesioned mice compared to the those induced by MFB. This downside comes with better post-surgery recovery time and easier care of animal. However, a limitation of this model is that it presents higher risks of not inducing

sufficient DA cell loss, principally due to the difficulty of the stereotaxic placement of the guide cannula.

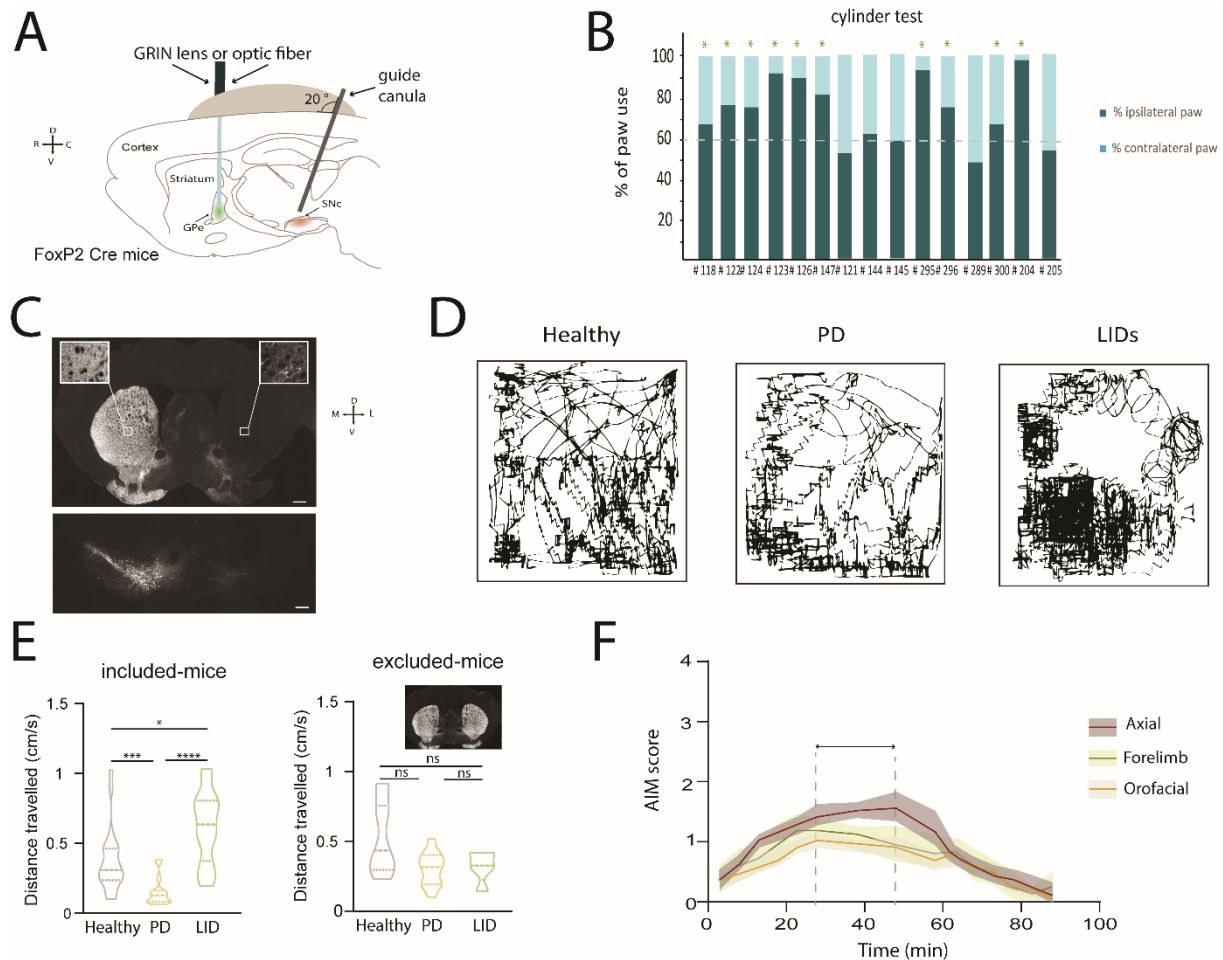


Figure 4.7. Motor assessment across different physio/pathological states using SNc-lesioned mice. **A**, Schematic representation of the experimental paradigm using FoxP2 Cre mice injected with an AAV-GCamp6s-WPRE.SV40 or an AAV-GCamp8f-WPRE.SV40 and implanted with an optic fiber or GRIN lens above the GPe. A cannula above the SNc was also implanted to directly infuse the toxin 6-OHDA in the proximity of DA neurons. **B**, Performance in the cylinder test was assessed 14 days after the 6-OHDA lesion. The results are expressed as the percentage of wall contacts performed by the paw contralateral to the lesion (left). **C**, Representative TH staining in the striatum and the substantia nigra pars compacta of one successfully-lesioned mouse (left) vs. non-lesioned mouse (right). **D**, Position tracking of one well-lesioned mouse for 10 min in an Openfield, in healthy vs. PD vs. LID states. **E**, Mean distance travelled for all lesioned (left) vs. non-lesioned (right) mice. *p=0.006 comparing healthy and PD, ***p=0.0355 comparing healthy and LID, ****p<0.0001 comparing PD and LID; ns=0.0880 comparing healthy and PD, ns=0.2495 comparing healthy and LID, ns=0.7693 comparing PD and LID. Tukey's multiple comparison test. **F**, The time profile of AIM scores per monitoring period. The temporal development of each AIM subtypes is shown with different colours (Axial: brown, Forelimb: green, Orofacial: orange). Colour shading indicates SEM. The horizontal arrow defines the chosen period for calcium imaging periods.

4.2.1.2 Calcium imaging of arkypallidal neurons activity across different health states using fiber photometry

In order to characterise the global change of activity in Arky-GPe neurons we compared the amplitude, the frequency, and the area under the curve of the calcium transients recorded across different health states (i.e. healthy, vs. parkinsonian, vs. dyskinetic) in the same animal. We first compared the calcium transient parameters recorded in the GPe ipsilateral to the lesion. We observed a significant decrease in the amplitude of the calcium transients in PD and LID states as compared to healthy condition (Figure 4.8-D). In parallel to this decrease in amplitude, we observed an increased frequency of the calcium transients in the PD condition (Figure 4.8-E). This increase was significantly reduced by the injection of L-DOPA in the LID condition to reach values similar to the one measured in healthy condition (Figure 4.8-E). No changes were observed when comparing the area under the curve (AUC) across the different conditions (Figure 4.8.F). As the calcium transients decreased in amplitude in PD and LID states with no changes in the AUC, this must imply that the duration of the transients increased in these disease states (to compensate for the loss in amplitude).

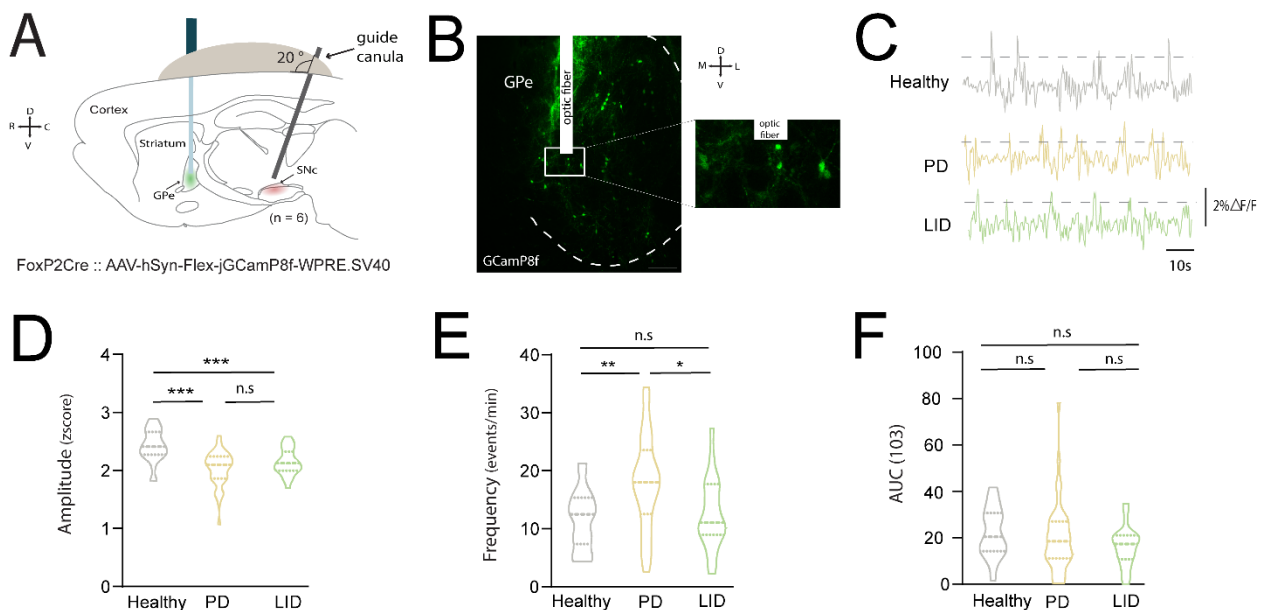


Figure 4.8. Comparison of calcium transient properties across healthy vs. PD vs. LID conditions. **A**, Schematic representation of the experimental paradigm using FoxP2 Cre mice injected with an AAV-DIO-GCamP8f-WPRE.SV40 and implanted with an optic fiber above the GPe and a cannula above the SNc. **B**, Representative GCamP8f transfection. **C**, Typical raw data signal obtain for one mouse in healthy (grey), PD (yellow), LID (green). Dashed line represent the threshold of peak detection. **D**, Amplitude of the included mice for healthy vs. PD vs. LID conditions. **p=0.0009 comparison between healthy vs. LID amplitude, ***p=0.0005 comparison between healthy vs. PD states. n.s.p=0.3475 comparison between PD and LID amplitude Tukey's multiple comparison test. **E**, Frequency of the included mice for healthy vs. PD vs. LID conditions. *p=0.0187 comparison between PD and LID,

p=0.042 comparison between healthy vs. PD states. ^{ns}p=0.8781 comparison between healthy vs. PD states Tukey's multiple comparisons test. **F, Area under the curve of the included mice for healthy vs. PD vs. LID conditions. ^{ns}p > 0.3. Tukey's multiple comparisons test.

Since the Arky-GPe global calcium signal was recorded in both hemispheres, we next compared how these parameters co-varied in ipsilateral vs. contralateral hemisphere for each condition.

Surprisingly, we observed a difference in the peak amplitude of the signal in healthy condition which was bigger in the ipsilateral in comparison to the contralateral GPe (Figure 4.9B). In PD, no differences were found in all of the parameters.

Finally, in the LID states, we observed a difference between both GPe signals, with an area under the curve smaller on the ipsilateral side of the lesion, compared to the contralateral side (Figure 4.9D).

The *post hoc* histological verification of these fiber photometry measures reveals the limitations of these experiments. Indeed, we realised that, although the placement of our optic fiber above GPe was adequate, the injection of the GCaMP virus had significantly leaked in the STR, which also contains many FoxP2+ neurons (Fong et al., 2018). As a consequence, the GCaMP signal measured above the GPe not only came from genuinely-labelled cell-bodies and axons of Arky-GPe neurons, but also from spurious axonal labelling of striatal neurons. Considering the global nature of such fiber photometry signals, it is nearly impossible to distinguish the contribution of fluorescence coming from Arky-GPe neurons vs. the fluorescence coming from striatal neurons. This issue has already been raised by others (Legaria et al., 2022). In addition, another limitation of the fiber photometry measures were the movement artefacts which were present in all conditions but exaggerated in the dyskinetic state. Although we tried our best to remove these artefacts (see methods), they most likely contaminated our measurements and therefore, also our analysis. Altogether, these important issues make the correct interpretation of the fiber photometry dataset difficult, if not impossible. This made us realise the importance of being able to monitor the calcium activity of single Arky-GPe neurons using *in vivo* miniscope-based calcium imaging.

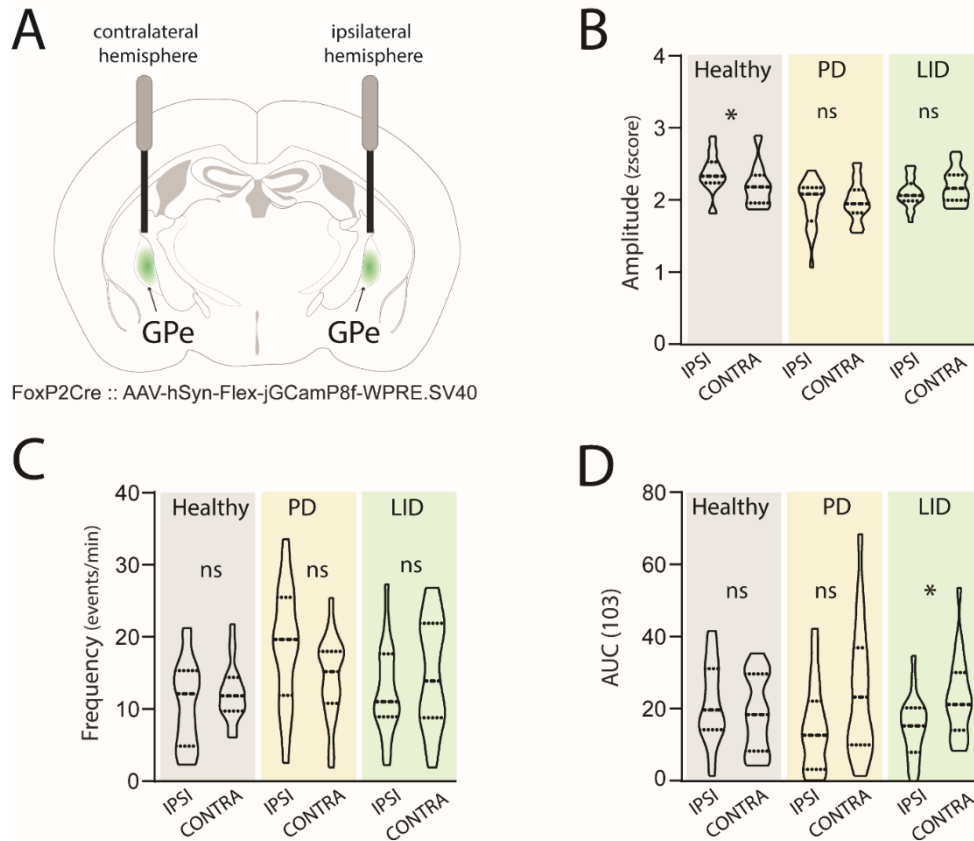


Figure 4.9: Comparison of calcium photometric signals between the contralateral and the ipsilateral side of the lesion across healthy, PD, and LID conditions. **A**, Coronal representation of the experimental approach. Mice received the AAV-hSyn-Flex-jGCaMP8f-WPRE.SV40 in both GPe and the 6-OHDA toxin in the ipsilateral hemisphere. **B**, Amplitude of the calcium transient measured in the contralateral and ipsilateral hemispheres in healthy vs. PD vs. LID states. **C**, Frequency of the calcium transient in the contralateral and ipsilateral hemispheres in healthy vs. PD vs. LID conditions. **D**, Area under the curve of the calcium transient in the contralateral and ipsilateral hemispheres in healthy vs. PD vs. LID conditions. * $p < 0.05$, unpaired t-test.

4.2.1.3 Calcium imaging of arypallidal neuron activity across different health states using *in vivo* miniscope

To monitor the individual activity of Arky-GPe neurons, we implanted miniature miniscopes in the GPe of FoxP2-Cre mice previously injected with a GCaMP virus (Figure 4.10A-B). In order to track the calcium activity across different health states, a guide cannula was cemented above the SNc, as previously described. Out of all the FoxP2-Cre mice implanted ($n=10$), only $n=4$ were used for further analysis. Indeed, $n=6$ mice were excluded due to either the absence of GCaMP+ cells for imaging in the field of view of the miniscope ($n=4$), or due to the lack of motor deficits in mice following the injection of 6-OHDA. In the latter case, this is likely resulting from a poor placement of the guide cannula in the SNc ($n=2$).

All of the mice included in the analysis showed a good behavioural response to both the 6-OHDA injection and L-DOPA treatment. Indeed, as expected, the 6-OHDA injection induced a significant decrease in the distance travelled by those mice in comparison to the healthy animals whereas the administration of L-DOPA reversed this effect and induced an increase in the distance travelled. That being said, these LID animals mostly displayed contralateral rotations and therefore not the natural locomotor activity present in healthy mice (Figure 4.10C).

All animals were perfused at the end of the behavioural sessions to verify the position of the GRIN lens and the level of DA depletion in the STR and in the SNc. We were able to validate the correct positioning of the GRIN lens in the GPe in two mice. The field of view of the imaged area in these mice revealed a low density of GCaMP+ cells compatible with the low number of Arky-GPe neurons in the GPe (Figure 4.10D), as reported by unbiased anatomical cell-counts (Abdi et al., 2015; Dodson et al., 2015). The soma of these cells was often in a fusiform shape which is also typical of Arky-GPe neurons (Mallet et al., 2012). On the opposite side, the remaining two mice had the GRIN lens partially implanted in the STR and their field of view revealed a higher density of GCaMP+ cells with a round-shape soma morphology, indicative of MSN neurons (Figure 4.10E). Indeed, as previously mentioned, the expression of FoxP2 is high in the STR and biased towards dMSNs as ~70% of FoxP2+ cells co-express the D1-R (Fong et al., 2018). It is possible that some Arky-GPe neurons were present in the field of view of these mice but, as we could not confidently identify them, we decided to separate the calcium imaging dataset into Arky-GPe vs. STR recordings. We independently analysed and compared the calcium transients recorded in each target area (GPe vs. STR) across different health states (Figure 4,10 D-E).

First, we compared the amplitude and frequency of the calcium transients for each health state. We observed a significant decrease in the transient amplitude of Arky-GPe neurons after the administration of L-DOPA. The number of events per minute also drastically reduced after the L-DOPA administration (Figure 4.10F). Interestingly, the effect size of these calcium variations in Arky-GPe neurons could positively correlate with the dyskinetic score of the animal. Indeed, we observed that the animal with a higher dyskinetic score had a strong silencing of the Arky-GPe response while the animal with a moderate dyskinetic score, showed a reduction in the Arky-GPe calcium activity. This observation suggests a causal link between a change in the activity of Arky-GPe neurons and the behavioural impact on dyskinesia. Looking at the change in calcium signals at the level of STR neurons, we observed that L-DOPA induced the opposite effect, compared to Arky-GPe neurons. Indeed, the number of transients this time increased in PD and LID conditions, in comparison to healthy states. In addition, the frequency of

transients significantly increased upon transition from the PD to the LID state after the administration of L-DOPA (Figure 4.10G). However, no significant changes were observed in the amplitude of the signal for the different transitions.

We also monitored the variation of calcium signals at different time points after the DA lesion: day 1, day 7, and day 14. For Arky-GPe neurons, we observed an increase in the transient amplitude 14 days after the lesion (Figure 4.10H), with no noticeable change for the frequency of these transients. Interestingly, for STR neurons, we observed the opposite response, that is a decrease in the peak frequency of the calcium transients at day 14 after the lesion (Figure 4.10 I).

Taken altogether, these results reveal that the calcium activity of Arky-GPe neurons changes differently depending on the health states. In particular, the dyskinetic state was associated with a strong and abnormal reduction in the activity of Arky-GPe neurons. Considering the normal function of Arky-GPe neurons in movement inhibition (Mallet, et al., 2016; Aristieta et al., 2021), it is tempting to speculate that this abnormal inhibition of Arky-GPe neurons could contribute to the generation of the hyperkinesia present in LID. The source of Arky-GPe inhibition is currently unknown, but previous work has established that the collateral of dMSNs specifically targets onto Arky-GPe neurons, making these striatal projections a putative candidate for the Arky-GPe inhibition (Ketzef et al., 2021). In agreement with this hypothesis, our data show that the response of Arky-GPe neurons seems to always be the opposite to the response measured in the striatum. Since a large majority of FoxP2+ cells in the STR are dMSNs (Fong et al., 2018) it is likely that our STR calcium recordings are biased towards dMSNs, which thus explains this opposition of activity response between Arky-GPe and STR calcium transients.

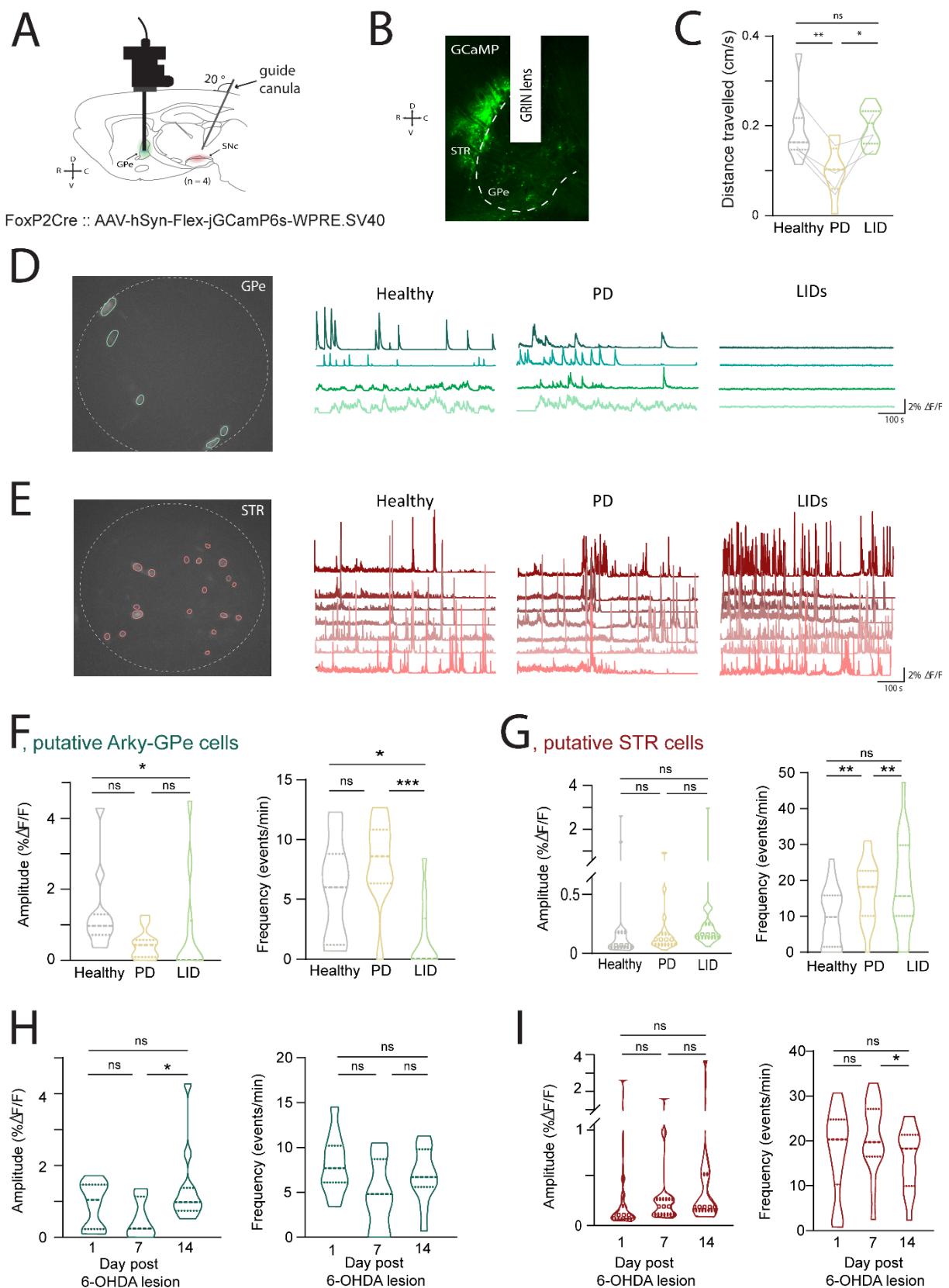


Figure 4.10. Longitudinal recordings of the calcium transients in Arky-GPe and STR neurons across different health states. **A**, Schematic representation of the experimental paradigm using FoxP2 Cre mice injected with an AAV-DIO-GCaMP-WPRE.SV40 and implanted with a GRIN lens into the GPe and a guide cannula above the SNc. **B**, Sagittal image illustrating the GCaMP labelling in the GPe and

STR. We can see that the virus injected in the GPe has leaked into the STR. In this mouse, the trace left by the lens is clearly visible in the GPe and represented by a white rectangle. **C**, Mean distance travelled by all of the mice included in this study across different behavioural conditions. ** $p=0.009$ healthy vs. PD states, * $p=0.0288$ PD vs. LID. Tukey's multiple comparison test. **D-E**, Representative maximal image projection of the GCaMP field of view (left) and raw calcium traces for sample cells across different health conditions (right) for one mouse recorded either in the GPe (**D**) or in the STR (**E**). **F**, Amplitude and frequency of calcium transients for putative GPe cells in healthy vs. PD vs. LID conditions. * $p=0.0294$ healthy vs. LID amplitude, * $p=0.0131$ healthy vs. LID frequency, *** $p=0.0009$ PD vs. LID frequency. Tukey's multiple comparison test. **G**, Amplitude and frequency of calcium transients recorded in putative STR cells in healthy vs. PD vs. LID conditions. ** $p=0.0039$ healthy vs. PD frequency, * $p=0.00023$ PD vs. LID frequency. Tukey's multiple comparison test. **H**, Amplitude and frequency recorded in putative GPe cells 1day, 7days and 14days after the 6-OHDA lesion. * $p=0.0151$ D7 vs. D14 peak amplitude. Tukey's multiple comparison test. **I**, Amplitude and frequency of putative STR cells 1day, 7days and 14days after the 6-OHDA lesion. * $p=0.0468$ D7 vs. D14 peak frequency. Tukey's multiple comparison test.

4.2.1.4 Characterisation of the *in vivo* firing rate changes in arkypallidal neurons in response to L-DOPA administration

To better interpret the decrease in calcium signals measured in Arky-GPe neurons during LID, we decided to characterise the firing rate changes of Arky-GPe neurons in response to L-DOPA administration using *in vivo* 32-channels silicon probes recordings in anesthetised FoxP2-Cre mice (Figure 4.11A). These mice were also rendered parkinsonian and presented dyskinetic behaviours in response to previous L-DOPA administration. The recording electrodes were coupled with an optic fiber to perform optogenetic stimulation on the recorded neurons (Figure 4.11B). The mice used for this project ($n=6$) were injected with an AAV-DIO-ChR2 virus in the GPe in order to distinguish Arky-GPe from Proto-GPe neurons in our recordings, based on an optotagging strategy (Figure 4.11C). This strategy relies on the response of neurons to a protocol of optogenetic stimulation using brief pulses of light (duration: 10 ms, intensity: 2.5 mW). In these conditions, only neurons expressing the excitatory opsin ChR2 (Arky-GPe neurons in our case) will show a fast excitatory response to the light-stimulation whereas the remaining neurons (i.e. prototypic neurons) would not have their firing modulated (Figure 4.11D). Following these experiments, we could record the firing activity of putative Arky-GPe (i.e. optotagged Arky-GPe, $n = 3$) or putative Proto-GPe ($n = 21$) in the parkinsonian condition and study their response to L-DOPA injection. We observed a decrease in the firing rate of Arky-GPe neurons 30 min after the injection of L-DOPA whereas Proto-GPe neurons activity was not affected overall (Figure 4.11E). Interestingly, the time-course of Arky-GPe firing inhibition parallels the time-course of dyskinesia generation that we had characterised in freely-moving mice (see Figure 4.3). Indeed, the decrease of Arky-GPe firing was evident within 10 minutes after L-DOPA injection and this inhibition lasted over 90 min. Unfortunately, due to stability issues in the course of the recording, we could only monitor such dynamic changes in activity for one optotagged Arky-GPe neuron. Therefore, future

experiments should be performed to increase n numbers and perform statistical analysis. However, these electrophysiological experiments indicated that the decrease in the calcium signal observed in Arky-GPe neurons in response to L-DOPA correlates with the inhibition of their firing activity *in vivo*. Altogether, our results so far show a clear correlation between the change in Arky-GPe activity and the development of LID which strongly questions the causal contribution of Arky-GPe neurons in the generation of LID.

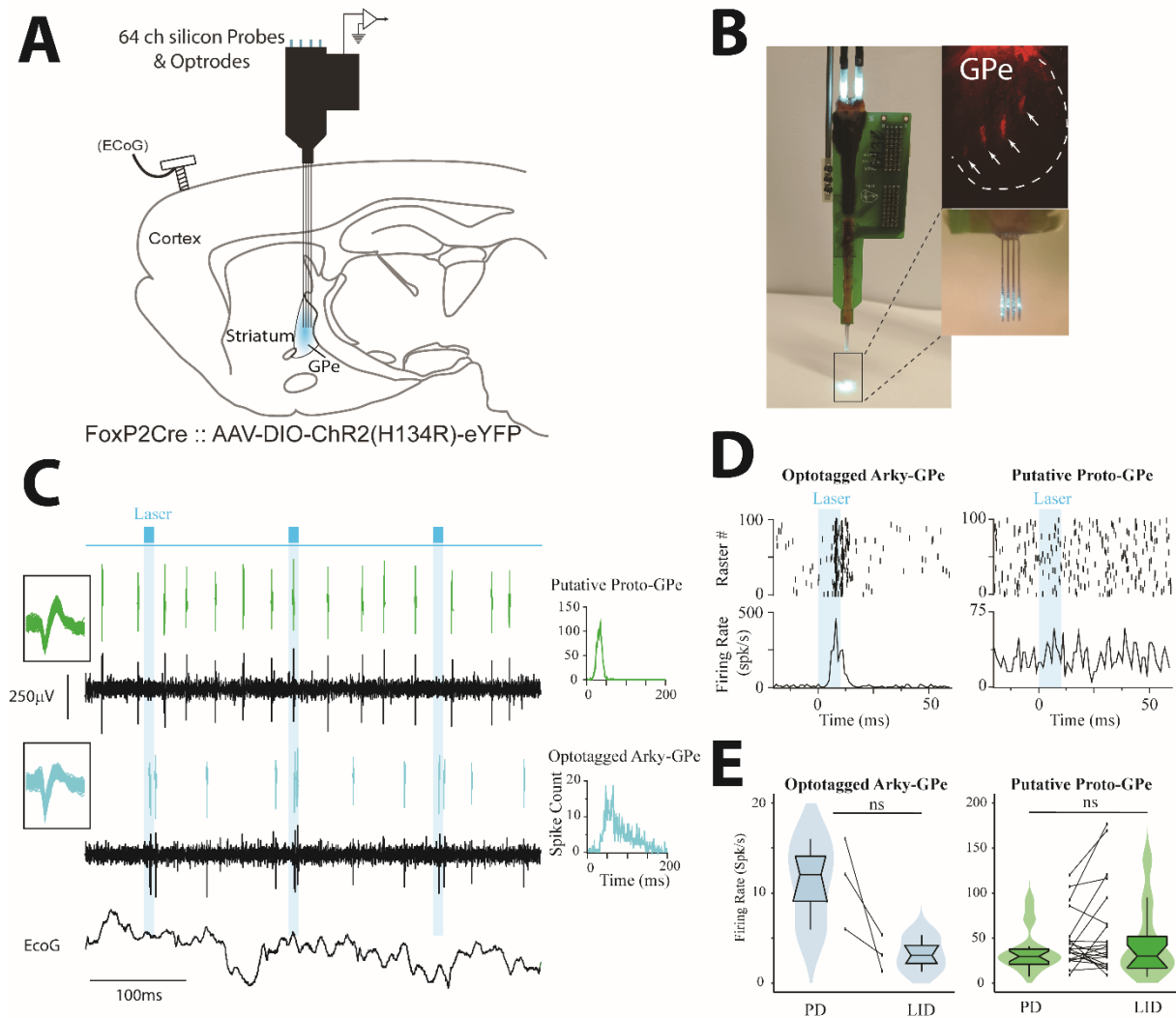


Figure 4.11. In vivo electrophysiological recordings and optotagging strategy in the GPe. **A**, Schematic representation of in vivo electrophysiological experiments using FoxP2-Cre mice injected with an AAV-DIO-ChR2-eYFP virus in the GPe. **B**, Pictures illustrating the 64-channel silicon probe recording opto-electrode used for neuronal network recording in the GPe in vivo. **C**, Typical example of raw data recordings showing an optotagged Arky-GPe (blue cell) and a putative Proto-GPe (green cell) neuron during the protocol of light stimulation. **D**, Representative example of the peri-stimulus histogram triggered by the light stimulation for the optotagged Arky-GPe and putative Proto-GPe neurons (same as in C). Note the strong excitation shortly present after the laser stimulation onset in the Arky-GPe cell (left) compared to the Proto-GPe neuron (right). **E**, Box-and-whisker plots illustrating the change of firing rate induced by the injection of L-DOPA in PD vs. LID mice for all the optotagged Arky-GPe (left plots)

and the Proto-GPe (right plots) neurons. ^{ns}p= 0.2500 PD vs. LID states (Arky-GPe); ^{ns}p= 0.4733 comparison between PD and LID states (Proto-GPe); Wilcoxon matched pairs signed rank test.

4.2.2 Causal contribution of Arky-GPe neurons in the genesis of L-DOPA-induced dyskinesia

Considering that: 1/ the firing of Arky-GPe neurons is tonic and above 10 Hz in the normal condition (Abdi et al., 2015; Mallet et al., 2016), and 2/ their key contribution to movement inhibition in normal conditions (Mallet et al., 2016; Aristieta et al., 2021), it seems logical to suggest that an abnormal reduction of their firing activity, as is present in the LID states, might have devastating consequences on motor behaviours. Here, we wanted to directly test this hypothesis and dissect the causal contribution of Arky-GPe neurons in the generation of LIDs. Having demonstrated the efficacy and specificity of our opto-excitatory approach on Arky-GPe neurons (see previous section 4.2.1.4), we decided to use this opto-strategy to restore a 'normal-like' activity of Arky-GPe neurons in dyskinetic mice and test whether the reduction of Arky-GPe neurons observed in LID state is a 'necessary' condition for the expression of LID. For this part, we thus combined optogenetic stimulation in parkinsonian or dyskinetic mice. AIMs were scored manually and the locomotion of the mice were tracked automatically using software-based analysis. Since the goal was to test the impact of Arky-GPe neurons excitation on the severity of dyskinesias, we decided to use MFB 6-OHDA lesioned mice for these experiments, as they more robustly express dyskinesia in comparison to the SNc 6-OHDA-lesioned mice.

4.2.2.1 Optogenetic stimulation of Arky-GPe neurons during LID in MFB-lesioned mice induces the restoration of normal behaviour

To test the impact of Arky-GPe neurons opto-excitation, we compared the level of AIMs and the number of contralateral rotations in the OFF, ON, and Post-ON laser stimulation periods.

All FoxP2-Cre mice (n=5), were injected with an AAV-DIO-ChR2-eYFP virus in the GPe and then implanted with an optic fiber on the side of the lesion (Figure 4.12A). The virus expression was localised in the GPe (Figure 4.12B, left panel) and the injection of the 6-OHDA into the MFB induced a near-total DA depletion in the lesioned hemisphere (Figure 4.12B, right panel).

Two weeks after the lesion, they received the first injection of L-DOPA and the evolution of each AIM subtype was scored (Figure 4.12C). AIMs reached peak values between 30 and 50 min post-injection. We therefore used this time window to test the effect of our light stimulation protocol.

The results of our Arky-GPe neurons opto-excitation showed that, for all the mice, the number of contralateral rotations, strongly present in L-DOPA-treated mice, significantly decreased during the light ON period (Figure 4.12D). In addition, the stimulation of Arky-GPe neurons decreased the severity of LID as evinced by the significant reduction in the mean AIM score during the ON epoch in comparison to the OFF and Post-ON epochs (Figure 4.12E, right panel).

Interestingly, the reduction of the overall AIM by Arky-GPe neurons excitation affected all but one mouse. Indeed, the animal that developed the most severe dyskinetic behaviours did not respond to the light stimulation (Figure 4.12E-F). Looking further into the consequences of these stimulations on the different subtypes of AIMs (i.e. axial, forelimb, orofacial), we found that the effect of the Arky-GPe-excitation could reduce axial and forelimb AIMs but not the severity of orofacial AIM (Figure 4.12F). The lack of a significant effect within the orofacial subtype could be due to anatomo-functional reasons such as the placement of the optic fiber in the dorsal part of the GPe which might have not functionally impacted the striatal region generating the orofacial AIM. Another explanation could be linked to the difficulty of collecting reliable data as they are rather difficult to record, and therefore score, on video.

Nevertheless, manipulating the Arky-GPe neurons leads to the rescue of normal-like behaviour. To illustrate this point, we plotted in three dimensions the locomotion of one mouse in figure 4.12-G. We can observe that the blue lines corresponding to the ON phases are more spread out than the grey lines corresponding to the OFF phases.

At this stage, the degree of recovery observed in our mouse model can be compared to the one observed in the seminal work by the Nelson's lab describing the reduction of LID following the opto-inhibition of D₁ neurons (dMSNs) (Girasole, 2018) potentially highlighting a common pathophysiological mechanism. That being said, since the manipulations of Arky-GPe or dMSN alone cannot fully suppress the dyskinetic phenotype in LID mice, it seems that additional neuronal mechanisms might contribute to maximising LID behaviour.

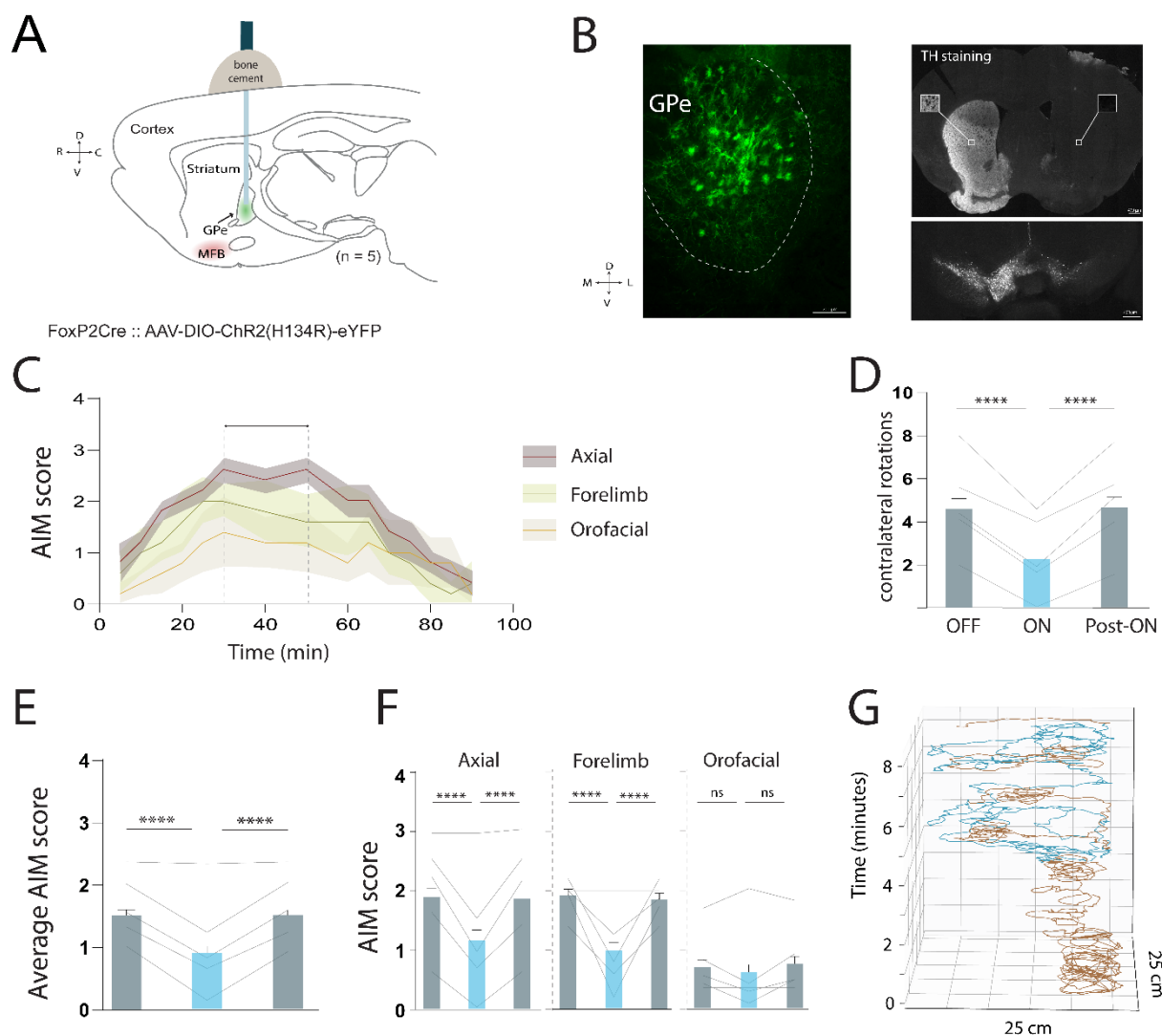


Figure 4.12. Stimulation of Arky-GPe neurons drastically reduces dyskinetic behaviour, in the MFB-lesioned model. **A**, Schematic representation of the experimental paradigm using FoxP2 Cre mice injected with an AAV-DIO-ChR2(H134R)-eYFP and implanted with an optic fiber above the GPe. **B**, Epifluorescence image of Arky-GPe transfected with an opsin, and eYFP immuno-labeling (left). Representative TH staining in the striatum and substantia nigra pars compacta (right). **C**, The time profile of AIM scores per monitoring period. The temporal development of each AIM subtype is shown with different colours (Axial: brown, Forelimb: green, Orofacial: orange). Colour shading indicates SEM. The horizontal arrow defines the chosen period for optogenetic protocols. **D**, The number of contralateral rotations is represented for the OFF, ON, and Post-ON periods. Grey lines represent individual mice. **E-F**, The average of the AIM score (**E**), and the detail for each AIM subtype (**F**) are represented for the OFF, ON, and Post-ON periods. Grey lines represent individual mice. **** $p < 0.0001$, Tukey's multiple comparison test. **G**, 3D plot of one mouse position during 10min. Blue: ON laser period (ARky-GPe activation). Brown: OFF laser period.

4.2.2.2 Optogenetic stimulation of Arky-GPe neurons in SNc-lesioned mice reduces dyskinetic behaviours

Although it is more variable to obtain a good DAergic lesion with 6-OHDA infusion in the SNc, it was important to link the results obtained from the calcium activity to those from behavioural modification induced by the Arky-GPe neurons opto-activation. So, we reproduced the same experiments of Arky-GPe neurons opto-excitation but this time, using SNc-lesioned mice (Figure 4.13).

Results were less pronounced in that case, but we still observed a significant reduction in the number of contralateral rotations induced by L-DOPA. We also observed a significant reduction of AIM axial and forelimb subtypes but, like for the MFB lesion, there were not changes for the orofacial AIMs (Figure 4.13-D).

It is likely that differences in the effect between both types of lesions can be explained by the lower level of dyskinetic behaviour present in the SNc-lesioned model.

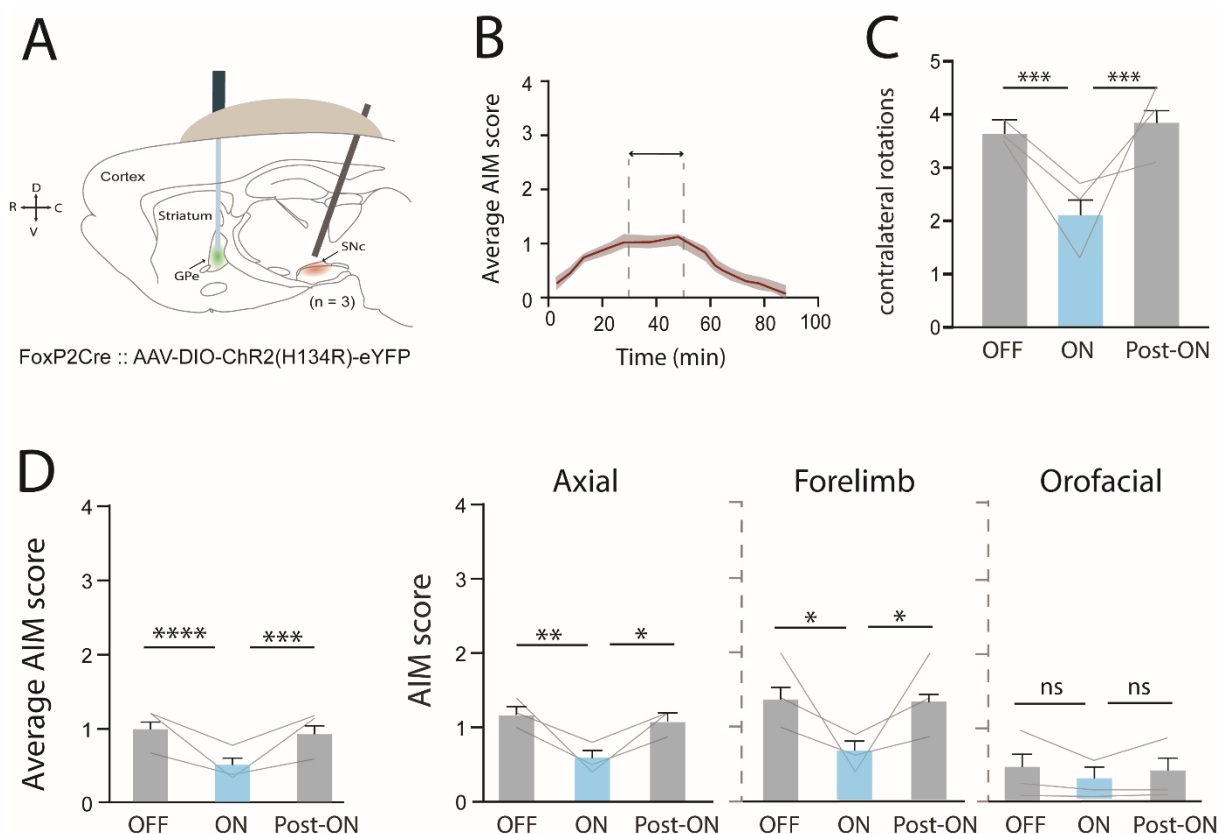


Figure 4.13. Stimulation of Arky-GPe neurons drastically reduces dyskinetic behaviour in the SNc-lesioned model. **A**, Schematic representation of the experimental paradigm using FoxP2 Cre mice injected with an AAV-DIO-ChR2(H134R)-eYFP and implanted with an optic fiber above the GPe and a cannula above the SNc for the infusion of 6-OHDA. **B**, 3D plot of the position of one mouse during 10min. Blue: ON laser period (Arky-GPe activation). Brown: OFF laser period. **C**, Distance travelled by

the same mouse across time. **C**, The number of contralateral rotations is represented for the OFF, ON, and Post-ON periods. Grey lines represent individual mice. *** $p=0.0002$ comparison between OFF vs. ON, **** $p<0.0001$ between ON and Post-ON. Tukey's multiple comparison test. **D**, The average of the AIM score (left), and the details for each AIM subtype is represented for the OFF, ON, and Post-ON periods. Grey lines represent individual mice. **** $p<0.0001$, ** $p<0.005$ Tukey's multiple comparison test.

4.2.2.3 The reduction of LID severity is specific to Arky-GPe neurons opto-excitation

In order to fully validate the specificity of our Arky-GPe neurons optogenetic manipulation on LIDs' reduction, and control the 'light' effect, we performed the same optogenetic experiments in mice injected with the DIO-CTL virus.

In these conditions, the FoxP2-Cre mice did not show any rescue of motor impairment during the light stimulation compared to the other opto-mice groups (Figure 4.14A-B). These results thus ruled out the possibility that the behavioural effect in LID was due to the light appearing in the field of view of the mouse, or to an effect of heat along the optic fiber. On the contrary, it confirms that the causal contribution of the increased activity of Arky-GPe neurons reduces LID severity.

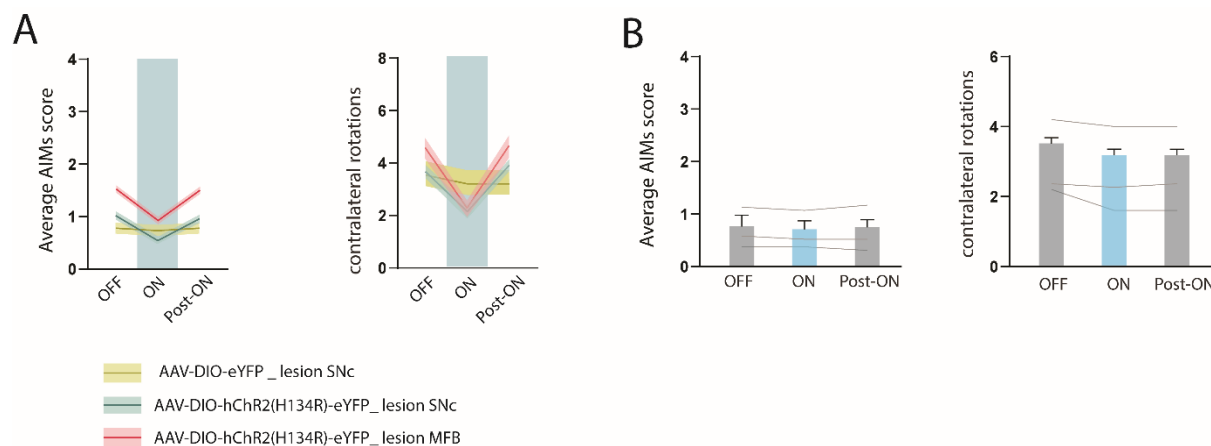


Figure 4.14. Validation of the excitatory opsin vs. CTL virus in the behavioural effect. **A**, Average AIM scores (left) and the number of contralateral rotations (right) for mice injected with the excitatory opsin ChR2(H134R) and the control virus. Yellow line: SNc-lesioned mice with DIO-control, Blue trace: SNc-lesioned mice with DIO-ChR2, Red line: MFB-lesioned mice with DIO-ChR2. Colour shading indicates SEM. **B**, Average AIM score (left) and the number of contralateral rotations (right) for control mice. The grey line indicates individual mice (n=3).

4.2.2.4 The inhibition of prototypical neuron activity during LIDs did not affect dyskinetic behaviour

As previously mentioned, Arky-GPe neurons receive inhibitory inputs from the STR (Ketzel et al., 2021) but also from the collateral of Proto-GPe neurons which powerfully controls the firing activity of Arky-GPe neurons (Ariestieta et al., 2021). So, in order to assess the contribution of Proto-GPe neurons in the generation of LIDs, we inhibited them during LID. Some transgenic Cre-mice lines exist that provide genetic access to specifically target the Proto-GPe neuronal population such as the Nkx2.1-Cre, the PV-Cre, or the Lh6x-Cre mice (Mastro et al., 2014; 2017; Dodson et al., 2015). Therefore, we first tested the contribution of Proto-GPe neurons using Nkx2.1-Cre and PV-Cre mice injected with the inhibitory opsine ArChT in the GPe (Figure 4.15 A). Our results show that the opto-inhibition of PV+ or Nkx2.1+ Proto-GPe neurons did not alter the expression of the AIM in LID mice (Figure 4.16 C-D) nor the number of contralateral rotations induce by the L-DOPA in the LID state (Figure 4.16 C-D). These results support the idea that collaterals of dMSN principally drive the inhibition of Arky-GPe neurons during LID. However, one confounding aspect of these experiments is the fact that these opto-inhibition of PV+ or Nkx2.1+ Proto-GPe neurons did not affect all the population of Proto-GPe neurons at the same time but rather major subgroups within this population. To address this issue, we used a global and non-specific chemogenetic inhibitory approach based on the constitutive expression of Designer Receptor Exclusively Activated by Designer Drugs (DREADDs) in GPe neurons.

In order to contrast the effect of CNO vs. the optogenetic stimulation of Arky-GPe neurons, this approach was used in FoxP2-Cre animals receiving a constitutive DREADD virus in the GPe, in addition to the excitatory opsin. A difference in the dynamic of LID's time course was observed, with a lower score of AIMs collected 30 minutes after the administration of L-DOPA in mice that received CNO (1mg/kg, i.p.). However, nothing emerged as significant (Figure 4.16 C).

Then, we compared the effect of the optogenetic manipulation of Arky-GPe with or without the previous administration of CNO (Figure 4.16-D). Once again, nothing appeared significantly different and the distribution of both drug protocols was similar (Figure 4.16-D). We looked at the AIM subtypes and the contralateral rotation of mice that received CNO before L-DOPA. We noted a reduction of the Arky-GPe effect on the number of contralateral rotations under CNO but this effect was due to the effect of CNO on the rotational behaviour in the OFF-laser stimulation (figure 4.16 E). For the axial and forelimb AIM subtypes, we observed the same tendency of CNO where it decreases the baseline AIM score in the OFF-laser epoch. As a

consequence of this slight decrease in baseline AIM score, the opto-excitation effect of Arky-GPe was not pronounced under CNO and the significant differences were still observed when comparing between OFF, ON, and Post-ON conditions. As before, no effect was observed in the orofacial AIM score. Taken altogether, we believe that the Proto-GPe neuron activity only plays a minor supportive role in the generation of dyskinesia. This parallels our *in vivo* electrophysiological recordings showing no changes in the firing activity of Proto-GPe neurons induced by the injection of L-DOPA (Figure 4.11 E). We conclude that the inhibition of Arky-GPe neurons induced by L-DOPA is not coming from Proto-GPe neurons but rather from the axon collaterals of D1-MSNs that seem to specifically contact Arky-GPe neurons.

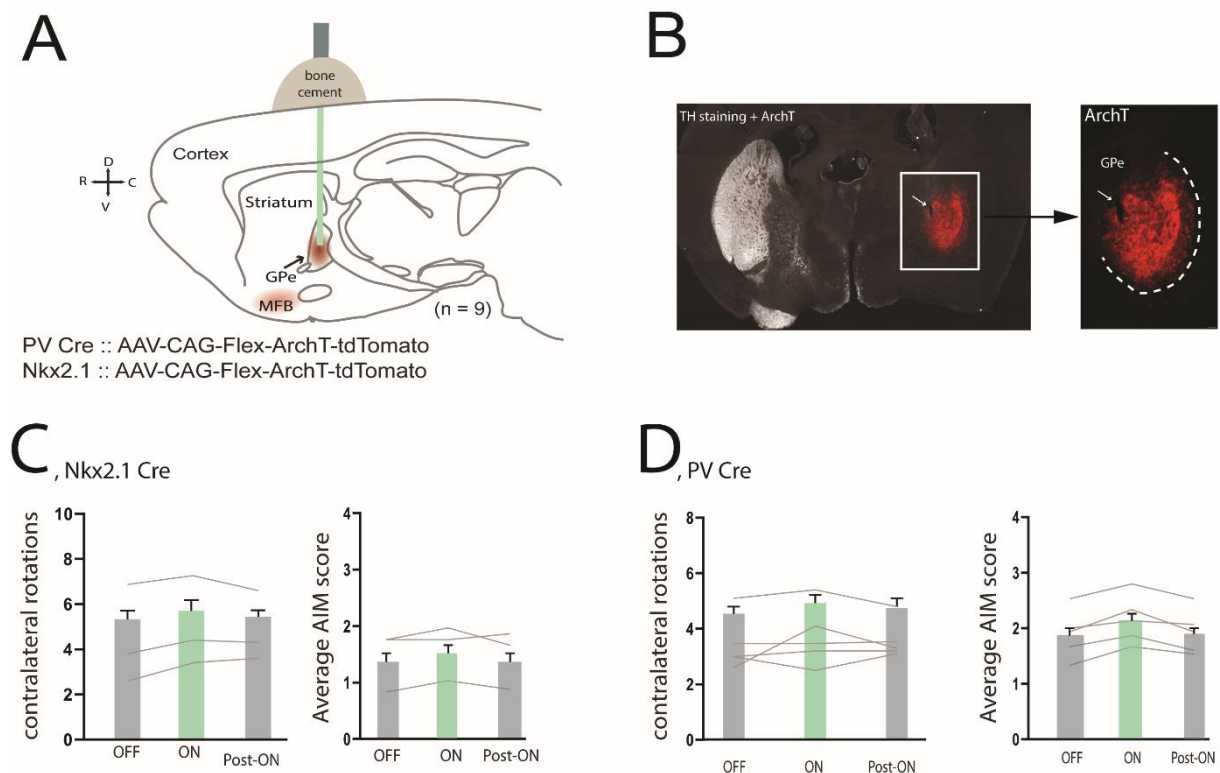


Figure 4.15. Effect of optogenetic inhibition of Proto-GPe neurons during LID in MFB-lesioned mice. **A**, Schematic representation of the experimental paradigm using PV Cre and Nkx2.1 Cre mice injected with an AAV-CAG-Flex-ArchT-tdTomato into the GPe. Mice were also implanted with an optic fiber above the GPe. **B**, Epifluorescence image of Proto-GPe transfected with theopsin (right hemisphere - red). Representative TH staining in the striatum. **C**, Number of contralateral rotations (left), and the AIM score average (right) of Nkx2.1 Cre mice for the OFF, ON, and Post-ON periods. The grey line indicates individual mice (n=3). **D**, Number of contralateral rotations (left), and the average of AIM score (right) of PV Cre mice for the OFF, ON, and Post-ON periods. The grey line indicates individual mice (n=6).

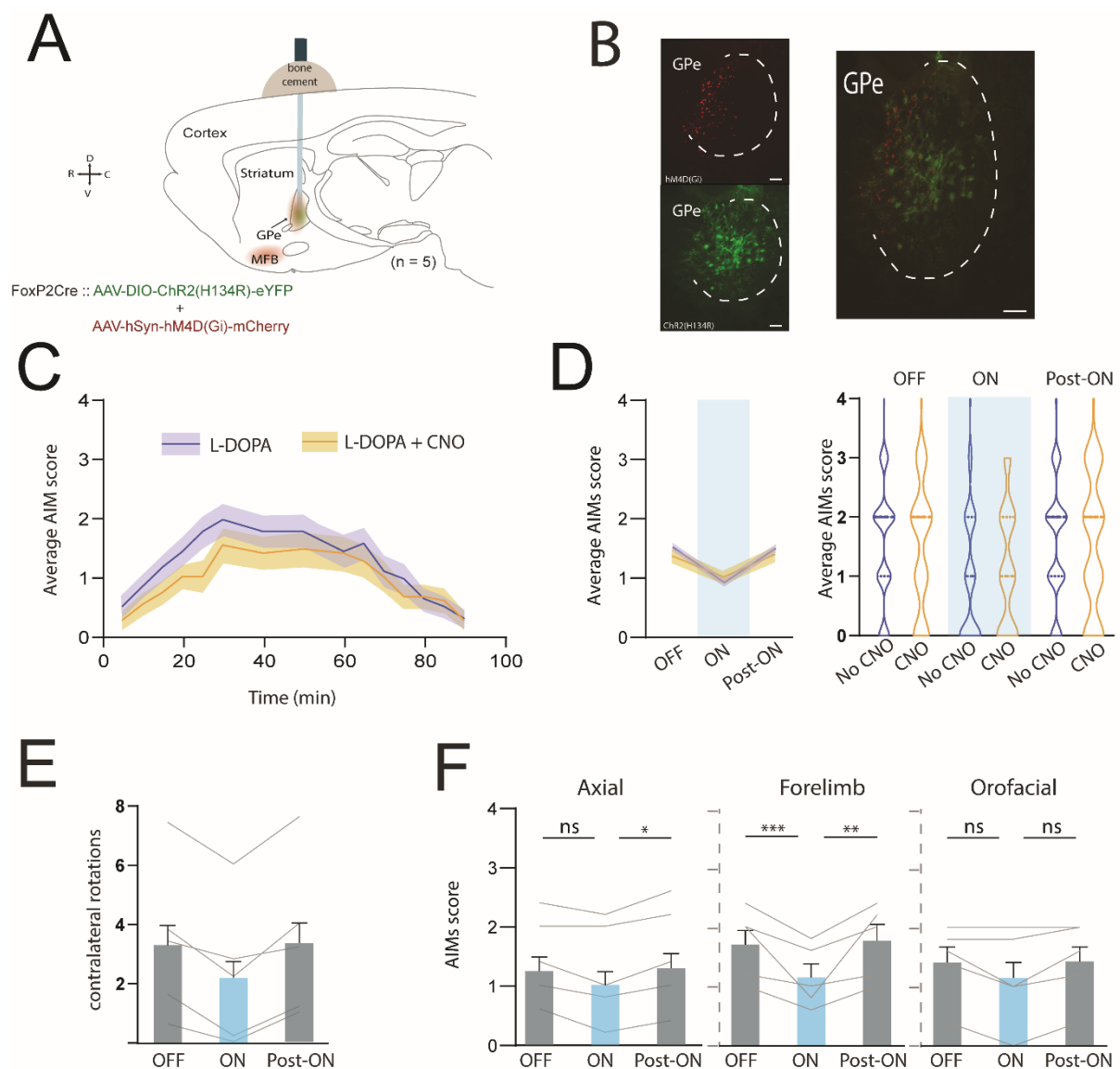


Figure 4.16: Effect of chemogenetic inhibition of Proto-GPe neurons during LID in MFB-lesioned mice. **A**, Schematic representation of the experimental paradigm using FoxP2 Cre mice injected with an AAV-DIO-ChR2(H134R)-eYFP and an AAV-hSyn-hM4D(Gi)-mCherry into the GPe. Mice were also implanted with an optic fiber above the GPe. **B**, Epifluorescence image of Arky-GPe transfected with the opsin-ChR2(H134R), eYFP immuno-labeling (green), and putative Arky-GPe, mCherry (red). **C**, The time profile of the average of the AIM scores per monitoring period. The temporal development of AIMs in mice receiving L-DOPA and L-DOPA+CNO is shown in different colours (Purple: L-DOPA, Orange: L-DOPA+CNO). Colour shading indicates SEM. **D**, Comparison of the average of the AIM scores for OFF, ON, and Post-ON periods. The same colors are used to differentiate each drug condition. **E**, The number of contralateral rotations is represented for the OFF, ON, and Post-ON periods. Grey lines represent individual mice. **F**, Different subtypes of AIM scores are represented for the OFF, ON, and Post-ON periods. Grey lines represent individual mice. *p=0.0145, **p=0.0018, ***p= 0.0002; Tukey's multiple comparison test.

4.3 Discussion

Previously described as sending a ‘cancel’ signal to the STR, Arky-GPe neurons have been proposed to play a crucial role in the cancellation of ongoing motor action. However, information about their activity in pathological conditions is lacking. Therefore, the main goal of this study was to characterise the dynamic changes of activity present in Arky-GPe neurons across different health states, from healthy conditions to two extreme pathophysiological states present in parkinsonism: the akinetic PD state in untreated subject and the hyperkinetic condition induced by L-DOPA in the LID state. Here, we found a change in the activity of Arky-GPe neurons in pathological conditions, especially under L-DOPA treatment where their calcium or spiking activity was strongly reduced. Relative to their activity in the healthy condition, the observed changes may be essential for considering the mechanisms underlying the genesis of LID.

Based on a recent study exploring the role of striatal populations in different pathological conditions (PD, LID) (Parker et al. 2018), we chose to use an SNc-lesioned mouse model. The implantation of a cannula above the SNc and the infusion of the 6-OHDA neurotoxin at two points of different depths, allowed us to obtain 67% of mice presenting a sufficient DA depletion and, more importantly, to perform a longitudinal investigation of the activity of Arky-GPe neurons across different health states.

Previous results in anaesthetised rats highlighted the effect of an acute injection of apomorphine to induce opposite effects on GPe neuron activity: an increase of the Proto-GPe neuron firing rate and of the silencing of Arky-GPe (data not published, carried out by our team). In this experiment, the changes in GPe activity directly correlated with the increase in gamma oscillations, which proves a dyskinetic state (Fogelson et al., 2005; Hutchison et al., 2009). Based on this observation, we tried to replicate these observations using L-DOPA injections in anaesthetised mice. Although we also observed a decrease in the firing rate of Arky-GPe neurons and no obvious changes in the firing rate of Proto-GPe neurons, the low number of neurons recorded over the time course of L-DOPA action (> 30 min) did not allow us to confirm the rat dataset nor to draw a strong conclusion on the effect of L-DOPA on the electrical activity of GPe neurons in mice. Consequently, our experiment constitutes an excellent indicator of firing changes present at the level of the GPe neuronal population but in no way does it provide any proof. Therefore, increasing n numbers is required to provide a definitive statistical significance. Moreover, in anaesthetised animals, confirmation of the drug’s correct action is

problematic considering the absence of behavioural output. As a solution, we are planning to perform in the near future similar electrophysiological recordings of optotagged Arky-GPe neurons but this time, applied to freely-moving mice.

To our knowledge, no data has ever reported the impact of L-DOPA on the activity of Arky-GPe in freely-moving animals. Population fluorescent imaging of calcium sensors is a powerful approach for recording cellular neural dynamics (Grienberger & Konnerth, 2012; Urai et al., 2022). Here, we used novel tools to record calcium modulation in Arky-GPe, during free exploration. First, we confirmed the variation of Arky-GPe activity after the DA depletion and under the effect of L-DOPA. For that purpose, we used the fiber photometry technique and recorded it at the population level. We observed a diminution of the fluorescent signal after the DAergic depletion and L-DOPA administration, however, the results are not as strong compared to what was expected. In the same experiment, we recorded the contralateral and ipsilateral hemispheres as a sort of control to better see the fluorescence variation. Once again, results were not as good as predicted, showing significant differences only for the area under the curve, after the administration of L-DOPA. Motion artefacts are prevalent in recordings of behaving animals. These artefacts can appear as signals of interest, reducing the interpretability of the data. Here, we tried to use methods to discard negative peaks but the frontier to remove or keep one peak is extremely thin and needs to be tweaked. In addition, non-specific expression of the GCaMP in striatal neurons could have contaminated the fluorescent signal measured in the GPe, causing miss-interpretation of the data.

Miniature miniscope offer a relatively similar approach to neuronal activity recording. Contrary to fiber photometry which only detects overall fluorescence from the region of interest, this system may image deep tissues with the resolution of a few micrometers (Stamatakis et al., 2021; Yang et al., 2017; Ghosh et al., 2011). Moreover, calcium imaging enables longitudinal studies at a single-cell resolution, but the GPe has never been imaged prior to our study. Here, we found interesting results imaging Arky-GPe neurons. In one mouse, where we were sure that the GRIN lens was positioned into the GPe, we recorded an increase in activity after the DAergic depletion and silencing of the same neurons after L-DOPA administration. Importantly, in the healthy condition, Arky-GPe neurons are not silent in the cortical activation state so it seems that during LIDs, Arky-GPe neurons receive important inhibitory inputs.

A recent study allows us to hypothesise that this over-inhibition induced by L-DOPA can be the result of dMSN collaterals. Indeed, using an electrophysiological *ex vivo* approach, Ketzef and colleagues demonstrated that dMSNs send collaterals to both populations of GPe neurons, with a bias to Arky-GPe neurons (Ketzef et al., 2021). These results, related to dMSNs being largely hyperactive and involved in the genesis of LID, is the first demonstration

that the Arky-GPe population can play a role in the generation and maintenance of LID-related mechanisms.

However, we obtained this result for only two mice. Imaging a deep structure close to a fiber bundle was not easy and so our methods need to be improved. In addition, we used the Cre line approach to specifically target Arky-GPe neurons, but the FoxP2 marker is not only a marker of Arky-GPe neurons. It has been shown that FoxP2 is highly expressed in the STR with a bias towards dMSN neurons (Fong et al., 2018). As a result, it is possible that our recordings were polluted by dMSNs and in a smaller proportion by iMSN neurons. In that sense, when looking at the GRIN lens position, we observed that two lenses were positioned in half of the STR. In these two mice, we observed neurons expressing a decrease in their fluorescence after the DAergic depletion and an increase under L-DOPA treatment. These specific cell responses seem to correspond to the calcium activity dynamics of dMSNs recorded by Parker and his colleagues across PD and LID (Parker et al., 2018). Although not restricted to the GPe and purely speculative, our results tend to confirm the opposite activity of Arky-GPe and dMSN neurons. However, to argue this we need to reproduce these data and go deeper into their analysis.

A previous study conducted in my host laboratory characterised the role of Arky-GPe neurons in the control of striatal circuit in action cancellation during normal locomotor behaviour (Aristieta et al., 2021). Added to our results in pathological conditions, the next step was to test the causal contribution of Arky-GPe neurons in the generation/maintenance of LID. In this experiment, we restore the activity of Arky-GPe during LID using optogenetic tools. The effect observed in our LID-mice model is consistent with our hypothesis about the implication of Arky-GPe in LID processes. However, we only reduced the dyskinetic behaviour without totally suppressing it. A similar reduction of dyskinetic behaviour was observed in previous optogenetic manipulations of D1-TRAPed neurons (Girasole et al., 2018). Overall, this supports the idea that the mechanisms of LID involve different actors, and cannot be reduced to the involvement of the STR (Giuseppe Di Giovanni et al., 2019; Porrás et al., 2014).

As already mentioned, the Proto-GPe neurons strongly innervate the Arky-GPe neurons (Aristieta et al., 2021; Ketzef et al., 2021). So, in order to define whether the Proto-GPe neurons can be responsible for the observed effect, we suppressed their activity during LID. Unlike Arky-GPe neurons, it is complicated to generate genetic mouse models to specifically target all the Proto-GPe neurons. Some genetic Cre lines exist to target Proto-GPe neurons (Nkx2.1 Cre, PV Cre, Lh6x Cre) but no one is able to manipulate all of the subpopulations at the same time. Here, in addition to using Nkx2.1 and PV Cre lines, we used inhibitory DREADDs injected in a FoxP2 Cre line to target all the GPe neurons. This approach is not

completely conventional but allowed us to show that even with a reduction of Proto-GPe innervation, the activation of Arky-GPe neurons is able to restore normal-like behaviour. Moreover, the inhibition of PV- or Nkx2.1-Proto-GPe neurons showed no effect on behavioural issues confirming the necessary effect led by the Arky-GPe neurons in the maintenance of LID.

On the other hand, all the AIM subtypes were not stopped by the Arky-GPe neurons manipulation. For instance, abnormal orofacial movements do not seem to be modified by the light. One of the explanations can be related to a study done in mice where orofacial movement is controlled by the ventral part of the striatum (Lee et al., 2020). Concerning the topography of each BG nucleus and their connectivity, it is plausible that like the STR, only a ventral part of the GPe is involved in this sort of abnormal movement. In this case, it is normal to not see any effects as we implanted the optic fiber in the dorsal part of the GPe.

More importantly, in this study, we used a traditional scoring of AIMS. However, this manual method presents the risk of including a scoring bias. As a solution, we are currently developing a machine-learning tool to classify and objectively quantify the normal or pathological motor behaviour. Indeed, using an adaptation of an unsupervised algorithm called “B-SOID” (Yttri et al., 2021), we analysed the video and extracted some features of behaviour which were then grouped into different clusters, such as grooming, normal walking, axial position, body angle, and contralateral rotations (See annex 1). Based on this unbiased analysis method established manually, the comparison of the time spent by the mice in each group in the OFF and ON Arky-GPe opto-excitation periods confirmed the restoration of ‘normal’ behaviour. This assisted method of analysis allowed us to compare changes in fine movement leads with the light. Interestingly, we observed a significant decrease of contralateral rotations initiated by the ipsilateral forepaw, as well as the time spent in the axial position with forelimb tremors (Annex 1-C). Moreover, the group corresponding to normal walking significantly improved with the light. Based on the new measure of dyskinesia established by Andreoli and her colleagues, we then calculated and compared the body angle formed by the intersection of two vectors: from the nose tip to the midpoint between the hind paws and the tail base (Andreoli et al., 2021). Once again this method highlights the effect of the light in restoring a normal body angle. We set up the threshold of a dyskinetic angle at 90° and observed the capacity of mice to restore a normal position of their body during Arky-GPe neurons stimulation. Here, the axial bending angle was markedly lower during the ON period of light, indicating a restoration of the spine bending during Arky-GPe neurons stimulation (Annex 1 D-E). Finally, we tested the probability of transition between two groups (Annex 1-F). We clearly saw that the probability of staying in the same group decreased (see rounded arrow in Annex1-F) except for group 5,

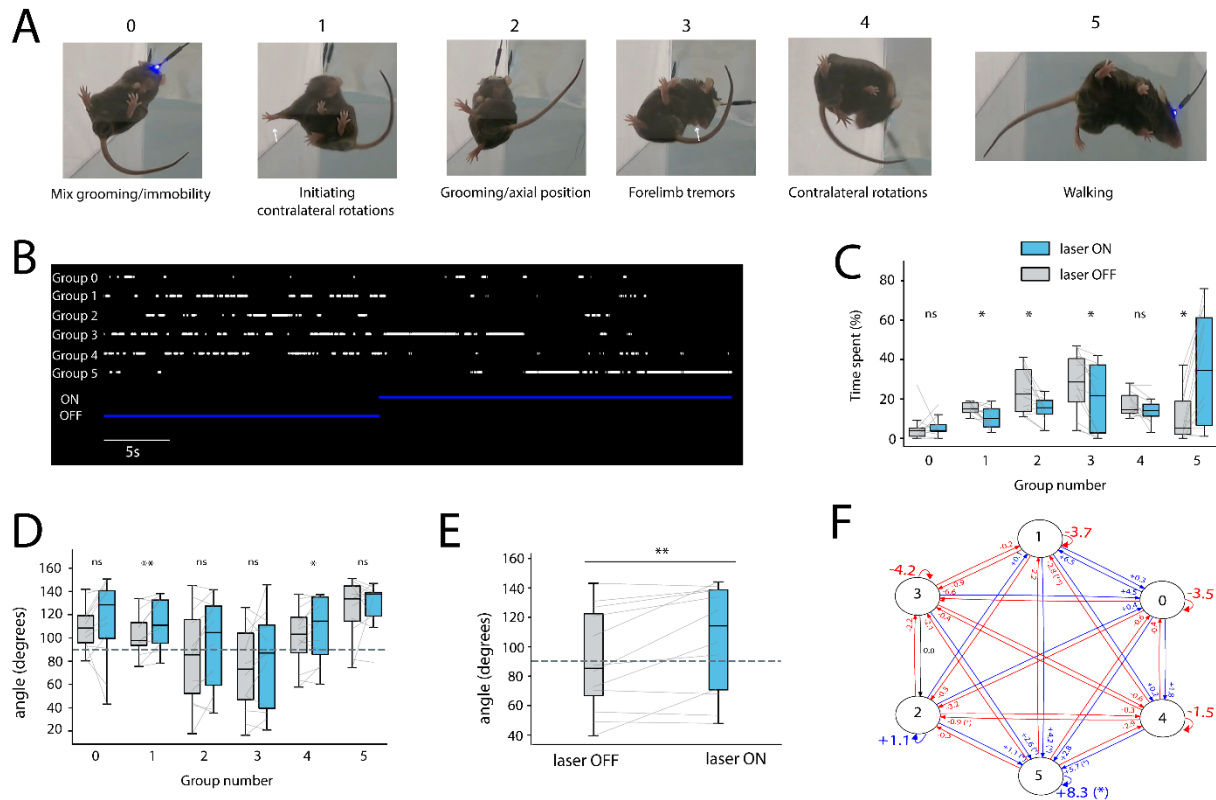
corresponding to 'normal' walking. Nowadays, the limitation in the study of LID lies in the biased method of scoring. To the best of our knowledge, this is the first unbiased analysis of dyskinetic features. Here, the results obtained indicate a strong confirmation of the effect induced by the Arky-GPe neurons activation during LID.

In summary, we obtained a lot of interesting results but this study also has some limitations. First, the diameter of the GRIN lens that we implanted into the GPe, was too large (500 μ m). Regarding our coordinates, it was easy to place the lens halfway from the STR and the GPe. Moreover, we injected a big volume of GCamP virus to be sure that the Arky-GPe neurons were transfected. However, we know that beyond 60nl, the virus leaks into the STR and may transfect all the dMSN and iMSN expressing the FoxP2 marker. So our experimental protocol needs to be refined to constrain GCamP expression only to Arky-GPe neurons.

Secondly, we quantified the number of orofacial AIMs but with the quality of our video, it was hard to follow this fine movement during the recording. Therefore, drawing conclusions encompassing this type of AIM is not entirely correct. Another drawback is the lack of electrophysiological data coming from dyskinetic freely-moving animals. Adding some data to the study of how the firing rate of Arky-GPe neurons is modified in each condition, would be helpful to understand the circuit mechanisms, although these experiments would not be able to track the activity of the same neurons across different health conditions.

Finally, we only have results for a small number of mice therefore, expanding the dataset has become one of our main objectives for the future of this project.

4.4 Annex



Annex1. Analysis of the impact of Arky-GPe opto-excitation on the motor-state transition in LID mice using an unsupervised classification method. **A**, Representative images illustrating different behavioural clusters identified in dyskinetic mice through unsupervised machine learning. Cluster 0: a mix of grooming and immobility; Cluster 1: typical contralateral rotation with the ipsilateral forepaw initiating the rotation; Cluster 2: a mix of axial position and grooming of the forepaw; Cluster 3: forelimb tremors, typical of the forelimb AIM subtype; Cluster 4: contralateral rotations; Cluster 5: walking and sequence with four paws on the ground. **B**, Example of cluster transitions mapped during 20s of OFF vs. 20s of ON laser period. The white points correspond to videoframes classified according to the motor behaviour they represent. We observed that during the ON period, transitions are less important and the majority of frames were placed in the forelimb tremor group that rapidly transitioned to the walking group. **C**, Percentage of time spent in each group for OFF and ON periods of light. Individual sessions (n=12) are shown in grey lines. *p=0.0269 comparison between OFF and ON for group 1; *p=0.0122 comparison between OFF and ON for group 2; *p=0.0207 comparison between OFF and ON for group 3; *p=0.0125 comparison between OFF and ON for group 5. Wilcoxon signed-rank test. **D**, Based on Andreoli et al. 2021, we calculated and compared the body angle of the mice as an index of axial dystonic behaviour in LID. This angle is generated from the intersection of two vectors traced from the midpoint between hind paws to the tail based and the nose tip. The dashed line corresponds to the threshold set to define normal or dyskinetic body angle. Below the threshold, the angle is considered dyskinetic. Individual sessions (n=12) are shown in grey lines. *p=0.03418 comparisons between OFF and ON periods for group 4; **p=0.00928 comparison between OFF and ON periods for the group 1. Wilcoxon signed-rank test. **E**, Comparison of the body angle during the OFF and ON periods. Individual sessions (n=12) are shown in grey lines. **p=0.021. Wilcoxon signed-rank test. **F**, Changes induced by Arky-GPe opto-excitation (i.e. ON-OFF periods) on the conditional transition probabilities between the five different motor clusters. *p<0.05 **p<0.01. Wilcoxon signed-rank test.

5. CONCLUSIONS

The results obtained in the aforementioned studies lead us to the following conclusions:

1. In control conditions, systemic administration of the 5-HT_{2A} receptor agonist TCB-2 showed a topographical-dependent effect with a specific regulatory action on limbic/cognitive territories of the SNr. TCB-2 dose-dependently stimulated medial SNr neuron activity, whereas it did not modify the electrical parameters of the lateral SNr neurons.
2. 5-HT_{2A} receptors have a preferential regulatory action on mPF BG circuits. Indeed, systemic administration of the 5-HT_{2A} receptor agonist TCB-2 favoured the cortico-nigral transmission through the direct pathway, since it induced an increase in the duration of the inhibitory response of medial SNr neurons evoked by mPFC stimulation and reduced the duration of the late excitation.
3. The effects triggered by TCB-2 on the spontaneous and cortically evoked SNr neuron activity are mediated by the 5-HT_{2A} receptor, since they were prevented by the pretreatment with the preferential antagonist MDL11939.
4. 5-HT_{2A} receptors do not tonically control the spontaneous or cortically evoked activity of SNr neurons, since neither the preferential 5-HT_{2A} receptor antagonist MDL11939 nor the non-selective 5-HT antagonist methiothepin caused any changes on their activity.
5. 5-HT depletion induced by pCPA treatment increases the basal firing rate of lateral SNr neurons and the cortico-nigral transmission through the direct pathway in mPF circuits. In addition, the absence of modulation of the SNr neuron activity following TCB-2 administration in pCPA-treated animals, highlights the participation of endogenous 5-HT in the observed effects.
6. The mobilisation of the endogenous 5-HT system by injecting the SSRI fluoxetine is not able to mimic the specific effects triggered by TCB-2. However, acute challenge of fluoxetine specifically decreased the lateral SNr neuron activity and caused important alterations in functionality in both motor and mPF circuits.

7. The Arky-GPe neuron activity is affected in different ways in PD and LID states. In mice, the DA depletion induces the activation of Arky-GPe neurons. In contrast, L-DOPA treatment leads to decrease of Arky-GPe calcium and spiking activity and even turned off in some cases. Importantly, this effect is specific on Arky-GPe neurons and disappears with the end of the drug effect.
8. Following L-DOPA administration, striatal FoxP2-MSN neurons have the opposite response to Arky-GPe neurons, i.e. increase their activity.
9. The activation of Arky-GPe neurons during dyskinetic behaviour leads to a restoration of normal-like behaviour. Recovery occurs for almost all the abnormal movement subtypes, is only observed during the stimulation period and it is not a long-term restoration.
10. The inhibition of Proto-GPe neurons during LID has no effect on AIMs, i.e Nkx2.1 or PV neurons inhibition neither improves nor worsens LID. However, the inhibition of Proto-GPe neurons at the same time as activation of Arky-GPe neurons slows down the restoration of normal movements.

6. BIBLIOGRAPHY

- Abdi, A., Mallet, N., Mohamed, F. Y., Sharott, A., Dodson, P. D., Nakamura, K. C., Suri, S., Avery, S. V., Larvin, J. T., Garas, F. N., Garas, S. N., Vinciati, F., Morin, S., Bezard, E., Baufreton, J., & Magill, P. J. (2015). Prototypic and Arkypallidal Neurons in the Dopamine-Intact External Globus Pallidus. *Journal of Neuroscience*, 35(17), 6667–6688. <https://doi.org/10.1523/JNEUROSCI.4662-14.2015>
- Abecassis, Z. A., Berceau, B. L., Win, P. H., Garcia, D., Xenias, H. S., Cui, Q., Pamucku, A., Cherian, S., Hernández, V. M., Chon, U., Lim, B. K., Justice, N. J., Awatramani, R., Kim, Y., Hooks, B. M., Gerfen, C. R., Boca, S. M., & Chan, C. S. (2019). Npas1+-Nkx2.1+ Neurons Are an Integral Part of the Cortico-pallido-cortical Loop. *BioRxiv*, 40(4), 743–768. <https://doi.org/10.1101/644674>
- Aceves, J. J., Rueda-Orozco, P. E., Hernandez-Martinez, R., Galarraga, E., & Bargas, J. (2011). Bidirectional plasticity in striatonigral synapses: A switch to balance direct and indirect basal ganglia pathways. *Learning and Memory*, 18(12), 764–773. <https://doi.org/10.1101/lm.023432.111>
- Albin, R. L., Young, A. B., & Penney, J. B. (1989). The functional anatomy of basal ganglia disorders. *Trends in Neurosciences*, 12(10), 366–375. [https://doi.org/10.1016/0166-2236\(89\)90074-X](https://doi.org/10.1016/0166-2236(89)90074-X)
- Alcacer, C., Andreoli, L., Sebastianutto, I., Jakobsson, J., Fieblinger, T., & Cenci, M. A. (2017). Chemogenetic stimulation of striatal projection neurons modulates responses to Parkinson's disease therapy. *Journal of Clinical Investigation*, 127(2), 720–734. <https://doi.org/10.1172/JCI90132>
- Alexander, G. E., & Crutcher, M. D. (1990). Functional Architecture of Basal Ganglia Circuits - Neural Substrates of Parallel Processing. *Trends in Neurosciences*, 13(7), 266–271.
- Aliane, V., Pérez, S., Nieoullon, A., Deniau, J. M., & Kemel, M. L. (2009). Cocaine-induced stereotypy is linked to an imbalance between the medial prefrontal and sensorimotor circuits of the basal ganglia. *European Journal of Neuroscience*, 30(7), 1269–1279. <https://doi.org/10.1111/j.1460-9568.2009.06907.x>
- Ammari, R., Lopez, C., Bioulac, B., Garcia, L., & Hammond, C. (2010). Subthalamic nucleus evokes similar long lasting glutamatergic excitations in pallidal, entopeduncular and nigral neurons in the basal ganglia slice. *Neuroscience*, 166(3), 808–818. <https://doi.org/10.1016/j.neuroscience.2010.01.011>
- Andreoli, L., Abbaszadeh, M., Cao, X., & Cenci, M. A. (2021). Distinct patterns of dyskinetic and

- dystonic features following D1 or D2 receptor stimulation in a mouse model of parkinsonism. *Neurobiology of Disease*, 157(June), 105429. <https://doi.org/10.1016/j.nbd.2021.105429>
- Antonazzo, M., Gutierrez-Ceballos, A., Bustinza, I., Ugedo, L., & Morera-Herreras, T. (2019). Cannabinoids differentially modulate cortical information transmission through the sensorimotor or medial prefrontal basal ganglia circuits. *British Journal of Pharmacology*, 176(8), 1156–1169. <https://doi.org/10.1111/bph.14613>
- Aristieta, A., Morera-Herreras, T., Ruiz-Ortega, J. A., Miguelez, C., Vidaurrezaga, I., Arrue, A., Zumarraga, M., & Ugedo, L. (2014). Modulation of the subthalamic nucleus activity by serotonergic agents and fluoxetine administration. *Psychopharmacology*, 231(9), 1913–1924. <https://doi.org/10.1007/s00213-013-3333-0>
- Aristieta, A., Ruiz-Ortega, J. A., Miguelez, C., Morera-Herreras, T., & Ugedo, L. (2016). Chronic L-DOPA administration increases the firing rate but does not reverse enhanced slow frequency oscillatory activity and synchronization in substantia nigra pars reticulata neurons from 6-hydroxydopamine-lesioned rats. *Neurobiology of Disease*, 89, 88–100. <https://doi.org/10.1016/j.nbd.2016.02.003>
- Aristieta, Asier, Barresi, M., Azizpour Lindi, S., Barrière, G., Courtand, G., de la Crompe, B., Guilhemsang, L., Gauthier, S., Fioramonti, S., Baufreton, J., & Mallet, N. P. (2021). A Disynaptic Circuit in the Globus Pallidus Controls Locomotion Inhibition. *Current Biology*, 31(4), 707-721.e7. <https://doi.org/10.1016/j.cub.2020.11.019>
- Aznar, S., & Hervig, M. E. S. (2016). The 5-HT_{2A} serotonin receptor in executive function: Implications for neuropsychiatric and neurodegenerative diseases. *Neuroscience and Biobehavioral Reviews*, 64, 63–82. <https://doi.org/10.1016/j.neubiorev.2016.02.008>
- Ballanger, B., Klinger, H., Eche, J., Lerond, J., Vallet, A.-E., Le Bars, D., Tremblay, L., Sgambato-Faure, V., Broussolle, E., & Thobois, S. (2012). Role of serotonergic 1A receptor dysfunction in depression associated with Parkinson's disease. *Movement Disorders*, 27(1), 84–89. <https://doi.org/10.1002/mds.23895>
- Ballanger, B., Strafella, A. P., Van Eimeren, T., Zurowski, M., Rusjan, P. M., Houle, S., & Fox, S. H. (2010). Serotonin 2A receptors and visual hallucinations in Parkinson disease. *Archives of Neurology*, 67(4), 416–421. <https://doi.org/10.1001/archneurol.2010.35>
- Balleine, B. W., & O'Doherty, J. P. (2010). Human and rodent homologues in action control: Corticostriatal determinants of goal-directed and habitual action. *Neuropsychopharmacology*, 35(1), 48–69. <https://doi.org/10.1038/npp.2009.131>
- Baron, M. S., Vitek, J. L., Bakay, R. A. E., Green, J., Kaneoke, Y., Hashimoto, T., Turner, R. S., Woodard, J. L., Cole, S. A., McDonald, W. M., & DeLong, M. R. (1996). Treatment of advanced

- Parkinson's disease by posterior GPi pallidotomy: 1-Year results of a pilot study. *Annals of Neurology*, 40(3), 355–366. <https://doi.org/10.1002/ana.410400305>
- Bastide, M. F., Meissner, W. G., Picconi, B., Fasano, S., Fernagut, P. O., Feyder, M., Francardo, V., Alcacer, C., Ding, Y., Brambilla, R., Fisone, G., Jon Stoessl, A., Bourdenx, M., Engeln, M., Navailles, S., De Deurwaerdère, P., Ko, W. K. D., Simola, N., Morelli, M., ... Bézard, E. (2015). Pathophysiology of L-dopa-induced motor and non-motor complications in Parkinson's disease. *Progress in Neurobiology*, 132, 96–168. <https://doi.org/10.1016/j.pneurobio.2015.07.002>
- Bateup, H. S., Santini, E., Shen, W., Birnbaum, S., Valjent, E., Surmeier, D. J., Fisone, G., Nestler, E. J., & Greengard, P. (2010). Distinct subclasses of medium spiny neurons differentially regulate striatal motor behaviors. *Proceedings of the National Academy of Sciences of the United States of America*, 107(33), 14845–14850. <https://doi.org/10.1073/pnas.1009874107>
- Benabid, A. L. (2003). Deep brain stimulation for Parkinson's disease. *Current Opinion in Neurobiology*, 13(6), 696–706. <https://doi.org/10.1016/j.conb.2003.11.001>
- Benabid, A. L., Chabardes, S., Mitrofanis, J., & Pollak, P. (2009). Deep brain stimulation of the subthalamic nucleus for the treatment of Parkinson's disease. *The Lancet Neurology*, 8(1), 67–81. [https://doi.org/10.1016/S1474-4422\(08\)70291-6](https://doi.org/10.1016/S1474-4422(08)70291-6)
- Benarroch, E. E. (2009). Serotonergic modulation of basal ganglia circuits: Complexity and therapeutic opportunities. *Neurology*, 73(11), 880–886. <https://doi.org/10.1212/WNL.0b013e3181b784e7>
- Benazzouz, A., Breit, S., Koudsie, A., Pollak, P., Krack, P., & Benabid, A. L. (2002). Intraoperative microrecordings of the subthalamic nucleus in Parkinson's disease. *Movement Disorders*, 17(SUPPL. 3), 145–149. <https://doi.org/10.1002/mds.10156>
- Bergman, H., Wichmann, T., Karmon, B., & DeLong, M. R. (1994). The primate subthalamic nucleus. II. Neuronal activity in the MPTP model of parkinsonism. *Journal of Neurophysiology*, 72(2), 507–520. <https://doi.org/10.1152/jn.1994.72.2.507>
- Betarbet, R., Sherer, T. B., Mackenzie, G., Garcia-osuna, M., Panov, A. V., & Greenamyre, J. T. (2000). Chronic systemic pesticide exposure produces pd symptoms Betarbet. *Nat. Neurosci.*, 26, 1301–1306. All Papers/B/Betarbet et al. 2000 - Chronic systemic pesticide exposure produces pd symptoms Betarbet.pdf
- Bevan, M. D. (1998). Selective innervation of neostriatal interneurons by a subclass of neuron in the globus pallidus of the rat. *Journal of Neuroscience*, 18(22), 9438–9452. <https://doi.org/10.1523/jneurosci.18-22-09438.1998>
- Bevan, M. D., Magill, P. J., Terman, D., Bolam, J. P., & Wilson, C. J. (2002). Move to the rhythm: Oscillations in the subthalamic nucleus-external globus pallidus network. *Trends in*

Neurosciences, 25(10), 525–531. [https://doi.org/10.1016/S0166-2236\(02\)02235-X](https://doi.org/10.1016/S0166-2236(02)02235-X)

- Beyeler, A., Kadiri, N., Navailles, S., Boujema, M. B., Gonon, F., Moine, C. L., Gross, C., & De Deurwaerdère, P. (2010). Stimulation of serotonin_{2C} receptors elicits abnormal oral movements by acting on pathways other than the sensorimotor one in the rat basal ganglia. *Neuroscience*, 169(1), 158–170. <https://doi.org/10.1016/j.neuroscience.2010.04.061>
- Bibbiani, F., Oh, J. D., & Chase, T. N. (2001). Serotonin 5-HT_{1A} agonist improves motor complications in rodent and primate parkinsonian models. *Neurology*, 57(10), 1829–1834. <https://doi.org/10.1212/WNL.57.10.1829>
- Bolam, J. P., Brown, M. T. C., Moss, J., & Magill, P. J. (2009). Basal Ganglia: Internal Organization. *Encyclopedia of Neuroscience*, 97–104. <https://doi.org/10.1016/B978-008045046-9.01294-8>
- Bonsi, P., Cuomo, D., Martella, G., Madeo, G., Schirinzi, T., Puglisi, F., Ponterio, G., & Pisani, A. (2011). Centrality of striatal cholinergic transmission in basal ganglia function. *Frontiers in Neuroanatomy*, 5(FEB), 1–9. <https://doi.org/10.3389/fnana.2011.00006>
- Bordia, T., Perez, X. A., Heiss, J. E., Zhang, D., & Quik, M. (2016). Optogenetic activation of striatal cholinergic interneurons regulates L-dopa-induced dyskinesias. *Neurobiology of Disease*, 91, 47–58. <https://doi.org/10.1016/j.nbd.2016.02.019>
- Braak, H., Rüb, U., Gai, W. P., & Del Tredici, K. (2003). Idiopathic Parkinson's disease: Possible routes by which vulnerable neuronal types may be subject to neuroinvasion by an unknown pathogen. *Journal of Neural Transmission*, 110(5), 517–536. <https://doi.org/10.1007/s00702-002-0808-2>
- Braak, Heiko, Ghebremedhin, E., Rüb, U., Bratzke, H., & Del Tredici, K. (2004). Stages in the development of Parkinson's disease-related pathology. *Cell and Tissue Research*, 318(1), 121–134. <https://doi.org/10.1007/s00441-004-0956-9>
- Brakedal, B., Toker, L., Haugarvoll, K., & Tzoulis, C. (2022). A nationwide study of the incidence, prevalence and mortality of Parkinson's disease in the Norwegian population. *Npj Parkinson's Disease*, 8(1), 1–8. <https://doi.org/10.1038/s41531-022-00280-4>
- Brücke, C., Huebl, J., Schönecker, T., Neumann, W. J., Yarrow, K., Kupsch, A., Blahak, C., Lütjens, G., Brown, P., Krauss, J. K., Schneider, G. H., & Kühn, A. A. (2012). Scaling of movement is related to pallidal γ oscillations in patients with dystonia. *Journal of Neuroscience*, 32(3), 1008–1019. <https://doi.org/10.1523/JNEUROSCI.3860-11.2012>
- Bubser, M., Backstrom, J. R., Sanders-Bush, E., Roth, B. L., & Deutch, A. Y. (2001). Distribution of serotonin 5-HT_{2A} receptors in afferents of the rat striatum. *Synapse*, 39(4), 297–304. [https://doi.org/10.1002/1098-2396\(20010315\)39:4<297::AID-SYN1012>3.0.CO;2-Q](https://doi.org/10.1002/1098-2396(20010315)39:4<297::AID-SYN1012>3.0.CO;2-Q)

- Calipari, E. S., Bagot, R. C., Purushothaman, I., Davidson, T. J., Yorgason, J. T., Peña, C. J., Walker, D. M., Pirpinias, S. T., Guise, K. G., Ramakrishnan, C., Deisseroth, K., & Nestler, E. J. (2016). In vivo imaging identifies temporal signature of D1 and D2 medium spiny neurons in cocaine reward. *Proceedings of the National Academy of Sciences of the United States of America*, 113(10), 2726–2731. <https://doi.org/10.1073/pnas.1521238113>
- Calne, D. B., & William Langston, J. (1983). Aetiology of Parkinson's Disease. *The Lancet*, 322(8365–8366), 1457–1459. [https://doi.org/10.1016/S0140-6736\(83\)90802-4](https://doi.org/10.1016/S0140-6736(83)90802-4)
- Carlsson, T. (1958). Reversal of dyskinesias in an animal model of Parkinson's disease by continuous L-DOPA delivery using rAAV vectors. *Brain*, 128(3), 559–569. <https://doi.org/10.1093/brain/awh374>
- Carta, A. R., Frau, L., Pontis, S., Pinna, A., & Morelli, M. (2008). Direct and indirect striatal efferent pathways are differentially influenced by low and high dyskinetic drugs: Behavioural and biochemical evidence. *Parkinsonism and Related Disorders*, 14(SUPPL.2), 165–168. <https://doi.org/10.1016/j.parkreldis.2008.04.023>
- Carta, M., & Bezard, E. (2011). Contribution of pre-synaptic mechanisms to L-DOPA-induced dyskinesia. *Neuroscience*, 198, 245–251. <https://doi.org/10.1016/j.neuroscience.2011.07.070>
- Carta, Manolo, Carlsson, T., Kirik, D., & Björklund, A. (2007). Dopamine released from 5-HT terminals is the cause of L-DOPA-induced dyskinesia in parkinsonian rats. *Brain*, 130(7), 1819–1833. <https://doi.org/10.1093/brain/awm082>
- Carta, Manolo, & Tronci, E. (2014). Serotonin system implication in L-DOPA-induced dyskinesia: From animal models to clinical investigations. *Frontiers in Neurology*, 5 MAY(May), 1–4. <https://doi.org/10.3389/fneur.2014.00078>
- Castrioto, A., Thobois, S., Carnicella, S., Maillet, A., & Krack, P. (2016). Emotional manifestations of PD: Neurobiological basis. *Movement Disorders*, 31(8), 1103–1113. <https://doi.org/10.1002/mds.26587>
- Castro, M. E., Pascual, J., Romón, T., Berciano, J., Figols, J., & Pazos, A. (1998). 5-HT_{1B} receptor binding in degenerative movement disorders. *Brain Research*, 790(1–2), 323–328. [https://doi.org/10.1016/S0006-8993\(97\)01566-7](https://doi.org/10.1016/S0006-8993(97)01566-7)
- Cazorla, M., deCarvalho, F. D., Chohan, M. O., Shegda, M., Chuhma, N., Rayport, S., Ahmari, S. E., Moore, H., & Kellendonk, C. (2014). Dopamine d2 receptors regulate the anatomical and functional balance of basal ganglia circuitry. *Neuron*, 81(1), 153–164. <https://doi.org/10.1016/j.neuron.2013.10.041>
- Cenci, M. A., Lee, C. S., & Björklund, A. (1998). L-DOPA-induced dyskinesia in the rat is associated

- with striatal overexpression of prodynorphin- and glutamic acid decarboxylase mRNA. *European Journal of Neuroscience*, 10(8), 2694–2706. <https://doi.org/10.1046/j.1460-9568.1998.00285.x>
- Chang, A., & Fox, S. H. (2016). Psychosis in Parkinson's Disease: Epidemiology, Pathophysiology, and Management. *Drugs*, 76(11), 1093–1118. <https://doi.org/10.1007/s40265-016-0600-5>
- Chatha, B. T., Bernard, V., Streit, P., & Bolam, J. P. (2000). Synaptic localization of ionotropic glutamate receptors in the rat substantia nigra. *Neuroscience*, 101(4), 1037–1051. [https://doi.org/10.1016/S0306-4522\(00\)00432-2](https://doi.org/10.1016/S0306-4522(00)00432-2)
- Compan, V., Segu, L., Buhot, M. C., & Daszuta, A. (1998). Selective increases in serotonin 5-HT(1B/1D) and 5-HT(2A/2C) binding sites in adult rat basal ganglia following lesions of serotonergic neurons. *Brain Research*, 793(1–2), 103–111. [https://doi.org/10.1016/S0006-8993\(98\)00168-1](https://doi.org/10.1016/S0006-8993(98)00168-1)
- Connolly, B. S., & Lang, A. E. (2014). Pharmacological Treatment of Parkinson Disease. *JAMA*, 311(16), 1670. <https://doi.org/10.1001/jama.2014.3654>
- Corvaja, N., Doucet, G., & Bolam, J. P. (1993). Ultrastructure and synaptic targets of the raphe-nigral projection in the rat. *Neuroscience*, 55(2), 417–427. [https://doi.org/10.1016/0306-4522\(93\)90510-M](https://doi.org/10.1016/0306-4522(93)90510-M)
- Crompe, B. de la, Aristieta, A., Leblois, A., Elsherbiny, S., Boraud, T., & Mallet, N. P. (2020). The globus pallidus orchestrates abnormal network dynamics in a model of Parkinsonism. *Nature Communications*, 11(1), 1–14. <https://doi.org/10.1038/s41467-020-15352-3>
- Crossman, A. R., Mitchell, I. J., Sambrook, M. A., & Jackson, A. (1988). Chorea and myoclonus in the monkey induced by gamma-aminobutyric acid antagonism in the lentiform complex: The site of drug action and a hypothesis for the neural mechanisms of chorea. *Brain*, 111(5), 1211–1233. <https://doi.org/10.1093/brain/111.5.1211>
- Cui, G., Jun, S. B., Jin, X., Pham, M. D., Vogel, S. S., Lovinger, D. M., & Costa, R. M. (2013). Concurrent activation of striatal direct and indirect pathways during action initiation. *Nature*, 494(7436), 238–242. <https://doi.org/10.1038/nature11846>
- Da Prada, M., Kettler, R., Zürcher, G., Schaffner, R., & Haefely, W. E. (1987). Inhibition of Decarboxylase and Levels of Dopa and 3-O-Methyldopa: A Comparative Study of Benserazide versus Carbidopa in Rodents and of Madopar Standard versus Madopar HBS in Volunteers. *European Neurology*, 27(1), 9–20. <https://doi.org/10.1159/000116170>
- Darmopil, S., Martín, A. B., De Diego, I. R., Ares, S., & Moratalla, R. (2009). Genetic Inactivation of Dopamine D1 but Not D2 Receptors Inhibits L-DOPA-Induced Dyskinesia and Histone Activation. *Biological Psychiatry*, 66(6), 603–613. <https://doi.org/10.1016/j.biopsych.2009.04.025>

- Dauer, W., & Przedborski, S. (2003). Parkinson's Disease. *Neuron*, 39(6), 889–909.
[https://doi.org/10.1016/S0896-6273\(03\)00568-3](https://doi.org/10.1016/S0896-6273(03)00568-3)
- Dautan, D., Huerta-Ocampo, I., Gut, N. K., Valencia, M., Kondabolu, K., Kim, Y., Gerdjikov, T. V., & Mena-Segovia, J. (2020). Cholinergic midbrain afferents modulate striatal circuits and shape encoding of action strategies. *Nature Communications*, 11(1), 1–19.
<https://doi.org/10.1038/s41467-020-15514-3>
- De Deurwaerdère, P., & Navailles, S. (2012). What can we expect from the serotonergic side of I-DOPA? *Revue Neurologique*, 168(12), 927–938. <https://doi.org/10.1016/j.neurol.2012.01.585>
- De Deurwaerdère, Philippe, & Di Giovanni, G. (2017). Serotonergic modulation of the activity of mesencephalic dopaminergic systems: Therapeutic implications. *Progress in Neurobiology*, 151, 175–236. <https://doi.org/10.1016/j.pneurobio.2016.03.004>
- de Montigny, C., & Aghajanian, G. K. (1977). Preferential action of 5-methoxytryptamine and 5-methoxydimethyltryptamine on presynaptic serotonin receptors: A comparative iontophoretic study with LSD and serotonin. *Neuropharmacology*, 16(12), 811–818.
[https://doi.org/10.1016/0028-3908\(77\)90142-3](https://doi.org/10.1016/0028-3908(77)90142-3)
- Dekundy, A., Lundblad, M., Danysz, W., & Cenci, M. A. (2007). Modulation of I-DOPA-induced abnormal involuntary movements by clinically tested compounds: Further validation of the rat dyskinesia model. *Behavioural Brain Research*, 179(1), 76–89.
<https://doi.org/10.1016/j.bbr.2007.01.013>
- Delicata, F., Bombardi, C., Pierucci, M., Di Maio, R., De Deurwaerdère, P., & Di Giovanni, G. (2018). Preferential modulation of the lateral habenula activity by serotonin-2A rather than -2C receptors: Electrophysiological and neuroanatomical evidence. *CNS Neuroscience and Therapeutics*, 24(8), 721–733. <https://doi.org/10.1111/cns.12830>
- DeLong, M. R., Crutcher, M. D., & Georgopoulos, A. P. (1983). Relations between movement and single cell discharge in the substantia nigra of the behaving monkey. *Journal of Neuroscience*, 3(8), 1599–1606. <https://doi.org/10.1523/jneurosci.03-08-01599.1983>
- DeLong, Mahlon R. (1990). Primate models of movement disorders of basal ganglia origin. *Trends in Neurosciences*, 13(7), 281–285. [https://doi.org/10.1016/0166-2236\(90\)90110-V](https://doi.org/10.1016/0166-2236(90)90110-V)
- Deniau, J. M., Mailly, P., Maurice, N., & Charpier, S. (2007). The pars reticulata of the substantia nigra: a window to basal ganglia output. *Progress in Brain Research*, 160, 151–172.
[https://doi.org/10.1016/S0079-6123\(06\)60009-5](https://doi.org/10.1016/S0079-6123(06)60009-5)
- Di Giovanni, G., Di Matteo, V., & Esposito, E. (2009). Birth, life and death of dopaminergic neurons in the substantia nigra. *Journal of Neural Transmission. Supplementum*, 73(73), 1 p preceeding

- Di Giovanni, Giuseppe, Chagraoui, A., Puginier, E., Galati, S., & De Deurwaerdère, P. (2019). Reciprocal interaction between monoaminergic systems and the pedunculopontine nucleus: Implication in the mechanism of L-DOPA. *Neurobiology of Disease*, 128, 9–18. <https://doi.org/10.1016/j.nbd.2018.08.014>
- Di Giovanni, Giuseppe, & De Deurwaerdère, P. (2018). TCB-2 [(7R)-3-bromo-2, 5-dimethoxy-bicyclo[4.2.0]octa-1,3,5-trien-7-yl]methanamine]: A hallucinogenic drug, a selective 5-HT_{2A} receptor pharmacological tool, or none of the above? *Neuropharmacology*, 142, 20–29. <https://doi.org/10.1016/j.neuropharm.2017.10.004>
- Di Matteo, V., Pierucci, M., Esposito, E., Crescimanno, G., Benigno, A., & Di Giovanni, G. (2008). Serotonin modulation of the basal ganglia circuitry: therapeutic implication for Parkinson's disease and other motor disorders. *Progress in Brain Research*, 172(08), 423–463. [https://doi.org/10.1016/S0079-6123\(08\)00921-7](https://doi.org/10.1016/S0079-6123(08)00921-7)
- Ding, S., Li, L., & Zhou, F. M. (2013). Presynaptic Serotonergic gating of the subthalamonigral glutamatergic projection. *Journal of Neuroscience*, 33(11), 4875–4885. <https://doi.org/10.1523/JNEUROSCI.4111-12.2013>
- Dodson, P. D., Dreyer, J. K., Jennings, K. A., Syed, E. C. J., Wade-Martins, R., Cragg, S. J., Bolam, J. P., Magill, P. J., & Malenka, R. C. (2016). Representation of spontaneous movement by dopaminergic neurons is cell-type selective and disrupted in parkinsonism. *Proceedings of the National Academy of Sciences of the United States of America*, 113(15), E2180–E2188. <https://doi.org/10.1073/pnas.1515941113>
- Dodson, P. D., Larvin, J. T., Butt, S. J. B., Magill, P. J., Dodson, P. D., Larvin, J. T., Duffell, J. M., Garas, F. N., Doig, N. M., & Kessaris, N. (2015). Distinct Developmental Origins Manifest in the Specialized Encoding of Movement by Adult Neurons of the External Globus Pallidus Distinct Developmental Origins Manifest in the Specialized Encoding of Movement by Adult Neurons of the External Globus Pallidus. *Neuron*, 86(2), 501–513. <https://doi.org/10.1016/j.neuron.2015.03.007>
- Dostrovsky, J., & Bergman, H. (2004). Oscillatory activity in the basal ganglia-relationship to normal physiology and pathophysiology. *Brain*, 127(4), 721–722. <https://doi.org/10.1093/brain/awh164>
- Dostrovsky, J. O., Levy, R., Wu, J. P., Hutchison, W. D., Tasker, R. R., & Lozano, A. M. (2000). Microstimulation-induced inhibition of neuronal firing in human globus pallidus. *Journal of Neurophysiology*, 84(1), 570–574. <https://doi.org/10.1152/jn.2000.84.1.570>
- Doucet, J. P., Nakabeppu, Y., Bedard, P. J., Hope, B. T., Nestler, E. J., Jasmin, B. J., Chen, J. S., Ladarola, M. J., St-Jean, M., Wigle, N., Blanchet, P., Grondin, R., & Robertson, G. S. (1996). Chronic alterations in dopaminergic neurotransmission produce a persistent elevation of AFosB-

- like protein(s) in both the rodent and primate striatum. *European Journal of Neuroscience*, 8(2), 365–381. <https://doi.org/10.1111/j.1460-9568.1996.tb01220.x>
- Dray, A., Gonye, T. J., Oakley, N. R., & Tanner, T. (1976). Evidence for the existence of a raphe projection to the substantia nigra in rat. *Brain Research*, 113(1), 45–57. [https://doi.org/10.1016/0006-8993\(76\)90005-6](https://doi.org/10.1016/0006-8993(76)90005-6)
- Edén, S., Bolle, P., & Modigh, K. (1979). Monoaminergic control of episodic growth hormone secretion in the rat: Effects of reserpine, A-methyl-P-tyrosine, P-chlorophenylalanine, and haloperidol. *Endocrinology*, 105(2), 523–529. <https://doi.org/10.1210/endo-105-2-523>
- Ehringer, H., & O., H. (1954). Verteilung von noradrenalin und dopamin im gehirn des menschen und ihr verhalten bei erkrankungen des extrapyramidalen systems. *Klinische Wochenschrift*, 1236–1239.
- Espay, A. J., Morgante, F., Merola, A., Fasano, A., Marsili, L., Fox, S. H., Bezard, E., Picconi, B., Calabresi, P., & Lang, A. E. (2018). Levodopa-induced dyskinesia in Parkinson disease: Current and evolving concepts. *Annals of Neurology*, 84(6), 797–811. <https://doi.org/10.1002/ana.25364>
- Everitt, B. J., Belin, D., Economidou, D., Pelloux, Y., Dalley, J. W., & Robbins, T. W. (2008). Neural mechanisms underlying the vulnerability to develop compulsive drug-seeking habits and addiction. *Philosophical Transactions of the Royal Society B: Biological Sciences*, 363(1507), 3125–3135. <https://doi.org/10.1098/rstb.2008.0089>
- F. Hernández, L., Castela, I., Ruiz-DeDiego, I., Obeso, J. A., & Moratalla, R. (2017). Striatal activation by optogenetics induces dyskinesias in the 6-hydroxydopamine rat model of Parkinson disease. *Movement Disorders*, 32(4), 530–537. <https://doi.org/10.1002/mds.26947>
- Faust, T. W., Assous, M., Shah, F., Tepper, J. M., & Koós, T. (2015). Novel fast adapting interneurons mediate cholinergic-induced fast GABAA inhibitory postsynaptic currents in striatal spiny neurons. *European Journal of Neuroscience*, 42(2), 1764–1774. <https://doi.org/10.1111/ejn.12915>
- Fitoussi, A., Dellu-Hagedorn, F., & De Deurwaerdère, P. (2013). Monoamines tissue content analysis reveals restricted and site-specific correlations in brain regions involved in cognition. *Neuroscience*, 255, 233–245. <https://doi.org/10.1016/j.neuroscience.2013.09.059>
- Fong, W. L., Kuo, H. Y., Wu, H. L., Chen, S. Y., & Liu, F. C. (2018). Differential and Overlapping Pattern of Foxp1 and Foxp2 Expression in the Striatum of Adult Mouse Brain. In *Neuroscience* (Vol. 388). IBRO. <https://doi.org/10.1016/j.neuroscience.2018.07.017>
- Foster, N. N., Barry, J., Korobkova, L., Garcia, L., Gao, L., Becerra, M., Sherafat, Y., Peng, B., Li, X., Choi, J. H., Gou, L., Zingg, B., Azam, S., Lo, D., Khanjani, N., Zhang, B., Stanis, J., Bowman, I.,

- Cotter, K., ... Dong, H. W. (2021). The mouse cortico–basal ganglia–thalamic network. *Nature*, 598(7879), 188–194. <https://doi.org/10.1038/s41586-021-03993-3>
- Fox, M. A., French, H. T., Laporte, J. L., Blackler, A. R., & Murphy, D. L. (2010). The serotonin 5-HT_{2A} receptor agonist TCB-2: A behavioral and neurophysiological analysis. *Psychopharmacology*, 212(1), 13–23. <https://doi.org/10.1007/s00213-009-1694-1>
- Francardo, V., Recchia, A., Popovic, N., Andersson, D., Nissbrandt, H., & Cenci, M. A. (2011). Impact of the lesion procedure on the profiles of motor impairment and molecular responsiveness to L-DOPA in the 6-hydroxydopamine mouse model of Parkinson's disease. *Neurobiology of Disease*, 42(3), 327–340. <https://doi.org/10.1016/j.nbd.2011.01.024>
- Freeze, B. S., Kravitz, A. V., Hammack, N., Berke, J. D., & Kreitzer, A. C. (2013). Control of basal ganglia output by direct and indirect pathway projection neurons. *Journal of Neuroscience*, 33(47), 18531–18539. <https://doi.org/10.1523/JNEUROSCI.1278-13.2013>
- Fries, P. (2009). Neuronal gamma-band synchronization as a fundamental process in cortical computation. *Annual Review of Neuroscience*, 32(April 2009), 209–224. <https://doi.org/10.1146/annurev.neuro.051508.135603>
- Fujiyama, F., Takahashi, S., & Karube, F. (2015). Morphological elucidation of basal ganglia circuits contributing reward prediction. *Frontiers in Neuroscience*, 9(FEB), 1–8. <https://doi.org/10.3389/fnins.2015.00006>
- Gage, G. J., Stoetzner, C. R., Wiltschko, A. B., & Berke, J. D. (2010). Selective Activation of Striatal Fast-Spiking Interneurons during Choice Execution. *Neuron*, 67(3), 466–479. <https://doi.org/10.1016/j.neuron.2010.06.034>
- Gagnon, D., Eid, L., Coudé, D., Whissel, C., Paolo, T. Di, Parent, A., & Parent, M. (2018). Evidence for sprouting of dopamine and serotonin axons in the pallidum of parkinsonian monkeys. *Frontiers in Neuroanatomy*, 12(May), 1–14. <https://doi.org/10.3389/fnana.2018.00038>
- Gerfen, C. R., Engber, T. M., Mahan, L. C., Susel, Z., Chase, T. N., Monsma, F. J., & Sibley, D. R. (1990). D₁ and D₂ Dopamine Receptor-regulated Gene Expression of Striatonigral and Striatopallidal Neurons. *Science*, 250(4986), 1429–1432. <https://doi.org/10.1126/science.2147780>
- Gerfen, C. R., & Surmeier, D. J. (2011). Modulation of striatal projection systems by dopamine. *Annual Review of Neuroscience*, 34, 441–466. <https://doi.org/10.1146/annurev-neuro-061010-113641>
- Gervais, J., & Rouillard, C. (2000). Modulates Dopaminergic Neurons in the Ventral Tegmental Area and Substantia Nigra. *Synapse*, 291(February 1999), 281–291.
- Ghosh, K. K., Burns, L. D., Cocker, E. D., Nimmerjahn, A., Ziv, Y., Gamal, A. El, & Schnitzer, M. J.

- (2011). Miniaturized integration of a fluorescence microscope. *Nature Methods*, 8(10), 871–878.
<https://doi.org/10.1038/nmeth.1694>
- Gilbertson, T., Lalo, E., Doyle, L., Di Lazzaro, V., Cioni, B., & Brown, P. (2005). Existing motor state is favored at the expense of new movement during 13-35 Hz oscillatory synchrony in the human corticospinal system. *Journal of Neuroscience*, 25(34), 7771–7779.
<https://doi.org/10.1523/JNEUROSCI.1762-05.2005>
- Girasole, A. E., Lum, M. Y., Nathaniel, D., Bair-Marshall, C. J., Guenther, C. J., Luo, L., Kreitzer, A. C., & Nelson, A. B. (2018). A Subpopulation of Striatal Neurons Mediates Levodopa-Induced Dyskinesia. *Neuron*, 97(4), 787-795.e6. <https://doi.org/10.1016/j.neuron.2018.01.017>
- Góngora-Alfaro, J. L., Hernández-López, S., Flores-Hernández, J., & Galarraga, E. (1997). Firing frequency modulation of substantia nigra reticulata neurons by 5-hydroxytryptamine. *Neuroscience Research*, 29(3), 225–231. [https://doi.org/10.1016/S0168-0102\(97\)00092-8](https://doi.org/10.1016/S0168-0102(97)00092-8)
- González-Hernández, T., & Rodríguez, M. (2000). Compartmental organization and chemical profile of dopaminergic and GABAergic neurons in the substantia nigra of the rat. *Journal of Comparative Neurology*, 421(1), 107–135. [https://doi.org/10.1002/\(SICI\)1096-9861\(20000522\)421:1<107::AID-CNE7>3.0.CO;2-F](https://doi.org/10.1002/(SICI)1096-9861(20000522)421:1<107::AID-CNE7>3.0.CO;2-F)
- Greene, A. W., Grenier, K., Aguilera, M. A., Muise, S., Farazifard, R., Haque, M. E., McBride, H. M., Park, D. S., & Fon, E. A. (2012). Mitochondrial processing peptidase regulates PINK1 processing, import and Parkin recruitment. *EMBO Reports*, 13(4), 378–385.
<https://doi.org/10.1038/embor.2012.14>
- Gremel, C. M., & Costa, R. M. (2013). Orbitofrontal and striatal circuits dynamically encode the shift between goal-directed and habitual actions. *Nature Communications*, 4(May).
<https://doi.org/10.1038/ncomms3264>
- Grienberger, C., & Konnerth, A. (2012). Imaging Calcium in Neurons. *Neuron*, 73(5), 862–885.
<https://doi.org/10.1016/j.neuron.2012.02.011>
- Guridi, J., González-Redondo, R., & Obeso, J. A. (2012). Clinical features, pathophysiology, and treatment of levodopa-induced dyskinesias in Parkinson's disease. *Parkinson's Disease*, 2012.
<https://doi.org/10.1155/2012/943159>
- Güttler, C., Altschüler, J., Tanev, K., Böckmann, S., Haumesser, J. K., Nikulin, V. V., Kühn, A. A., & van Riesen, C. (2021). Levodopa-Induced Dyskinesia Are Mediated by Cortical Gamma Oscillations in Experimental Parkinsonism. *Movement Disorders*, 36(4), 927–937.
<https://doi.org/10.1002/mds.28403>
- Haber, S. N. (2003). The primate basal ganglia: Parallel and integrative networks. *Journal of Chemical*

- Neuroanatomy*, 26(4), 317–330. <https://doi.org/10.1016/j.jchemneu.2003.10.003>
- Haider, B., & McCormick, D. A. (2009). Rapid Neocortical Dynamics: Cellular and Network Mechanisms. *Neuron*, 62(2), 171–189. <https://doi.org/10.1016/j.neuron.2009.04.008>
- Hammond, C., Bergman, H., & Brown, P. (2007). Pathological synchronization in Parkinson's disease: networks, models and treatments. *Trends in Neurosciences*, 30(7), 357–364. <https://doi.org/10.1016/j.tins.2007.05.004>
- Hang, L., Thundiyil, J., & Lim, K. L. (2015). Mitochondrial dysfunction and Parkinson disease: a Parkin–AMPK alliance in neuroprotection. *Annals of the New York Academy of Sciences*, 1350(1), 37–47. <https://doi.org/10.1111/nyas.12820>
- Haynes, W. I. A., & Haber, S. N. (2013). The organization of prefrontal-subthalamic inputs in primates provides an anatomical substrate for both functional specificity and integration: Implications for basal ganglia models and deep brain stimulation. *Journal of Neuroscience*, 33(11), 4804–4814. <https://doi.org/10.1523/JNEUROSCI.4674-12.2013>
- Herna, V. M., Hegeman, D. J., Cui, Q., Kelder, D. A., Fiske, M. P., Glajch, K. E., Pitt, J. E., Huang, T. Y., Justice, N. J., & Chan, X. C. S. (2015). *Parvalbumin 2 Neurons and Npas1 2 Neurons Are Distinct Neuron Classes in the Mouse External Globus Pallidus*. 35(34), 11830–11847. <https://doi.org/10.1523/JNEUROSCI.4672-14.2015>
- Higley, M. J., Gittis, A. H., Oldenburg, I. A., Balthasar, N., Seal, R. P., Edwards, R. H., Lowell, B. B., Kreitzer, A. C., & Sabatini, B. L. (2011). Cholinergic interneurons mediate fast VGluT3-dependent glutamatergic transmission in the striatum. *PLoS ONE*, 6(4). <https://doi.org/10.1371/journal.pone.0019155>
- Huang, K. W., Ochandarena, N. E., Philson, A. C., Hyun, M., Birnbaum, J. E., Cicconet, M., & Sabatini, B. L. (2019). Molecular and anatomical organization of the dorsal raphe nucleus. *ELife*, 8, 1–34. <https://doi.org/10.7554/eLife.46464>
- Huot, P., Fox, S. H., & Brotchie, J. M. (2011). The serotonergic system in Parkinson's disease. *Progress in Neurobiology*, 95(2), 163–212. <https://doi.org/10.1016/j.pneurobio.2011.08.004>
- Huot, P., Johnston, T. H., Darr, T., Hazrati, L. N., Visanji, N. P., Pires, D., Brotchie, J. M., & Fox, S. H. (2010). Increased 5-HT_{2A} receptors in the temporal cortex of Parkinsonian patients with visual hallucinations. *Movement Disorders*, 25(10), 1399–1408. <https://doi.org/10.1002/mds.23083>
- Hutchison, W. D., Dostrovsky, J. O., Walters, J. R., Courtemanche, R., Borraud, T., Goldberg, J., & Brown, P. (2004). Neuronal oscillations in the basal ganglia and movement disorders: Evidence from whole animal and human recordings. *Journal of Neuroscience*, 24(42), 9240–9243. <https://doi.org/10.1523/JNEUROSCI.3366-04.2004>

- Ibáñez-Sandoval, O., Tecuapetla, F., Unal, B., Shah, F., Koós, T., & Tepper, J. M. (2010). Electrophysiological and morphological characteristics and synaptic connectivity of tyrosine hydroxylase-expressing neurons in adult mouse striatum. *Journal of Neuroscience*, *30*(20), 6999–7016. <https://doi.org/10.1523/JNEUROSCI.5996-09.2010>
- Ibáñez-Sandoval, O., Tecuapetla, F., Unal, B., Shah, F., Koós, T., & Tepper, J. M. (2011). A novel functionally distinct subtype of striatal neuropeptide Y interneuron. *Journal of Neuroscience*, *31*(46), 16757–16769. <https://doi.org/10.1523/JNEUROSCI.2628-11.2011>
- Ito, H., Nyberg, S., Halldin, C., Lundkvist, C., & Farde, L. (1998). PET imaging of central 5-HT(2A) receptors with carbon-11-MDL 100,907. *Journal of Nuclear Medicine*, *39*(1), 208–214.
- Jin, X., Tecuapetla, F., & Costa, R. M. (2014). Basal ganglia subcircuits distinctively encode the parsing and concatenation of action sequences. *Nature Neuroscience*, *17*(3), 423–430. <https://doi.org/10.1038/nn.3632>
- Karube, F., Takahashi, S., Kobayashi, K., & Fujiyama, F. (2019). Motor cortex can directly drive the globus pallidus neurons in a projection neuron type-dependent manner in the rat. *eLife*, *8*, 1–25. <https://doi.org/10.7554/eLife.49511>
- Kawaguchi, Y., Wilson, C. J., Augood, S. J., & Emson, P. C. (1995). Striatal interneurons: chemical, physiological and morphological characterization. *Trends in Neurosciences*, *18*(12), 527–535. [https://doi.org/10.1016/0166-2236\(95\)98374-8](https://doi.org/10.1016/0166-2236(95)98374-8)
- Keifman, E., Ruiz-DeDiego, I., Pafundo, D. E., Paz, R. M., Solís, O., Murer, M. G., & Moratalla, R. (2019). Optostimulation of striatonigral terminals in substantia nigra induces dyskinesia that increases after L-DOPA in a mouse model of Parkinson's disease. *British Journal of Pharmacology*, *176*(13), 2146–2161. <https://doi.org/10.1111/bph.14663>
- Ketzef, M., & Silberberg, G. (2021). Article Differential Synaptic Input to External Globus Pallidus Neuronal Subpopulations In Vivo II Differential Synaptic Input to External Globus Pallidus Neuronal Subpopulations In Vivo. *Neuron*, *109*(3), 516-529.e4. <https://doi.org/10.1016/j.neuron.2020.11.006>
- Kha, H. T., Finkelstein, D. I., Tomas, D., Drago, J., Pow, D. V., & Horne, M. K. (2001). Projections from the substantia nigra pars reticulata to the motor thalamus of the rat: Single axon reconstructions and immunohistochemical study. *The Journal of Comparative Neurology*, *440*(1), 20–30. <https://doi.org/10.1002/cne.1367>
- Kita, H., & Kitai, S. T. (1987). Efferent projections of the subthalamic nucleus in the rat: Light and electron microscopic analysis with the PHA-L method. *Journal of Comparative Neurology*, *260*(3), 435–452. <https://doi.org/10.1002/cne.902600309>

- Kita, Hitoshi, Tokuno, H., & Nambu, A. (1999). Monkey globus pallidus external segment neurons projecting to the neostriatum. *NeuroReport*, 10(7), 1467–1472. <https://doi.org/10.1097/00001756-199905140-00014>
- Koketsu, D., Chiken, S., Hisatsune, T., Miyachi, S., & Nambu, A. (2021). Elimination of the Cortico-Subthalamic Hyperdirect Pathway Induces Motor Hyperactivity in Mice. *Journal of Neuroscience*, 41(25), 5502–5510. <https://doi.org/10.1523/JNEUROSCI.1330-20.2021>
- Kolomiets, B. P., Deniau, J. M., Glowinski, J., & Thierry, A. M. (2003). Basal ganglia and processing of cortical information: Functional interactions between trans-striatal and trans-subthalamic circuits in the substantia nigra pars reticulata. *Neuroscience*, 117(4), 931–938. [https://doi.org/10.1016/S0306-4522\(02\)00824-2](https://doi.org/10.1016/S0306-4522(02)00824-2)
- Koshimizu, Y., Fujiyama, F., Nakamura, K. C., Furuta, T., & Kaneko, T. (2013). Quantitative analysis of axon bouton distribution of subthalamic nucleus neurons in the rat by single neuron visualization with a viral vector. *Journal of Comparative Neurology*, 521(9), 2125–2146. <https://doi.org/10.1002/cne.23277>
- Kravitz, A. V., Freeze, B. S., Parker, P. R. L., Kay, K., Myo, T., Deisseroth, K., & Kreitzer, A. C. (2010). Control of Basal Ganglia Circuitry. *Nature*, 466(7306), 622–626. <https://doi.org/10.1038/nature09159.Regulation>
- Kühn, A. A., Kupsch, A., Schneider, G. H., & Brown, P. (2006). Reduction in subthalamic 8-35 Hz oscillatory activity correlates with clinical improvement in Parkinson's disease. *European Journal of Neuroscience*, 23(7), 1956–1960. <https://doi.org/10.1111/j.1460-9568.2006.04717.x>
- Lacombe, E., Khaindrava, V., Melon, C., Oueslati, A., Kerkerian-Le Goff, L., & Salin, P. (2009). Different functional basal ganglia subcircuits associated with anti-akinetic and dyskinesigenic effects of antiparkinsonian therapies. *Neurobiology of Disease*, 36(1), 116–125. <https://doi.org/10.1016/j.nbd.2009.07.002>
- Lagière, M., Bosc, M., Whitestone, S., Benazzouz, A., Chagraoui, A., Millan, M. J., & Deurwaerdère, P. De. (2020). A subset of purposeless oral movements triggered by dopaminergic agonists is modulated by 5-HT_{2C} receptors in rats: Implication of the subthalamic nucleus. *International Journal of Molecular Sciences*, 21(22), 1–22. <https://doi.org/10.3390/ijms21228509>
- Lavian, H., Almog, M., Madar, R., Loewenstern, Y., Bar-Gad, I., Okun, E., & Korngreen, A. (2017). Dopaminergic modulation of synaptic integration and firing patterns in the rat entopeduncular nucleus. *Journal of Neuroscience*, 37(30), 7177–7187. <https://doi.org/10.1523/JNEUROSCI.0639-17.2017>
- Leal, P. C., Bispo, J. M. M., Engelberth, R. C. G. J., Kayo, K. D., Meurer, Y. R., Ribeiro, A. M., Silva, R. H., Marchioro, M., & Santos, J. R. (2019). Serotonergic dysfunction in a model of

- parkinsonism induced by reserpine. *Journal of Chemical Neuroanatomy*, 96(December 2018), 73–78. <https://doi.org/10.1016/j.jchemneu.2018.12.011>
- Lee, J., Wang, W., & Sabatini, B. L. (2020). Anatomically segregated basal ganglia pathways allow parallel behavioral modulation. *Nature Neuroscience*. <https://doi.org/10.1038/s41593-020-00712-5>
- Legaria, A. A., Matikainen-Ankney, B. A., Yang, B., Ahanonu, B., Licholai, J. A., Parker, J. G., & Kravitz, A. V. (2022). Fiber photometry in striatum reflects primarily nonsomatic changes in calcium. *Nature Neuroscience*, 25(9), 1124–1128. <https://doi.org/10.1038/s41593-022-01152-z>
- Liu, D., Li, W., Ma, C., Zheng, W., Yao, Y., Tso, C. F., Zhong, P., Chen, X., Song, J. H., Choi, W., Paik, S. B., Han, H., & Dan, Y. (2020). A common hub for sleep and motor control in the substantia nigra. *Science*, 367(6476), 440–445. <https://doi.org/10.1126/science.aaz0956>
- López-Giménez, J. F., Mengod, G., Palacios, J. M., & Vilaró, M. T. (1997). Selective visualization of rat brain 5-HT(2A) receptors by autoradiography with [3H]MDL 100,907. *Naunyn-Schmiedeberg's Archives of Pharmacology*, 356(4), 446–454. <https://doi.org/10.1007/PL00005075>
- Lundblad, M., Picconi, B., Lindgren, H., & Cenci, M. A. (2004). A model of L-DOPA-induced dyskinesia in 6-hydroxydopamine lesioned mice: Relation to motor and cellular parameters of nigrostriatal function. *Neurobiology of Disease*, 16(1), 110–123. <https://doi.org/10.1016/j.nbd.2004.01.007>
- Lyons, K. E. (2018). *Amantadine extended-release capsules for levodopa-induced dyskinesia in patients with Parkinson ' s disease*. 665–673.
- Mallet, N., Micklem, B. R., Henny, P., Brown, M. T., Williams, C., Bolam, J. P., Nakamura, K. C., & Magill, P. J. (2012). Dichotomous Organization of the External Globus Pallidus. *Neuron*, 74(6), 1075–1086. <https://doi.org/10.1016/j.neuron.2012.04.027>
- Mallet, N., Schmidt, R., Leventhal, D., Chen, F., Amer, N., Boraud, T., & Berke, J. D. (2016). Arkypallidal Cells Send a Stop Signal to Striatum. *Neuron*, 89(2). <https://doi.org/10.1016/j.neuron.2015.12.017>
- Martín-Ruiz, R., Puig, M. V., Celada, P., Shapiro, D. A., Roth, B. L., Mengod, G., & Artigas, F. (2001). Control of Serotonergic Function in Medial Prefrontal Cortex by Serotonin-2A Receptors through a Glutamate-Dependent Mechanism. *The Journal of Neuroscience*, 21(24), 9856–9866. <https://doi.org/10.1523/JNEUROSCI.21-24-09856.2001>
- Masliyah, E., Rockenstein, E., Mante, M., Crews, L., Spencer, B., Adame, A., Patrick, C., Trejo, M., Ubhi, K., Rohn, T. T., Mueller-Steiner, S., Seubert, P., Barbour, R., McConlogue, L., Buttini, M., Games, D., & Schenk, D. (2011). Passive immunization reduces behavioral and

- neuropathological deficits in an alpha-synuclein transgenic model of lewy body disease. *PLoS ONE*, 6(4). <https://doi.org/10.1371/journal.pone.0019338>
- Mastro, K. J., Bouchard, R. S., Holt, H. A. K., & Gittis, A. H. (2014). *Transgenic Mouse Lines Subdivide External Segment of the Globus Pallidus (GPe) Neurons and Reveal Distinct GPe Output Pathways*. 34(6), 2087–2099. <https://doi.org/10.1523/JNEUROSCI.4646-13.2014>
- Mastro, K. J., Zitelli, K. T., Willard, A. M., Leblanc, K. H., Kravitz, A. V., & Gittis, A. H. (2017). Cell-specific pallidal intervention induces long-lasting motor recovery in dopamine-depleted mice. *Nature Neuroscience*, 20(6), 815–823. <https://doi.org/10.1038/nn.4559>
- Mathis, A., Mamidanna, P., Cury, K. M., Abe, T., Murthy, V. N., Mathis, M. W., & Bethge, M. (2018). DeepLabCut: markerless pose estimation of user-defined body parts with deep learning. *Nature Neuroscience*, 21(9), 1281–1289. <https://doi.org/10.1038/s41593-018-0209-y>
- Matsuda, W., Furuta, T., Nakamura, K. C., Hioki, H., Fujiyama, F., Arai, R., & Kaneko, T. (2009). Single nigrostriatal dopaminergic neurons form widely spread and highly dense axonal arborizations in the neostriatum. *The Journal of Neuroscience : The Official Journal of the Society for Neuroscience*, 29(2), 444–453. <https://doi.org/10.1523/JNEUROSCI.4029-08.2009>
- Maurice, N., Deniau, J. M., Glowinski, J., & Thierry, A. M. (1999). Relationships between the prefrontal cortex and the basal ganglia in the rat: Physiology of the cortico-nigral circuits. *Journal of Neuroscience*, 19(11), 4674–4681. <https://doi.org/10.1523/jneurosci.19-11-04674.1999>
- McElvain, L. E., Chen, Y., Moore, J. D., Brigidi, G. S., Bloodgood, B. L., Lim, B. K., Costa, R. M., & Kleinfeld, D. (2021). Specific populations of basal ganglia output neurons target distinct brain stem areas while collateralizing throughout the diencephalon. *Neuron*, 109(10), 1721-1738.e4. <https://doi.org/10.1016/j.neuron.2021.03.017>
- Meissner, W., Ravenscroft, P., Reese, R., Harnack, D., Morgenstern, R., Kupsch, A., Klitgaard, H., Bioulac, B., Gross, C. E., Bezard, E., & Boraud, T. (2006). Increased slow oscillatory activity in substantia nigra pars reticulata triggers abnormal involuntary movements in the 6-OHDA-lesioned rat in the presence of excessive extracellular striatal dopamine. *Neurobiology of Disease*, 22(3), 586–598. <https://doi.org/10.1016/j.nbd.2006.01.009>
- Mela, F., Marti, M., Dekundy, A., Danyasz, W., Morari, M., & Cenci, M. A. (2007). Antagonism of metabotropic glutamate receptor type 5 attenuates L-DOPA-induced dyskinesia and its molecular and neurochemical correlates in a rat model of Parkinson's disease. *Journal of Neurochemistry*, 101(2), 483–497. <https://doi.org/10.1111/j.1471-4159.2007.04456.x>
- Miczek, K. A., Altman, J. L., Appel, J. B., & Boggan, W. O. (1975). Para-chlorophenylalanine, serotonin and killing behavior. *Pharmacology, Biochemistry and Behavior*, 3(3), 355–361. [https://doi.org/10.1016/0091-3057\(75\)90043-X](https://doi.org/10.1016/0091-3057(75)90043-X)

- Middleton, F. A., & Strick, P. L. (2000). Basal ganglia and cerebellar loops: Motor and cognitive circuits. *Brain Research Reviews*, 31(2–3), 236–250. [https://doi.org/10.1016/S0165-0173\(99\)00040-5](https://doi.org/10.1016/S0165-0173(99)00040-5)
- Miguelé, C., Navailles, S., De Deurwaerdère, P., & Ugedo, L. (2016). The acute and long-term L-DOPA effects are independent from changes in the activity of dorsal raphe serotonergic neurons in 6-OHDA lesioned rats. *British Journal of Pharmacology*, 2135–2146. <https://doi.org/10.1111/bph.13447>
- Miguelé, Cristina, Morera-Herreras, T., Torrecilla, M., Ruiz-Ortega, J. A., & Ugedo, L. (2014). Interaction between the 5-HT system and the basal ganglia: functional implication and therapeutic perspective in Parkinson's disease. *Frontiers in Neural Circuits*, 8(March), 1–9. <https://doi.org/10.3389/fncir.2014.00021>
- Miller, D. W., Miller, D. W., Abercrombie, E. D., & Abercrombie, E. D. (1999). *Role of High-Affinity Dopamine Uptake and Impulse Activity in the Appearance of Extracellular Dopamine in Striatum After Administration of Exogenous*. 1516–1522.
- Mink, J. W. (2003). The Basal Ganglia and Involuntary Movements. *Archives of Neurology*, 60(10), 1365. <https://doi.org/10.1001/archneur.60.10.1365>
- Miyamoto, S., Duncan, G. E., Marx, C. E., & Lieberman, J. A. (2005). Treatments for schizophrenia: A critical review of pharmacology and mechanisms of action of antipsychotic drugs. *Molecular Psychiatry*, 10(1), 79–104. <https://doi.org/10.1038/sj.mp.4001556>
- Montagu, K. A. (1957). Catechol Compounds in Rat Tissues and in Brains of Different Animals. *Nature*, 180(4579), 244–245. <https://doi.org/10.1038/180244a0>
- Morilak, D. A., & Ciaranello, R. D. (1993). 5-HT₂ receptor immunoreactivity on cholinergic neurons of the pontomesencephalic tegmentum shown by double immunofluorescence. *Brain Research*, 627(1), 49–54. [https://doi.org/10.1016/0006-8993\(93\)90747-B](https://doi.org/10.1016/0006-8993(93)90747-B)
- Muir, J., Lorsch, Z. S., Ramakrishnan, C., Deisseroth, K., Nestler, E. J., Calipari, E. S., & Bagot, R. C. (2018). In vivo fiber photometry reveals signature of future stress susceptibility in nucleus accumbens. *Neuropsychopharmacology*, 43(2), 255–263. <https://doi.org/10.1038/npp.2017.122>
- Murer, M. Gustavo, Riquelme, L. A., Tseng, K. Y., & Pazo, J. H. (1997). Substantia nigra pars reticulata single unit activity in normal and 6OHDA-lesioned rats: Effects of intrastriatal apomorphine and subthalamic lesions. *Synapse*, 27(4), 278–293. [https://doi.org/10.1002/\(SICI\)1098-2396\(199712\)27:4<278::AID-SYN2>3.0.CO;2-9](https://doi.org/10.1002/(SICI)1098-2396(199712)27:4<278::AID-SYN2>3.0.CO;2-9)
- Murer, Mario Gustavo, & Moratalla, R. (2011). Striatal signaling in L-DOPA-induced dyskinesia: Common mechanisms with drug abuse and long term memory involving D1 dopamine receptor

- stimulation. *Frontiers in Neuroanatomy*, 5(AUG), 1–12. <https://doi.org/10.3389/fnana.2011.00051>
- Nambu, A., Tokuno, H., & Takada, M. (2002). Functional significance of the cortico-subthalamo-pallidal “hyperdirect” pathway. *Neuroscience Research*, 43(2), 111–117. [https://doi.org/10.1016/S0168-0102\(02\)00027-5](https://doi.org/10.1016/S0168-0102(02)00027-5)
- Näslund, J., Studer, E., Nilsson, K., Westberg, L., & Eriksson, E. (2013). Serotonin depletion counteracts sex differences in anxiety-related behaviour in rat. *Psychopharmacology*, 230(1), 29–35. <https://doi.org/10.1007/s00213-013-3133-6>
- Naslund, J., Studer, E., Pettersson, R., Hagsater, M., Nilsson, S., Nissbrandt, H., & Eriksson, E. (2015). Differences in anxiety-like behavior within a batch of wistar rats are associated with differences in serotonergic transmission, enhanced by acute sri administration, and abolished by serotonin depletion. *International Journal of Neuropsychopharmacology*, 18(8), 1–9. <https://doi.org/10.1093/ijnp/pyv018>
- Navailles, S., Bioulac, B., Gross, C., & De Deurwaerdère, P. (2011). Chronic L-DOPA therapy alters central serotonergic function and L-DOPA-induced dopamine release in a region-dependent manner in a rat model of Parkinson's disease. *Neurobiology of Disease*, 41(2), 585–590. <https://doi.org/10.1016/j.nbd.2010.11.007>
- Nikulin, V. V., & Brismar, T. (2005). Long-range temporal correlations in electroencephalographic oscillations: Relation to topography, frequency band, age and gender. *Neuroscience*, 130(2), 549–558. <https://doi.org/10.1016/j.neuroscience.2004.10.007>
- Nonomura, S., Nishizawa, K., Sakai, Y., Kawaguchi, Y., Kato, S., Uchigashima, M., Watanabe, M., Yamanaka, K., Enomoto, K., Chiken, S., Sano, H., Soma, S., Yoshida, J., Samejima, K., Ogawa, M., Kobayashi, K., Nambu, A., Isomura, Y., & Kimura, M. (2018). Monitoring and Updating of Action Selection for Goal-Directed Behavior through the Striatal Direct and Indirect Pathways. *Neuron*, 99(6), 1302–1314.e5. <https://doi.org/10.1016/j.neuron.2018.08.002>
- North, R. A., & Uchimura, N. (1989). 5-Hydroxytryptamine acts at 5-HT₂ receptors to decrease potassium conductance in rat nucleus accumbens neurones. *The Journal of Physiology*, 417(1), 1–12. <https://doi.org/10.1113/jphysiol.1989.sp017786>
- Obeso, J. A., Rodríguez-Oroz, M. C., Rodríguez, M., Arbizu, J., & Giménez-Amaya, J. M. (2002). The basal ganglia and disorders of movement: Pathophysiological mechanisms. *News in Physiological Sciences*, 17(2), 51–55. <https://doi.org/10.1152/nips.01363.2001>
- Obeso, J. A., Rodríguez-Oroz, M. C., Rodríguez, M., Lanciego, J. L., Artieda, J., Gonzalo, N., & Olanow, C. W. (2000). Pathophysiology of the basal ganglia in Parkinson's disease. *Trends in Neurosciences*, 23(Box 1), S8–S19. [https://doi.org/10.1016/S1471-1931\(00\)00028-8](https://doi.org/10.1016/S1471-1931(00)00028-8)

- Oh, Y. M., Karube, F., Takahashi, S., Kobayashi, K., Takada, M., Uchigashima, M., Watanabe, M., Nishizawa, K., Kobayashi, K., & Fujiyama, F. (2017). Using a novel PV-Cre rat model to characterize pallidonigral cells and their terminations. *Brain Structure and Function*, 222(5), 2359–2378. <https://doi.org/10.1007/s00429-016-1346-2>
- Olanow, C. W., Stern, M. B., & Sethi, K. (2009). The scientific and clinical basis for the treatment of Parkinson disease (2009). *Neurology*, 72(21 SUPPL. 4). <https://doi.org/10.1212/WNL.0b013e3181a1d44c>
- Oueslati, A., Sgambato-Faure, V., Melon, C., Kachidian, P., Gubellini, P., Amri, M., Goff, L. K. Le, & Salin, P. (2007). High-frequency stimulation of the subthalamic nucleus potentiates L-DOPA-induced neurochemical changes in the striatum in a rat model of Parkinson's disease. *Journal of Neuroscience*, 27(9), 2377–2386. <https://doi.org/10.1523/JNEUROSCI.2949-06.2007>
- Pagano, G., Niccolini, F., & Politis, M. (2018). The serotonergic system in Parkinson's patients with dyskinesia: evidence from imaging studies. *Journal of Neural Transmission*, 125(8), 1217–1223. <https://doi.org/10.1007/s00702-017-1823-7>
- Parent, A., & Hazrati, L. N. (1995). Functional anatomy of the basal ganglia. II. The place of subthalamic nucleus and external pallidum in basal ganglia circuitry. *Brain Research Reviews*, 20(1), 128–154. [https://doi.org/10.1016/0165-0173\(94\)00008-D](https://doi.org/10.1016/0165-0173(94)00008-D)
- Parent, A., & Hazrati, L. N. (1997). Functional anatomy of the basal ganglia. *Revista de Neurologia*, 25 Suppl 2, S121–S128. <https://doi.org/10.1002/mds.10138>
- Parker, J. G., Marshall, J. D., Ahanonu, B., Wu, Y. W., Kim, T. H., Grewe, B. F., Zhang, Y., Li, J. Z., Ding, J. B., Ehlers, M. D., & Schnitzer, M. J. (2018). Diametric neural ensemble dynamics in parkinsonian and dyskinetic states. In *Nature* (Vol. 557, Issue 7704). Springer US. <https://doi.org/10.1038/s41586-018-0090-6>
- Perese, D. A., Ulman, J., Viola, J., Ewing, S. E., & Bankiewicz, K. S. (1989). A 6-hydroxydopamine-induced selective parkinsonian rat model. *Brain Research*, 494(2), 285–293. [https://doi.org/10.1016/0006-8993\(89\)90597-0](https://doi.org/10.1016/0006-8993(89)90597-0)
- Pettersson, R., Hagsäter, S. M., & Eriksson, E. (2016). Serotonin depletion eliminates sex differences with respect to context-conditioned immobility in rat. *Psychopharmacology*, 233(8), 1513–1521. <https://doi.org/10.1007/s00213-016-4246-5>
- Peyron, C., Petit, J. M., Rampon, C., Jouvet, M., & Luppi, P. H. (1997). Forebrain afferents to the rat dorsal raphe nucleus demonstrated by retrograde and anterograde tracing methods. *Neuroscience*, 82(2), 443–468. [https://doi.org/10.1016/S0306-4522\(97\)00268-6](https://doi.org/10.1016/S0306-4522(97)00268-6)
- Phillips, J. G., Bradshaw, J. L., Iansek, R., & Chiu, E. (1993). Biological Research biologische

- Forschung Motor functions of the basal ganglia. *Psychol Res*, 55, 175–181.
- Pickrell, A. M., & Youle, R. J. (2015). The roles of PINK1, Parkin, and mitochondrial fidelity in parkinson's disease. *Neuron*, 85(2), 257–273. <https://doi.org/10.1016/j.neuron.2014.12.007>
- Pinborg, L. H., Adams, K. H., Svarer, C., Holm, S., Hasselbalch, S. G., Haugbøl, S., Madsen, J., & Knudsen, G. M. (2003). Quantification of 5-HT_{2A} receptors in the human brain using [18F]altanserin-PET and the bolus/infusion approach. *Journal of Cerebral Blood Flow and Metabolism*, 23(8), 985–996. <https://doi.org/10.1097/01.WCB.0000074092.59115.23>
- Politis, M., Wu, K., Loane, C., Brooks, D. J., Kiferle, L., Turkheimer, F. E., Bain, P., Molloy, S., & Piccini, P. (2014). Serotonergic mechanisms responsible for levodopa-induced dyskinesias in Parkinson's disease patients. *Journal of Clinical Investigation*, 124(3), 1341–1349. <https://doi.org/10.1172/JCI71640>
- Pompeiano, M., Palacios, J. M., & Mengod, G. (1994). Distribution of the serotonin 5-HT₂ receptor family mRNAs: comparison between 5-HT_{2A} and 5-HT_{2C} receptors. *Molecular Brain Research*, 23(1–2), 163–178. [https://doi.org/10.1016/0169-328X\(94\)90223-2](https://doi.org/10.1016/0169-328X(94)90223-2)
- Porras, G., De Deurwaerdere, P., Li, Q., Marti, M., Morgenstern, R., Sohr, R., Bezard, E., Morari, M., & Meissner, W. G. (2014). L-dopa-induced dyskinesia: Beyond an excessive dopamine tone in the striatum. *Scientific Reports*, 4, 6–10. <https://doi.org/10.1038/srep03730>
- Querejeta, E., Oviedo-Chávez, A., Araujo-Alvarez, J. M., Quiñones-Cárdenas, A. R., & Delgado, A. (2005). In vivo effects of local activation and blockade of 5-HT_{1B} receptors on globus pallidus neuronal spiking. *Brain Research*, 1043(1–2), 186–194. <https://doi.org/10.1016/j.brainres.2005.02.055>
- Ramirez-Zamora, A., & Ostrem, J. L. (2018). Globus pallidus interna or subthalamic nucleus deep brain stimulation for Parkinson disease a review. *JAMA Neurology*, 75(3), 367–372. <https://doi.org/10.1001/jamaneurol.2017.4321>
- Rav-Acha, M., Bergman, H., & Yarom, Y. (2008). Pre- and postsynaptic serotonergic excitation of globus pallidus neurons. *Journal of Neurophysiology*, 100(2), 1053–1066. <https://doi.org/10.1152/jn.00845.2007>
- Reznitsky, M., Plenge, P., & Hay-Schmidt, A. (2016). Serotonergic projections from the raphe nuclei to the subthalamic nucleus; a retrograde- and anterograde neuronal tracing study. *Neuroscience Letters*, 612, 172–177. <https://doi.org/10.1016/j.neulet.2015.11.035>
- Riad, M., Wu, C., Cornea-he, V., Singh, S. K., & Descarries, L. (1999). Cornéa-Hébert et al. 1999.pdf. *The Journal of Comparative Neurology*, 209(November 1998), 187–209.
- Rick, C. E., Stanford, I. M., & Lacey, M. G. (1995). Excitation of rat substantia nigra pars reticulata

- neurons by 5-hydroxytryptamine in vitro: Evidence for a direct action mediated by 5-hydroxytryptamine 2C receptors. *Neuroscience*, 69(3), 903–913. [https://doi.org/10.1016/0306-4522\(95\)00283-O](https://doi.org/10.1016/0306-4522(95)00283-O)
- Riss, P. J., Hong, Y. T., Williamson, D., Caprioli, D., Sitnikov, S., Ferrari, V., Sawiak, S. J., Baron, J. C., Dalley, J. W., Fryer, T. D., & Aigbirhio, F. I. (2011). Validation and quantification of 18 Faltanserin binding in the rat brain using blood input and reference tissue modeling. *Journal of Cerebral Blood Flow and Metabolism*, 31(12), 2334–2342. <https://doi.org/10.1038/jcbfm.2011.94>
- Rizzi, G., & Tan, K. R. (2019). Synergistic Nigral Output Pathways Shape Movement. *Cell Reports*, 27(7), 2184–2198.e4. <https://doi.org/10.1016/j.celrep.2019.04.068>
- Rogóz, Z., & Gołembiowska, K. (2010). Effect of metyrapone on the fluoxetine-induced change in extracellular dopamine, serotonin and their metabolites in the rat frontal cortex. *Pharmacological Reports*, 62(6), 1015–1022. [https://doi.org/10.1016/S1734-1140\(10\)70363-7](https://doi.org/10.1016/S1734-1140(10)70363-7)
- Saunders, A., Huang, K. W., & Sabatini, B. L. (2016). Globus Pallidus Externus Neurons Expressing parvalbumin Interconnect the Subthalamic Nucleus and Striatal Interneurons. *PLoS ONE*, 11(2), 1–20. <https://doi.org/10.1371/journal.pone.0149798>
- Saunders, A., Oldenburg, I. A., Berezovskii, V. K., Johnson, C. A., Kingery, N. D., Elliott, H. L., Xie, T., Gerfen, C. R., & Sabatini, B. L. (2015). A direct GABAergic output from the basal ganglia to frontal cortex. *Nature*, 521(7550), 85–89. <https://doi.org/10.1038/nature14179>
- Sawada, M., Kato, K., Kunieda, T., Mikuni, N., Miyamoto, S., Onoe, H., Isa, T., & Nishimura, Y. (2014). *Research | reports* 24. 788.
- Schober, A. (2004). Classic toxin-induced animal models of Parkinson's disease: 6-OHDA and MPTP. *Cell and Tissue Research*, 318(1), 215–224. <https://doi.org/10.1007/s00441-004-0938-y>
- Schwartz, R. K. W., & Huston, J. P. (1996). Unilateral 6-hydroxydopamine lesions of meso-striatal dopamine neurons and their physiological sequelae. *Progress in Neurobiology*, 49(3), 215–266. [https://doi.org/10.1016/S0301-0082\(96\)00015-9](https://doi.org/10.1016/S0301-0082(96)00015-9)
- Sgambato-Faure, V., Worbe, Y., Epinat, J., Féger, J., & Tremblay, L. (2016). Cortico-basal ganglia circuits involved in different motivation disorders in non-human primates. *Brain Structure and Function*, 221(1), 345–364. <https://doi.org/10.1007/s00429-014-0911-9>
- Sherathiya, V. N., Schaid, M. D., Seiler, J. L., Lopez, G. C., & Lerner, T. N. (2021). GuPPy, a Python toolbox for the analysis of fiber photometry data. *Scientific Reports*, 11(1), 1–9. <https://doi.org/10.1038/s41598-021-03626-9>
- Smith, Y., Bevan, M. D., Shink, E., & Bolam, J. P. (1998). Microcircuitry of the direct and indirect pathways of the basal ganglia. *Neuroscience*, 86(2), 353–387. <https://doi.org/10.1016/S0306->

- Stamatakis, A. M., Resendez, S. L., Chen, K. S., Favero, M., Liang-Gualpa, J., Nassi, J. J., Neufeld, S. Q., Visscher, K., & Ghosh, K. K. (2021). Miniature microscopes for manipulating and recording in vivo brain activity. *Microscopy*, 70(5), 399–414. <https://doi.org/10.1093/jmicro/dfab028>
- Stanford, I. M., Kantaria, M. A., Chahal, H. S., Loucif, K. C., & Wilson, C. L. (2005). 5-Hydroxytryptamine induced excitation and inhibition in the subthalamic nucleus: Action at 5-HT_{2C}, 5-HT₄ and 5-HT_{1A} receptors. *Neuropharmacology*, 49(8), 1228–1234. <https://doi.org/10.1016/j.neuropharm.2005.09.003>
- Stansley, B. J., & Yamamoto, B. K. (2014). Chronic L-Dopa decreases serotonin neurons in a subregion of the dorsal raphe nucleus. *Journal of Pharmacology and Experimental Therapeutics*, 351(2), 440–447. <https://doi.org/10.1124/jpet.114.218966>
- Stefano, G. B., Ptáček, R., Kuželová, H., Mantione, K. J., Raboch, J., Papezova, H., & Kream, R. M. (2013). Convergent dysregulation of frontal cortical cognitive and reward systems in eating disorders. *Medical Science Monitor*, 19(1), 353–358. <https://doi.org/10.12659/MSM.889133>
- Stein, E., & Bar-Gad, I. (2013). Beta oscillations in the cortico-basal ganglia loop during parkinsonism. *Experimental Neurology*, 245, 52–59. <https://doi.org/10.1016/j.expneurol.2012.07.023>
- Steinbusch, H. W. M. (1981). Distribution of serotonin-immunoreactivity in the central nervous system of the rat-Cell bodies and terminals. In *Neuroscience* (Vol. 6, Issue 4). [https://doi.org/10.1016/0306-4522\(81\)90146-9](https://doi.org/10.1016/0306-4522(81)90146-9)
- Tepper, J. M., Martin, L. P., & Anderson, D. R. (1995). GABA(A) receptor-mediated inhibition of rat substantia nigra dopaminergic neurons by pars reticulata projection neurons. *Journal of Neuroscience*, 15(4), 3092–3103. <https://doi.org/10.1523/jneurosci.15-04-03092.1995>
- Tepper, James M., Koós, T., Ibanez-Sandoval, O., Tecuapetla, F., Faust, T. W., & Assous, M. (2018). Heterogeneity and diversity of striatal GABAergic interneurons: Update 2018. *Frontiers in Neuroanatomy*, 12(November), 1–14. <https://doi.org/10.3389/fnana.2018.00091>
- Thiruchelvam, M., Richfield, E. K., Baggs, R. B., Tank, A. W., & Cory-Slechta, D. A. (2000). The nigrostriatal dopaminergic system as a preferential target of repeated exposures to combined paraquat and maneb: Implications for Parkinson's disease. *Journal of Neuroscience*, 20(24), 9207–9214. <https://doi.org/10.1523/jneurosci.20-24-09207.2000>
- Tremblay, L., Worbe, Y., Thobois, S., Sgambato-Faure, V., & Féger, J. (2015). Selective dysfunction of basal ganglia subterritories: From movement to behavioral disorders. *Movement Disorders*, 30(9), 1155–1170. <https://doi.org/10.1002/mds.26199>
- Tseng, K. Y., Kasanetz, F., Kargieman, L., Pazo, J. H., Murer, M. G., & Riquelme, L. A. (2001).

- Subthalamic nucleus lesions reduce low frequency oscillatory firing of substantia nigra pars reticulata neurons in a rat model of Parkinson's disease. *Brain Research*, 904(1), 93–103. [https://doi.org/10.1016/S0006-8993\(01\)02489-1](https://doi.org/10.1016/S0006-8993(01)02489-1)
- Tsybko, A. S., Ilchibaeva, T. V., Filimonova, E. A., Eremin, D. V., Popova, N. K., & Naumenko, V. S. (2020). The Chronic Treatment With 5-HT_{2A} Receptor Agonists Affects the Behavior and the BDNF System in Mice. *Neurochemical Research*, 45(12), 3059–3075. <https://doi.org/10.1007/s11064-020-03153-5>
- Tysnes, O. B., & Storstein, A. (2017). Epidemiology of Parkinson's disease. *Journal of Neural Transmission*, 124(8), 901–905. <https://doi.org/10.1007/s00702-017-1686-y>
- Uhlhaas, P. J., & Singer, W. (2006). Neural Synchrony in Brain Disorders: Relevance for Cognitive Dysfunctions and Pathophysiology. *Neuron*, 52(1), 155–168. <https://doi.org/10.1016/j.neuron.2006.09.020>
- Vegas-Suárez, S., Morera-Herreras, T., Requejo, C., Lafuente, J. V., Moratalla, R., Miguélez, C., & Ugedo, L. (2022). Motor cortico-nigral and cortico-entopeduncular information transmission and its modulation by bupropion in control and after dopaminergic denervation. *Frontiers in Pharmacology*, 13(August), 1–17. <https://doi.org/10.3389/fphar.2022.953652>
- Venzi, M., David, F., Bellet, J., Cavaccini, A., Bombardi, C., Crunelli, V., & Di Giovanni, G. (2016). Role for serotonin_{2A} (5-HT_{2A}) and 2C (5-HT_{2C}) receptors in experimental absence seizures. *Neuropharmacology*, 108, 292–304. <https://doi.org/10.1016/j.neuropharm.2016.04.016>
- Vijayakumar, D., & Jankovic, J. (2016a). Drug-Induced Dyskinesia, Part 1: Treatment of Levodopa-Induced Dyskinesia. *Drugs*, 76(7), 759–777. <https://doi.org/10.1007/s40265-016-0566-3>
- Vijayakumar, D., & Jankovic, J. (2016b). Drug-Induced Dyskinesia, Part 2: Treatment of Tardive Dyskinesia. *Drugs*, 76(7), 779–787. <https://doi.org/10.1007/s40265-016-0568-1>
- Volle, J., Bregman, T., Scott, B., Diwan, M., Raymond, R., Fletcher, P. J., Nobrega, J. N., & Hamani, C. (2018). Deep brain stimulation and fluoxetine exert different long-term changes in the serotonergic system. *Neuropharmacology*, 135, 63–72. <https://doi.org/10.1016/j.neuropharm.2018.03.005>
- Wallace, M. L., Saunders, A., Huang, K. W., Philson, A. C., Goldman, M., Macosko, E. Z., McCarroll, S. A., & Sabatini, B. L. (2017). Genetically Distinct Parallel Pathways in the Entopeduncular Nucleus for Limbic and Sensorimotor Output of the Basal Ganglia. *Neuron*, 94(1), 138–152.e5. <https://doi.org/10.1016/j.neuron.2017.03.017>
- Watabe-Uchida, M., Zhu, L., Ogawa, S. K., Vamanrao, A., & Uchida, N. (2012). Whole-Brain Mapping of Direct Inputs to Midbrain Dopamine Neurons. *Neuron*, 74(5), 858–873.

<https://doi.org/10.1016/j.neuron.2012.03.017>

Wichmann, T., & Dostrovsky, J. O. (2011). Pathological basal ganglia activity in movement disorders. *Neuroscience*, 198, 232–244. <https://doi.org/10.1016/j.neuroscience.2011.06.048>

Wiest, C., Tinkhauser, G., Pogosyan, A., He, S., Baig, F., Morgante, F., Mostofi, A., Pereira, E. A., Tan, H., Brown, P., & Torrecillos, F. (2021). Subthalamic deep brain stimulation induces finely-tuned gamma oscillations in the absence of levodopa. *Neurobiology of Disease*, 152(January). <https://doi.org/10.1016/j.nbd.2021.105287>

Wilson, M. A. (1993). *GONADECTOMY AND SEX MODULATE SPONTANEOUS ACTIVITY Electrophysiological Techniques : SN reticulata recording in vivo Electrophysiological analysis of single unit activity and microiontophoretic*. 53, 217–225.

Wright, D. E., Seroogy, K. B., Lundgren, K. H., Davis, B. M., & Jennes, L. (1995). Comparative Localization of Subtype mRNAs in Rat Brain. *In Situ*, 357373.

Xiang, Z., Wang, L., & Kitai, S. T. (2005). Modulation of spontaneous firing in rat subthalamic neurons by 5-HT receptor subtypes. *Journal of Neurophysiology*, 93(3), 1145–1157. <https://doi.org/10.1152/jn.00561.2004>

Yang, H. H. H., St-Pierre, F., Sun, X., Ding, X., Lin, M. Z. Z., & Clandinin, T. R. R. (2016). Subcellular Imaging of Voltage and Calcium Signals Reveals Neural Processing In Vivo. *Cell*, 166(1), 245–257. <https://doi.org/10.1016/j.cell.2016.05.031>

Yawata, S., Yamaguchi, T., Danjo, T., Hikida, T., & Nakanishi, S. (2012). Pathway-specific control of reward learning and its flexibility via selective dopamine receptors in the nucleus accumbens. *Proceedings of the National Academy of Sciences of the United States of America*, 109(31), 12764–12769. <https://doi.org/10.1073/pnas.1210797109>

Zappia, M., Annesi, G., Nicoletti, G., Arabia, G., Annesi, F., Messina, D., Pugliese, P., Spadafora, P., Tarantino, P., Carrideo, S., Civitelli, D., De Marco, E. V., Cirò-Candiano, I. C., Gambardella, A., & Quattrone, A. (2005). Sex differences in clinical and genetic determinants of levodopa peak-dose dyskinesias in Parkinson disease: An exploratory study. *Archives of Neurology*, 62(4), 601–605. <https://doi.org/10.1001/archneur.62.4.601>

Zhai, S., Shen, W., Graves, S. M., & Surmeier, D. J. (2019). Dopaminergic modulation of striatal function and Parkinson's disease. *Journal of Neural Transmission*, 0(0), 0. <https://doi.org/10.1007/s00702-019-01997-y>

Zhang, G., & Stackman, R. W. (2015). The role of serotonin 5-HT_{2A} receptors in memory and cognition. *Frontiers in Pharmacology*, 6(OCT), 1–17. <https://doi.org/10.3389/fphar.2015.00225>

Zhou, F. M., & Lee, C. R. (2011). Intrinsic and integrative properties of substantia nigra pars reticulata

neurons. *Neuroscience*, 198, 69–94. <https://doi.org/10.1016/j.neuroscience.2011.07.061>

Zhou, Fu Ming, Wilson, C. J., & Dani, J. A. (2002). Cholinergic interneuron characteristics and nicotinic properties in the striatum. *Journal of Neurobiology*, 53(4), 590–605.
<https://doi.org/10.1002/neu.10150>